Università degli Studi di Napoli Federico II
Dottorato in Scienze Chimiche – XXIV Ciclo (2008-2011)
Indirizzo: Chimica Macromolecolare e Catalisi

Interaction among reinforcing fibres, adhesive layer and rubber in tyres

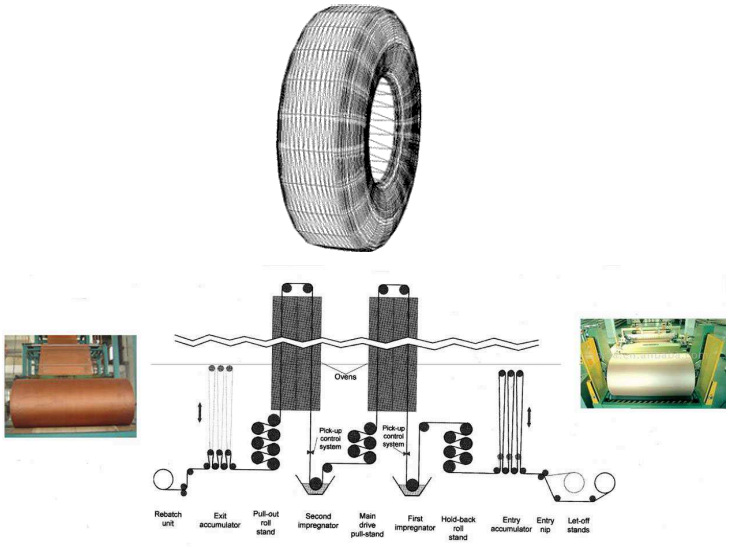

Dott. Paolo Vollaro

Tutor: *Ch.mo Prof.* Claudio De Rosa

Co-tutor: *Ch.mo Prof.* Finizia Auriemma

Supervisor: *Ch.mo Prof.* Ugo Caruso

Coordinator: *Ch.mo* Prof. Lucio Previtera

CONTENTS

Chapter 1
Introduction to the tyre world

1.1 Introduction: History of tyres

The tyre history begins about two centuries ago. In the early 1800s, Charles McIntosh is experimenting with latex, the sap from a tree found in the Amazon basin of South America. The latex is studied in this country after explorers have seen Indians using sheets of 'rubber' as waterproofing. Unfortunately, these 'rubber' sheets show undesirable qualities. In cold weather the sheets become brittle; in hot weather they become very sticky. Rubber experimentation is so widespread both in Europe and North America to try to stabilise its properties. It is in 1839 that Charles Goodyear discovers that by adding sulphur to melted latex the much sought-after attributes of elasticity and strength are attainable. This new vulcanised rubber is used initially as 'cushioning tyres' for carriages and cycles.

The modern pneumatic tyre, like so many inventions, is born out of a need to solve an individual problem rather than for a desire for fame and fortune. So in 1888, when a Scotsman John Boyd Dunlop is looking for a way to make his son's bicycle journeys more comfortable, he could hardly image the great discovery made. However Dunlop's discovery is not without its controversy. Unbeknown to him another Scot, Robert William Thomson, have already patented[1] a pneumatic rubber tyre in 1845. Dunlop fights and wins a legal battle with Thomson and creates the famous Dunlop Rubber Company.

Despite Thomson getting there quicker, it is Dunlop's tyre *design* that give him the claim to have invented the pneumatic tyre. But sadly Dunlop, a veterinary surgeon, sells the patent and the company early on and so from a financial point of view have not benefited greatly from his invention.
In late 1891 the first detachable pneumatic tyre is invented by two agricultural engineers in Clermont-Ferrand in Central France. These brothers Andre and Edouard Michelin market their ideas strongly and successfully. Their tyre consists of a separate tube with an outer bolt fix to the rim by means of a huge washer.

Within a few years W.E. Barlett has invented an improved detachable tyre and rim. At the same time Welch, in conjunction with the newly-formed Dunlop Company, invents something reminiscent of modern wheels and tyres.

It is in 1915 that the Palmer Tyre Company of Detroit makes a great stride forward. They create the first ‘cord’ fabric covered by rubber and make the first ‘Cord Tyre’. The fabric they used is not woven. All the strands of cord are laid parallel to each other and pressed into sheet rubber. Experimentation continues and the search for stronger and more resistant cord materials is ceaseless; in 1937 the steel cords are introduced for the first time in truck tyre manufacture. At last, in 1947 the first radial tyre comes, a tyre that has revolutionised the transport industry. This new type of pneumatic tyre has a long life and less rolling resistance increasing the mileage of a vehicle.

1.2 Cord/rubber composites

Cord-rubber composites can be found in every day life. Examples of applications are car and bicycle tyres, high-pressure hoses and conveyor belts. Some essential under-the-hood applications are made of cord-rubber composites as well: timing belts, V-belts and radiator hoses are examples. By far the largest of all these examples is the car tyre. The application of cords in tyres is essential because the cords prevent large deformations of the rubber material when excessive forces are applied. These forces are caused by the air pressure of the tyre, and by accelerating, breaking and cornering of the car. The network of cords that provides the tyre with its strength and its shape is called the carcass. There are two types of carcass constructions in use, thereby dividing virtually all tyres in two categories: radial and bias tyres, Figure 1.1.[2]

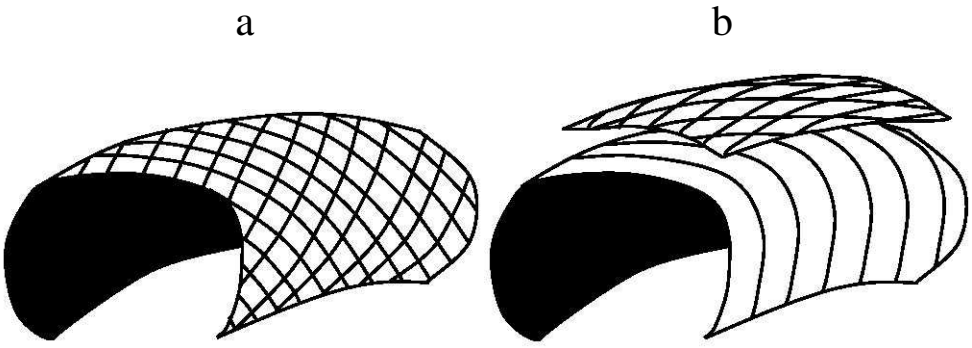

Figure 1.1: Schematic representation of the two tyre constructions: bias (a) and radial (b).[2]

Bias and radial tyres

The oldest tyre construction is called bias or cross ply: Figure 1.1a. A bias tyre has a casing which is made of stacked reinforcing layers of cords, called plies, crossing over each other at an angle of 30° to 40° to the centre line of the tyre. These stacked plies reinforce both the tread and the sidewall and must therefore resist the forces caused by cornering, accelerating and breaking, but also maintain the shape of the tyre. Because of the required flexibility of the tyre sidewall, the all-sided reinforcement causes the tread to deform as well when driving over obstacles. This causes rapid wear, lower traction and higher fuel consumption compared to more recent radial tyres.

The first commercial tyre with radial belt construction was produced by Michelin in 1948: the 'Michelin X'. A schematic reproduction of a radial tyre carcass is shown in Figure 1.1b. Textile cords are placed at 90° to the direction of travel from bead to bead, designed to hold the air pressure and carry the load of the car. These cords are flexible and large deflections are allowed to absorb obstacles on the road for comfort. However, positioning the reinforcing cords in this direction, there is insufficient stabilisation of the circumference of the tyre, and the control and steering properties would be completely unacceptable. Therefore, additional plies of high modulus cords, usually steel, are placed at an angle of 16° to 25° underneath the tread. These plies are designed to carry the load caused by accelerating, breaking and cornering. The radial tyre separates the functions of the tread and the sidewall, where the bias tyre compromises the two.

1.3 Fibres in tyres applications

Fibre reinforced rubber compounds play a crucial role in tyres. Until about 1890, only natural fibres are available. Just before the end of the 19th century the first synthetic fibres based on cellulose are developed.

Cellulose is an insoluble substance and in order to make this soluble, several derivations are tried. The first attempt is nitration, but cellulose nitrate proves to be more useful as guncotton than as a fibre. Cooper rayon and viscose rayon follow; the latter become the first large-volume synthetic fibre material. [2,3]

These cellulose yarns are considered to be half-synthetic, because the raw material is still a natural polymer: cellulose.

DuPont develops the first fully synthetic fibre Nylon® 6,6 or Polyamide 6,6; it is commercially introduced in 1936 (Carothers).[4] A few years later, Polyamide 6 (Schlack, 1938)[5] and Polyester (Whinfield & Dickson, 1941)[6] are introduced.

The development of "advanced fibres" takes place around 1970. Most of these fibres are produced from fully aromatic polymers with high temperature stability. This lead to the discovery of the liquid-crystalline behaviour of PPTA (paraphenylene terephthalamide), the first super-strong fibre. The companies DuPont and Akzo Nobel start a patent conflict in 1979. The patents of DuPont[7-10] as well as the patent of Akzo Nobel[11] are necessary to produce this fibre. In 1988, the two companies reach a compromise. Nowadays, the PPTA fibre of DuPont is called Kevlar®. Akzo sells its fibre division and the PPTA fibre is now owned by Teijin; the brand name is Twaron®. The second super-strong fibre is gelspun polyethylene (Dyneema® of DSM, 1979).[12]

The types of fibres used for reinforcing rubber are listed in Table 1.1 together with the year the fibre is invented and the year it is introduced in tyre reinforcement.[13]

Table 1.1: Types of fibres produced throughout history for tyre reinforcement.[13]

Type of fibre	Year of invention	Introduction in tyre reinforcement
Cotton	app. 7000 years ago	1900
Viscose rayon	1885	1938
Polyamide 6,6	1935	1947
Polyamide 6	1938	1947
Polyethylene terephthalate	1941	1962
Aromatic polyamide	1969	1974
Gelspun polyethylene	1979	-

In Table 1.2, the types of fibres used in various parts of tyres are listed.[14,15] In Figure 1.2, a cross section of a tyre is shown with the description of the various tyre parts.[15] The types of fibres used in tyres are limited to polyamide, rayon, polyester, aramid and steel, because these materials are sufficiently temperature-resistant to survive the vulcanisation step in tyre manufacturing without weakening or complete disintegration.

There is a large variety between these fibres in price and performance, hence the change in type of reinforcement with increasing demands. The main properties of the fibres are listed in Table 1.3.[15]

Table 1.2: Type of fibres used in tyres.[14,15]

Tyre part \ Tyre type	Standard	High performance	Ultra high performance (>300 km/h)	Racing	Run flat	Ultra light
Carcass	PET Rayon	PET Rayon	PET Rayon PEN	Rayon Aramide	Rayon Steel PET	Rayon Aramide
Belt	Steel	Steel Aramid	Steel PEN	Aramid	Steel	Aramid
Capply	no	Polyamide Aramid	Polyamide Aramid	Polyamide Aramid	Polyamide Aramid	Polyamide Aramid
Chafer	no	Polyamide Aramid	Polyamide Aramid	Aramid	Polyamide	Aramid
Bead	Steel	Steel	Steel	Steel Aramid	Steel	Steel Aramid

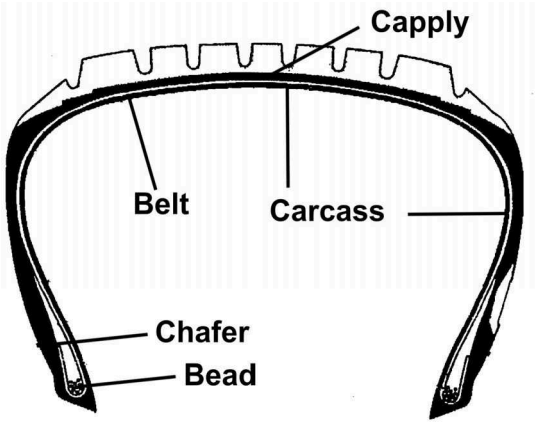

Figure 1.2: Cross section of a tyre, indicating the areas important for fibre reinforcement.[15]

Table 1.3: Properties and performance of several types of fibres.[15]

	Rayon	Polyamide 6	Polyamide 6,6	Polyester	Aramid
Density (kg/m^3)	1520	1140	1140	1380	1440
Moisture content* (%)	12 – 14	4	4	0.4	1.2 – 7
Decomp. temp (°C)	210	-	-	-	500
Melting temp. (°C)	-	255	255	285	-
Glass transition temperature (°C)	-	50	57	69	>300
E-mod (cN/tex)	600 – 800	300	500	850	4000
Tensile strength (MPa)	685 – 850	850	850	1100	2750

* measured at 65% relative humidity at 20°C

The properties of Rayon are significantly improved between the 1930's and the 1970's. This is realised by making the Rayon denser and more uniform in structure. A major disadvantage of Rayon is its sensitivity to moisture. In moist conditions, its loss in strength is significant.

Polyamide 6 is mostly used in automobile tyres in India and South America; polyamide 66 is used on a larger scale. For rubber reinforcement, polyamide 6 and polyamide 66 have the disadvantage of a low melting point and a low modulus. Therefore, they cannot be used in the carcass but only as a cap ply, above or around the steel belt.

Polyester fibres have a high modulus and a high tensile strength and are the single most important reinforcing material for tyres. However, there are two problems involved in using polyester for reinforcing rubber. The first problem is that polyester is chemically rather inert and it is therefore more difficult to obtain a sufficient level of adhesion to rubber compared to rayon and polyamide. The second problem is the thermal shrinkage. Various grades of polyester are available with varying shrinkage/modulus ratios.

Aramid fibres have a very high modulus and tensile strength. However, this is coupled to a very low value of elongation at break. The major disadvantage of this low elongation occurs when aramid is used in

several layers. When flat, each layer contributes its own share of strength, but upon bending the outer layer causes a compression deformation of the inner layers: aramid performs poorly under compression. The elongation at break of an aramid fibre can be improved by applying a large twist factor. Next to this, there is the problem of poor adhesion, similar to polyester.

1.4 Adhesive treatment of fibres

When using fibres in combination with rubber, good adhesion is essential especially for high safety products such as tyres. The adhesion between untreated fibres and rubber is always low, because there is a significant chemical incompatibility (for example in modulus and polarity) between the reinforcing fibres and the rubber matrix. The type of adhesive treatment is dependent on the type of fibre used. In the case of cotton, one of the first fibres used in rubber, the only adhesive treatment necessary is drying the fibre. Cotton fibres are not smooth; filaments are sticking out of the surface of the fibre. These filaments are anchored in the rubber matrix. The frictional forces that need to be overcome to pull or strip the fibre out of the rubber result in a significant adhesion.

The (semi) man-made fibres such as regenerated cellulose (Rayon) and polyamide have a smooth surface; therefore, there is no interlocking of filaments. Furthermore, the mechanical properties of these fibres are higher compared to cotton and therefore a higher strength of the adhesion is required. The aim to find some systems able to give good adhesion between these fibres and rubber lead to a first series of adhesives. These are originally based on a latex and casein, but the casein component is soon replaced with a resorcinol/formaldehyde (RF) resin. This Resorcinol-

Formaldehyde-Latex treatment (RFL-DIP treatment) is invented by W.H. Charch and D.B. Maney.[16]

For polyester fibres, the RFL-DIP treatment alone is not sufficient due to the lack of polar and hydrogen bonding groups in its chemical structure. In case of aramid fibres, the bulky aromatic groups sterically hinder the amide functionalities. Therefore, both polyester and aramid fibres are treated with a preDIP (epoxy or isocyanate treatment)[17-22] before being treated with a standard RFL-DIP. An outline of the RFL-treatment is schematically depicted in Figure 1.3.[15]

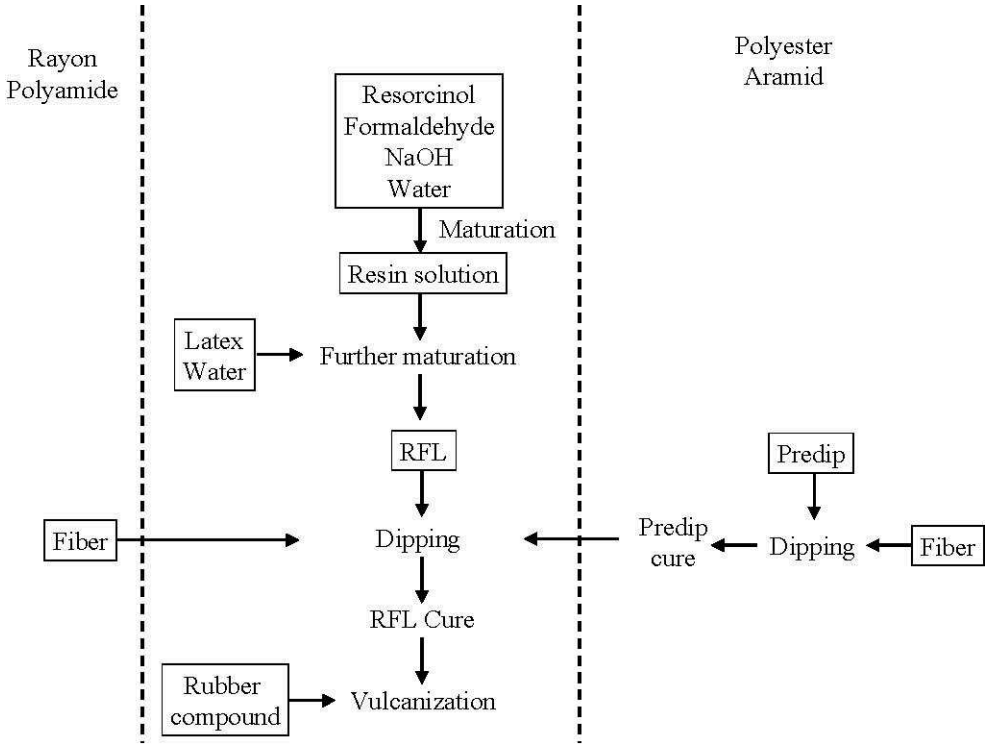

Figure 1.3: Schematic representation of the various fibre treatments, including RFL-DIP treatment and the adhesion to rubber compounds.[15]

1.5 RFL-DIP composition

The RFL-DIP is an emulsion of rubber latex in a solution of resorcinol and formaldehyde in water. If latex alone would be applied to the cords, it would provide an interaction with the rubber matrix of the compound but not with the fibre itself; furthermore, the latex layer would have weak mechanical properties. By adding resorcinol and formaldehyde, the DIP layer increases in polarity and mechanical properties.

The preparation of a RFL-DIP takes place in two stages. First, an aqueous solution of resorcinol and formaldehyde is matured for several hours at room temperature. By adding sodium hydroxide, this mixture becomes basic. During the maturation process, some degree of condensation takes place. Second, the resin solution is added to a mixture of latex and water. The amount and ratio of latex and water can be varied to achieve the desired RFL-DIP. A RFL-DIP has a typical solid content of around 20 wt% and a pH of around 10. Several studies have shown that the structure of the cured RFL consists of a continuous resin phase and dispersed latex particles.[23,24] A visualisation of the morphology is shown in Figure 1.4.

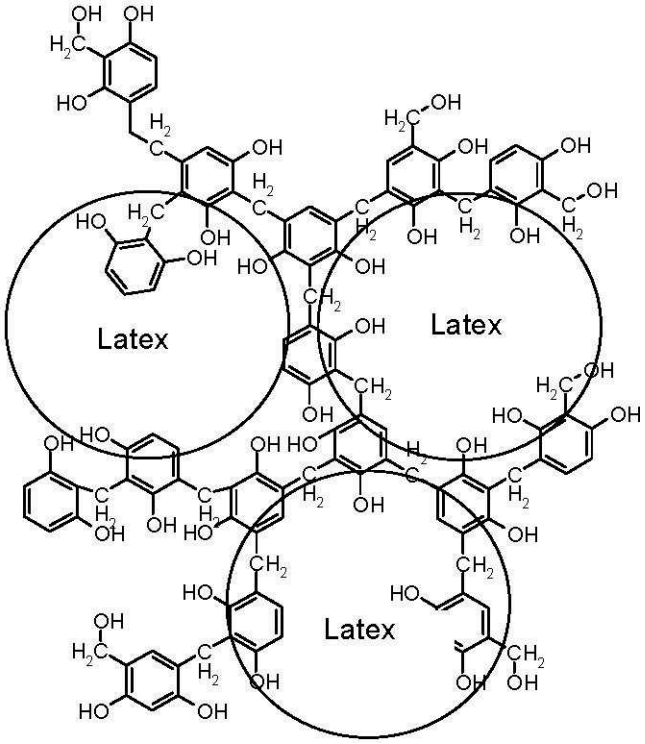

Figure 1.4: Proposed RFL morphology.

1.6 Dipping process

A general scheme for a dipping process unit[25] is given in Figure 1.5. In this picture, the cord is moving from the right to the left. When a feed roll is empty, the entry accumulator is used to gain time to attach a new feed roll. Before entering the impregnator bathes and after the ovens, series of rolls are present. These rolls have a relative velocity between each other, allowing application of a certain stress on the cord during dipping and drying. After the cord has passed an impregnator bath, the amount of DIP on the cord (DIP pickup) is regulated by the so-called pickup control system. This is mostly a squeeze roll unit, but can also be a vacuum unit or a beater. The second dipping unit functions similar to the first one. The exit accumulator works the opposite way as the entry accumulator, as a buffer

for the rebatch unit. Parameters that are adjusted during the dipping process are: cure temperature of the preDIP, cure temperature of the RFL-DIP, tensile forces on the cord when passing the ovens and residence times in the ovens. The residence times in the ovens can be adjusted either by changing the speed of the cord or by adjusting the number of loops which the cord makes through the ovens.

All these parameters need optimisation for every type of reinforcing fibre, the type of RFL and the type of rubber to adhere to. It is therefore not surprising that the knowledge of cord to rubber adhesion to date is very pragmatic rather than scientific. Many RFL variables such as formaldehyde to resin ratio, resin to latex ratio, dip pickup, acidity of the dip, cure time and temperature of the dip and environmental aspects such as UV and ozone attack are investigated and their influence on the adhesion reported in a variety of papers.[26-36] The references reported here only represent a selection of the most useful articles.

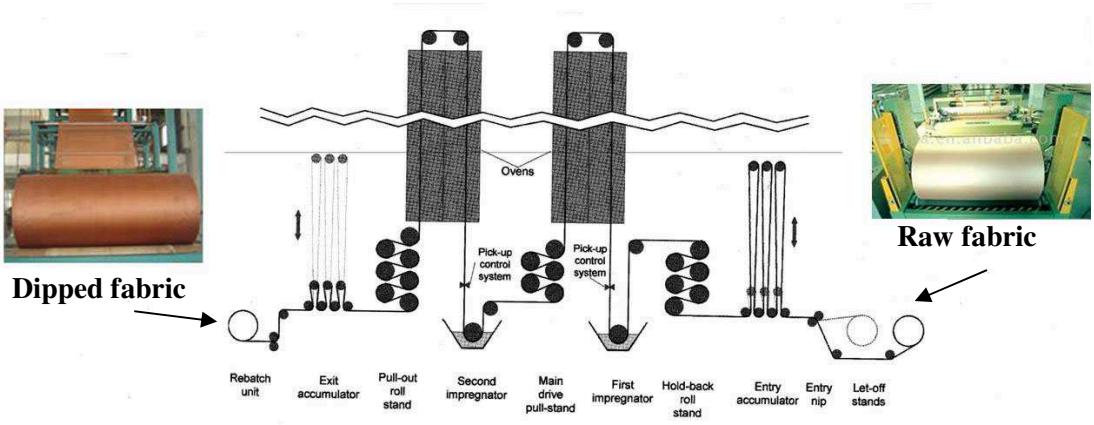

Figure 1.5: General drawing of a fabric treatment unit for a two dip system.

Formaldehyde to resorcinol ratio: Formaldehyde and resorcinol react in a similar manner as in the formation of Bakelite.[37] The reactions take place in a basic environment. The reaction scheme is depicted in Figure 1.6.

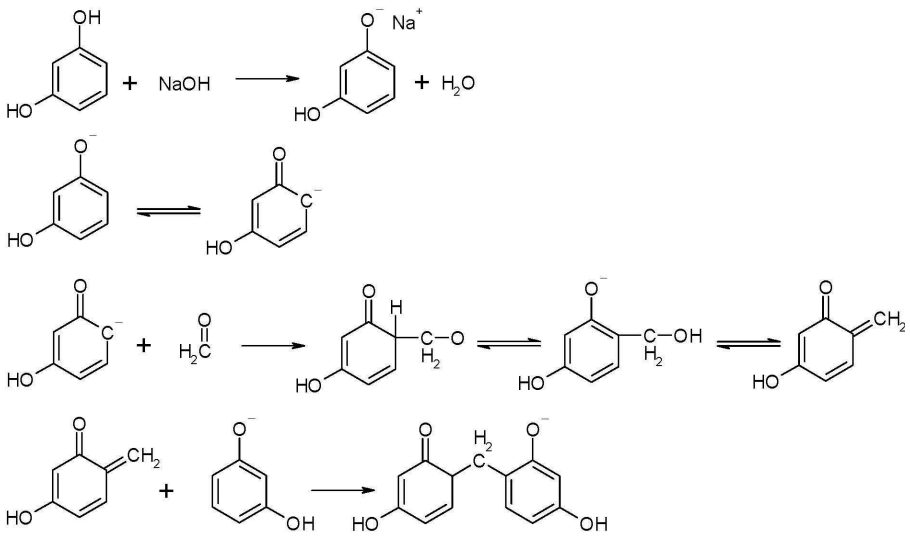

Figure 1.6: Reaction of formaldehyde and resorcinol in a basic environment.

Increasing the amount of formaldehyde increases the rate and amount of methylol formation.[15,38] Due to this methylol functionality, reaction can take place with another resorcinol molecule according to the scheme. Increasing the formaldehyde to resorcinol ratio increases both the degree of condensation and the degree of branching. The concentration, the maturation time and temperature of the resin solution, as well as the curing time and temperature of the RFL-DIP influence the rate of condensation.

The influence of the formaldehyde to resorcinol ratio of the RFL-DIP on the adhesion to rubber compounds has been the subject of various review articles in the 1950's and 60's.

In Figure 1.7 is reported the formaldehyde and resorcinol ratio versus the pullout force (force required to pull the fibres from the rubbery matrix). All studies indicate an optimum in formaldehyde and resorcinol ratio. Porter[30] studied the effect, using a styrene butadiene (SBR) rubber compound containing N-tert-butyl-benzothiazole sulphenamide (TBBS), tetramethyl thiuram disulphide (TMTD) and sulphur as curatives. He found that the optimum amount of formaldehyde relative to resorcinol is 2 to 1 for all three fibres: polyester, polyamide and Rayon. The research of Miller and Robison[31] was based on butylrubber reinforced with rayon fibres. Dietrick[32] used polyamide in a Natural Rubber (NR) compound using mercapto benzothiazole disulphide (MBTS) and sulphur as curatives. The results of Solomon[39] were published in an educational book without the type of fibre or rubber being mentioned. The rate of methylol formation, molecular weight and the network structure of the RF-resin vary with the formaldehyde to resorcinol ratio.[28,29]

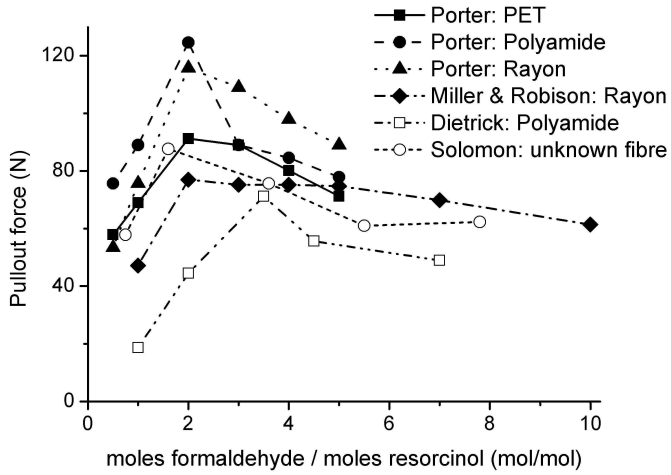

Figure 1.7: Effect of resin composition on pullout force.

***Resin to latex ratio**:* The influence of the amount of resin versus latex on the adhesion is reported in the same publications as the influence of resin composition. If only the latex would be applied on the cord, the bonding force would be very low due to lack of interaction with the fibre. According to all publications, the pullout force increases significantly when resin is added to the latex in the DIP.[28,29] However a too high content of resin results in a DIP which is too stiff and has poor flex properties.[29] This type of DIP shows a lack of interaction with the rubber phase.

Type of rubber latex: The most commonly used latex is based on a terpolymer of styrene, butadiene and vinylpyridine, the so-called VP-latex. The structural formula of VP-latex is given in Figure 1.8. It is empirically believed that vinylpyridine monomer is indispensable to obtain sufficient rubber adhesion. However, the reason for this is unknown.

Wootton[40] reported that a blend of 80% VP-latex with 20% SBR-latex results in an optimum adhesion for Rayon tyre cord. However, for polyamide the use of only VP-latex was beneficial. The adhesion was measured to a NR compound. No explanation was given for these observations.

Porter[27,30,41] investigated the adhesion of RFL-dipped polyester and polyamide with varying VP-monomer contents. The VP-content was varied by mixing a copolymer of 70% butadiene and 30% VP with SBR-latex and by copolymerising different amounts of the VP-monomer in the latex. The adhesion was measured to a SBR-compound with TBBS, TMTD and sulphur as curatives. All the results indicated that a VP-content of 15 wt% in the latex was the optimum value that resulted in the highest adhesion.

Hupjé[26] explained the choice of the tyre industry for the more expensive VP-latex by the fact that higher DIP-cure temperatures can be

used for VP-latex than for SBR-latex. Furthermore, VP has a better interaction with the resorcinol formaldehyde resin component of the RFL-DIP.

Takeyama[42] claimed that for a NR/SBR compound the use of VP-latex was preferred over the use of NR-latex or SBR-latex. However, due to the high modulus of the VP-terpolymer, the fatigue properties of a RFL-DIP containing VP-latex were worse.

Solomon[43] gave three possible reasons for the good performance of the VP-latex: (1) vulcanised VP-latex shows high strength; (2) the polarity of the VP-monomer is high, thereby increasing the interaction with the fibre; and (3) the VP-monomer improves the interaction with the resorcinol formaldehyde (RF) resin. The last was verified by Xue.[44] He found that 2-ethylpyridin undergoes hydrogen bonding with the RF-resin.

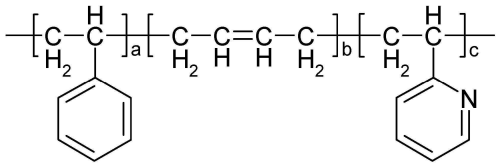

Figure 1.8 Structural formula of styrene-butadiene-vinylpyridine latex.

DIP pickup: The amount of DIP on the cord after the dipping process is called dip pickup. The DIP pickup influences the adhesion. The adhesion increases as a function of DIP pickup and reaches a saturation point. In practice, a DIP pickup of around 7 wt% is preferred.[29] The exact mechanism by which the DIP pickup influences the adhesion is not given by any author.[26, 30-32, 39]

Initial pH of the DIP: In Figure 1.9, the influence of initial pH of the resorcinol formaldehyde resin on the pullout force of a polyamide fibre in a NR compound is shown.[32] Two types of catalyst were used: ammonium hydroxide and sodium hydroxide. The optimum adhesion is achieved by using sodium hydroxide at a pH between 8 and 9. When using ammonium hydroxide, the resulting adhesion is less sensitive to pH. The same results are obtained by Porter[30] for polyester, polyamide and rayon fibres. Solomon reported an optimum in pH at a value of around 9.7 using NaOH as catalyst.[39]

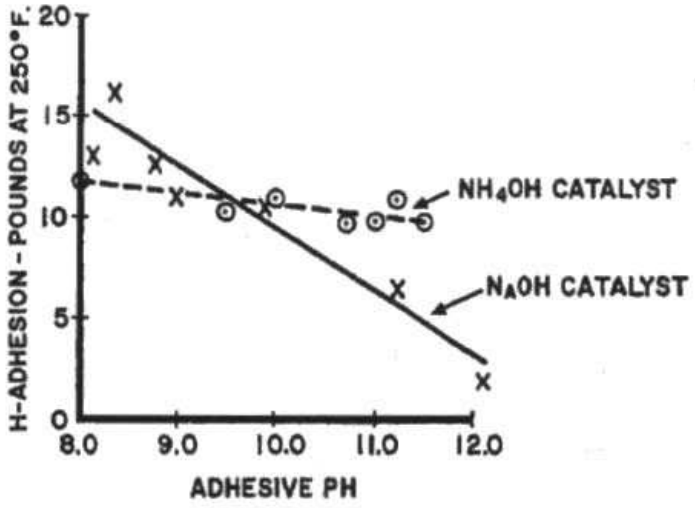

Figure 1.9: Influence of initial pH of the resin solution on the H-pullout force.[32]

Cure time and temperature of the RFL-DIP: Takeyama[29] investigated the influence of cure time and temperature of the RFL-DIP on the adhesion to rubber. Takeyama published Figure 1.10 in a review article and did not mention the type of rubber or fibre used. According to Figure 1.10, an increasing temperature results in a shorter optimum cure time. The cure time also becomes more critical with increasing temperature because the

graphs in Figure 1.10 become narrower. The obtained adhesion remains on the same level for all temperatures.

However, usually, the cure temperature used for rayon varies around 160°C, polyamide between 200 and 230°C and for polyester and aramid fibres even higher temperatures can be used, because these are temperature-stable fibres.

The explanations for the dependence of adhesion on cure time and temperature vary widely. Explanations are based on the mechanical properties of the DIPS, the presence of methylol groups and oxidative breakdown of the DIP layer.

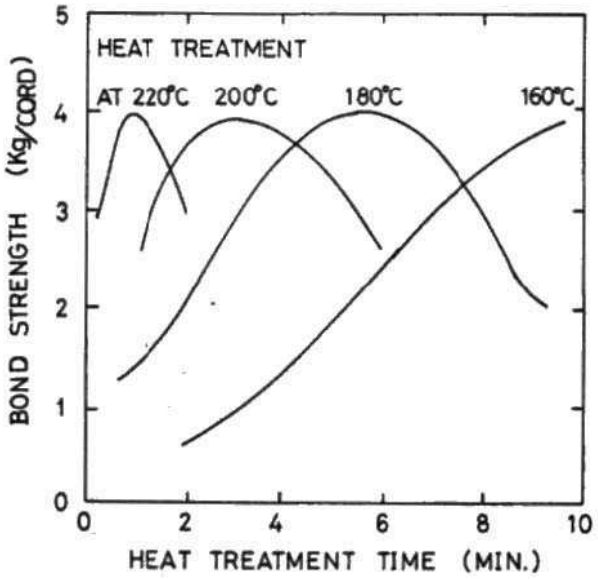

Figure 1.10: Effect of cure time and temperature of the RFL-treatment on the adhesion.[29]

Environmental aspects: The properties of the RFL-layer are influenced to a large extent when the treated fibre is exposed to ozone, humidity, UV light or heat.[36,45] After vulcanising the exposed fibre to a rubber compound, the adhesion is deteriorated to a large extent, not because of cohesive failure in the RFL-DIP itself, but rather at the surface and the interface between RFL and rubber, due to lack of reactive sites in the latex where vulcanisation can take place.

1.7 Aim of this PhD thesis

Textile cords used in rubber applications are commonly treated with the so-called Resorcinol-Formaldehyde-Latex (RFL-DIP). Despite the relevance of good adhesion between cords and rubber, and although this system dates back as far as 1938[3] and is still commonly used for rubber reinforcement till today, the mechanism by which the adhesion is obtained has remained unclear.

The level of knowledge of adhesion between RFL-treated cords and rubber today is empirical rather than scientific. With the introduction of new material in recent years, it is considered appropriate to revisit the physical and/or chemical processes at the basis of the interactions between latex and resin in the RFL-DIP traditional systems and to define also the nature of interactions among the RFL components and the reinforcing fibers and the RFL components and rubber. Based on the results obtained from the understanding of these interactions, a study on the possibility of developing alternative DIP systems free of formaldehyde is carried out. Currently, in fact, there are restrictions on the industrial use of formaldehyde based on the proven carcinogenic properties.[46]

Chapter 2 deals with a mechanical characterization of PET fibers produced by three different suppliers in order to establish the material with the best properties in terms of tensile creep and fatigue strength at break and that can be subjected to the treatment of dipping.

In **Chapter 3** RFL-DIP traditional systems are characterized in the solid state in order to understand the nature and mechanism of interaction between Resorcinol-Formaldehyde resin (RF) and Latex. Solid samples of RFL, obtained from aqueous solution by means of casting, are analyzed using techniques of Optical Microscopy (OM) and Raman and Fourier transform infrared (FTIR) spectroscopies.

In **Chapter 4** the study of the interactions between the reinforcing fibers and RFL and of the interface RFL/rubber is reported. Raman, FT-IR attenuated total reflection (FT-IR/ATR), ^{13}C NMR spectroscopies and mechanical and thermogravimetric (TGA) analysis are used to obtain much information as possible about these interactions.

A bibliographic study of alternative DIP systems free of formaldehyde is reported in **Chapter 5**. Two possible systems have been identified: soy-based DIP and starch-based DIP that will be tested as potential substitutes of traditional RFL-DIP systems.

In **Chapter 6,** this thesis is completed by summarising the results.

Chapter 2

Study of mechanical properties of PET fibres

2.1 Introduction

High performance thermoplastic fibres find wide use in technical applications such as the reinforcement of tyres and belting, in the field of geo-textiles or in assemblies of numerous yarns in mooring ropes or climbing ropes.

The use of cords in tyres is essential because the cords prevent large deformations of the rubber material when excessive forces are applied. Since the reinforcing effect of fibres in tyres depends on their ability of resisting to crack initiation, a better understanding of mechanism subtending to the rupture of fibres is desirable. In this study, conducted at the Ecole Nationale Supérieure des Mines de Paris under the supervision of prof. Anthony Robert Bunsell, the mechanical properties of poly(ethylene terephthalate) (PET) fibres, produced by three different companies and used as reinforcing agents for tyres, have been analyzed. The study is made on single filaments extracted from these fibres, in order to identify the fibre with the best tensile, creep and fatigue strength at break. The fibre with the best mechanical properties can be subjected to a dipping process and used in a tyre.

2.2 Materials and methods

Materials: PET fibres production and properties.

In the textile industry, polyester is the general name given to the fibres from poly-ethylene terephtalate (PET). The synthetic route for PET production is given in figure 2.1. Ethylene glycol is prepared by the oxidation of ethylene to ethylene oxide, which for hydrolysis yields the glycol (Figure 2.1 A). Therephthalic acid is obtained by direct oxidation of *p*-xylene (Figure 2.1 B).[47]

There are two methods for polymer preparation. In Europe, the more widely used route is by ester interchange via dimethyl terephthalate (Figure 2.1 Ci), but in USA, the direct esterification of the acid with ethylene glycol is the favoured method (Figure 2.1 Cii).

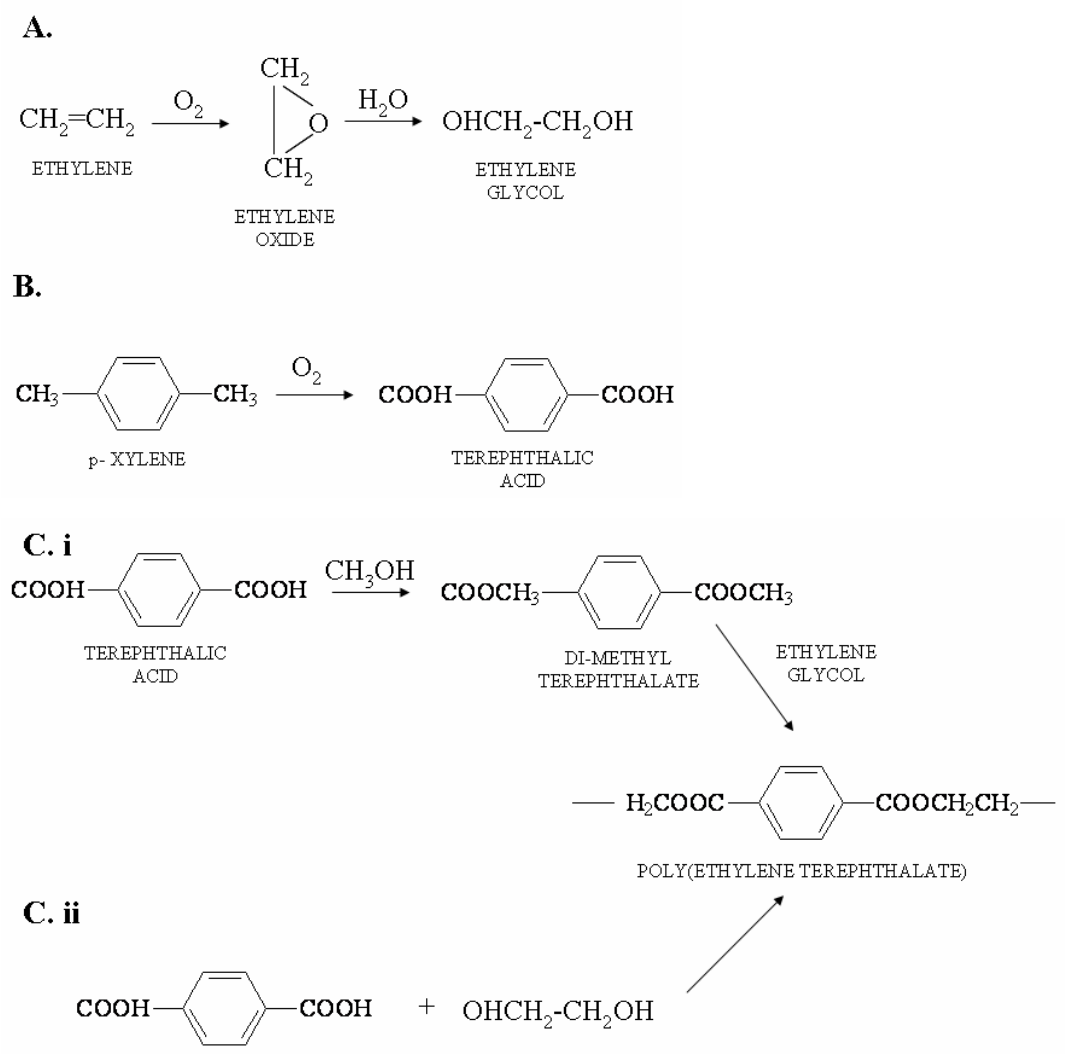

Figure 2.1: The polyester process. A-B-Ci: PET production process via di-methylterephthalate; A-B-Cii PET production process via direct esterification of terphthalic acid with ethylene glycol.

The properties of PET fibres are reported in many publications.[48-56] Polyester molecule contains aromatic rings making it less flexible than the molecule of polyamide.[48] The consequence of this increased molecular rigidity is the increase of the module of polyester fibres compared to polyamide fibres. The softening point of PET fibres is approximately 260°C.[49] At about 180°C, tenacity of the PET fibres is about half of its value at room temperature. PET fibres have excellent resistance to

oxidation and reduction and to most organic solvents and common hydrocarbons. The range of chemicals that dissolve the PET fibres is limited. PET fibres have a moisture resistance considerably higher, due to their low water absorption. PET fibres have excellent mechanical properties such as fracture toughness and elastic modulus high, moderate elastic resilience, good resistance to heat and light.[49]

Industrial PET fibres are classified as medium tenacity fibres (MT), high tenacity (HT), high modulus (HM), low shrinkage (LS) and the newly developed grade of high modulus/low shrinkage (HM/LS) also called the "dimensionally" stable (DSP). Many of the PET fibres products are used in composite materials reinforced with fibres. Among them, fibre HM/LS, recently developed, are widely used in tyres, seat belts, conveyor belts and other mechanical products using a rubber matrix. Thanks to their high dimensional stability, PET fibres HM/LS or DSP are today the most advanced fibres for the reinforcement of tyres. The fibres HM/LS offer same tenacity that the nylon fibres of high strength. Their withdrawal is typically 6% against 8-12% for Nylon 6,6. For the reinforcement of tyres, PET fibres have better resistance to fatigue and "flat spotting" compared to nylon fibres.

In this PhD thesis a mechanical characterization of three types of high performance PET fibres has been performed. The fibres are produced by different manufacturers and the details of the processes are not known. However all types of fibres are made for use in tyre cords. The monofilaments extracted from fibres will be referred in this thesis as PET-A, PET-B and PET-C.

Methods

Measure of monofilaments diameters

The evaluation of the section of monofilaments is an important step, since this size is necessary to calculate the nominal stress in the mechanical tests.

The monofilament diameter is estimated with an accuracy of ± 0.1 microns using a laser Mitutoyo LSM-6000 showed in figure 2.2. Once the single filament is mounted on the measuring system, it is horizontal and vertical optimally adjusted using two micrometer screws. The determination of the diameter is based on the estimation of the shadow created by the monofilament when it encounters the laser beam. More precisely, how long the monofilament is an obstacle during the scanning of the laser beam is estimated. The output voltage varies with the duration of the switch off of the beam. The data obtained are processed and displayed in digital form to be direct read by the user.

For each type of filament, the device has been calibrated by means of standard monofilaments, with a diameter previously evaluated by a scanning electron microscope (SEM). For each single filament, three diameter measurements are made along the length of gauge and the average of these measures is used to obtain the diameter.

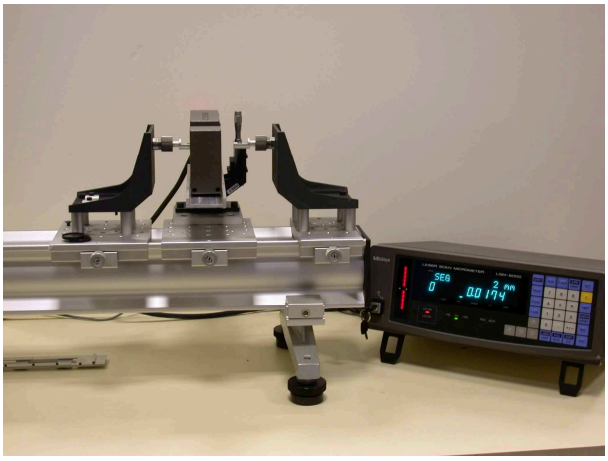

Figure 2.2: A Mitutoyo laser apparatus used for measuring the diameters of filaments

Mechanical tests

In order to obtain unambiguous results concerning the failure processes in fibres it is necessary to test single filaments. This is because when a multifilament fibre is loaded, it is unclear if all the filaments are subjected to same load. For this reason a machine has been developed at the Ecole des Mines to make tensile, creep and fatigue tests on single filaments. The machine is known as the Universal Fibre Tester[57] and is shown with the associated electronic units in Figure 2.3.

The filaments are held between two clamps, one mounted on the cross-head and connected by a screw thread to a motor controlled by a servo-system controlled by the chosen load or displacement. The other grip is fixed for tensile and creep tests or connect to a vibrator for fatigue tests.

The mechanical tests can be load and displacement controlled with a very high accuracy. The load is monitored by a piezoelectric transducer with a sensitivity of 0.01 g ($9.81*10^{-5}$ N), the displacement of the cross-head by a LVDT transducer with a sensitivity of 1 μm, and the cyclic deformation, produced by a vibrator acting on the same principal as a loud speaker, by a capacitive transducer with a sensitivity of 6 μm.

A tensile test consists of a controlled increase of deformation at constant chosen speed until failure.

Creep tests are conducted forcing the machine to keep the load on the monofilament constant. This is the most efficient way of conducting a creep test on a single filament and ensures that the test is not perturbed by transient vibrations originating outside the test procedure.

For fatigue tests, a cyclic load, induced by the imposed cyclic deformation, is superimposed on a steady load and the maximum load is maintained constant with an automatic compensation for elongation due to creep or plastic deformation. The measured maximum load is continuously compared, by the servo-mechanism, to the required load level which is maintained constant to within 0.1 g ($9.81*10^{-4}$ N). The apparatus can be used from 0 up to 100 g ($9.81*10^{-1}$ N), with a precision of 0.01 g ($9.81*10^{-5}$ N), a maximum displacement of 20 mm with a precision of 1 μm and a cyclic displacement, at 50 Hz, which is within the range of interest for tyre applications, of up to ±3 mm. A PC linked to the fibre tester via a National Instrument Interface Card and ATS software from Sysma is used for data acquisition. The gauge length used in all mechanical tests is 30 mm.

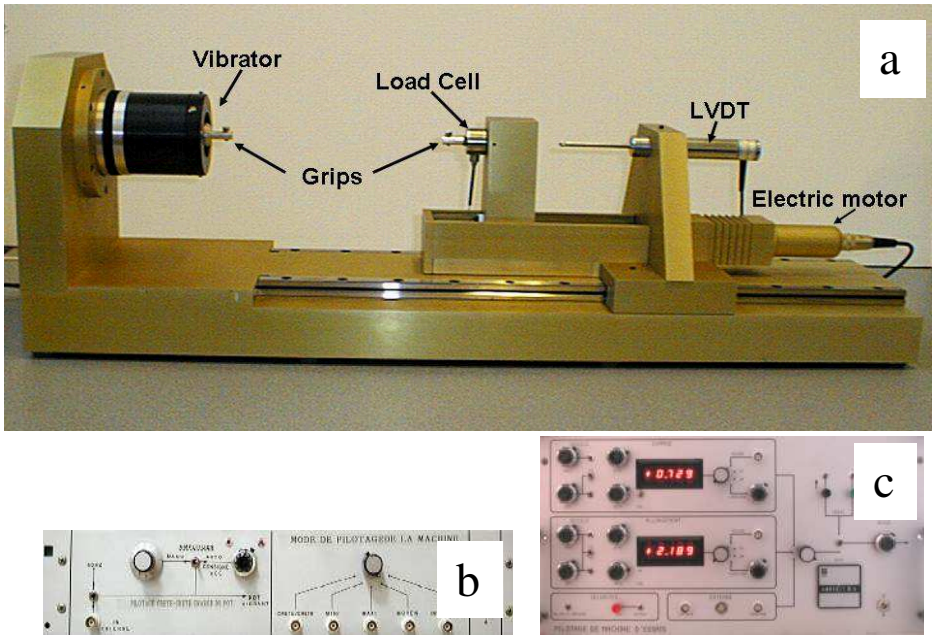

Figure 2.3: (a) Universal Fibre Tester, (b) Vibrator controls, (c) Machine controls.

Transmission optical microscopy (OM)

The main interest of transmission optical microscopy (OM) comes from the transparency of thick samples of polymers such as polyester or polyamide. A microscope Leica equipped with a Nikon digital camera coupled with the Leica im1000 software has been used in this thesis. Several objectives with magnifications from 20 to 100 xs are used. Monofilaments are held between a slide and a cover glass and are immersed in a mineral oil with a refractive index of 1.515, close to that of the polymer refractive index, in order to avoid optical reflection and refraction at the curved surface of the filament. In the best optical conditions, the optical resolution was better than 0.4µm.

Scanning Electron Microscope (SEM)

The scanning electron microscope (SEM) is used to study the surfaces of filaments, the fracture surface and for measuring the diameters of the filaments. The use of SEM for the study of organic fibre allows a better understanding of the mechanisms of deformation and damage of filaments after a mechanical stress.

Hearle et al.[58] are the first to use scanning electron microscopy for observe the tensile and fatigue fracture surface. Based on their observations, the different failure mechanisms of fibre have been identified and classified.[59-61]

However, the major drawback of using scanning electron microscopy to characterize polymers is the sensitivity of such materials to superheat, combined with their non-conductive. With a classic thermionic SEM, it is necessary to work with accelerating voltages of the order of tens of kV, to obtain an image with a suitable signal to noise ratio. Strong metallization of the material is essential to the expansion of the detail of observation.

Instead, with a field effect SEM a very low accelerating voltage can be obtained, with a very small electron beam, which greatly reduces the risk of damaging the samples and lead to excellent observation.

In this thesis a Zeiss Gemini 982 microscope equipped with a digital field emission gun is used. This microscope can operate at accelerating voltages below 1 kV.

The accuracy measurement of the images is of the order of percent. For this reason, the SEM is also used to calibrate the laser used to measure filaments diameters.

For SEM observation, samples are plated by applying a layer of gold-palladium of 2.5 nm, using a spray generation (Cressington 208HR) under

high vacuum, allowing a controlled deposition of uniform thickness over the entire surface of the samples. An acceleration tension of 3 kV is applied, but in some cases it is decreased to 1kV to avoid field effects on the samples. A working distance of 4 mm is maintained in most observations. The secondary electron signal is mostly used.

2.3 Results and discussion

Three kind of PET single filaments (called as PET-A, PET-B and PET-C) extracted from technical yarn produced by different companies have been tested.

During the manufacturing process, the fibres may be subject to several sources damage. Therefore, a careful analysis of the monofilaments surface, before they are tested mechanically, is essential. The presence of defects and heterogeneities, in fact, can cause stress leading to the initiation and propagation of cracks. It is important to determine the existence of initial defects in order to distinguish the real contribute of mechanical stress on the initiation and propagation of the crack.

The surface of PET-A, PET-B and PET-C samples is studied using a scanning electron microscope. SEM observations are conducted on several samples with a length of about 20 cm, cut into pieces and placed on an aluminium support. SEM images of PET samples are shown in Figure 2.4.

The surface of all PET filaments seems quite smooth with only few visible defects due to the manufacturing process of fibre (Figure 2.4).

SEM observations obtained are also useful to calibrate the laser device used to measure filaments diameters.

In table 2.1 the average diameters (<d>) of PET-A, PET-B and PET-C samples obtained by a Mitutoyo Laser (see figure 2.2), after calibration with SEM results, are reported. PET-A filaments have an average diameter of 20.5 μm, while as regards PET-B and PET-C has 23.3 and 21.1 μm respectively. The accuracy of these measures is 0.1 μm.

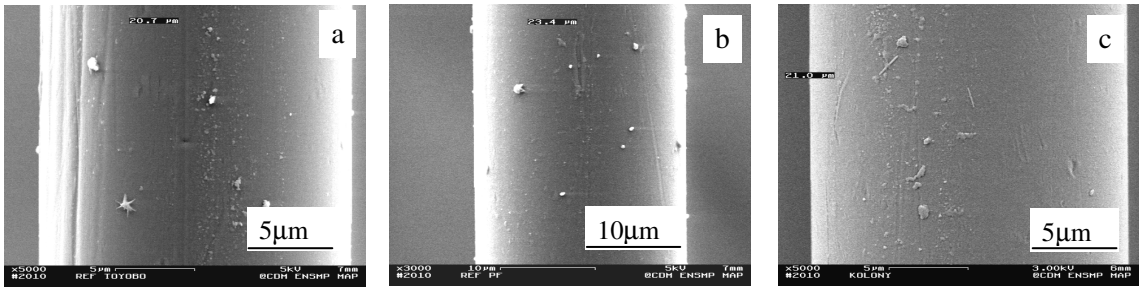

PET-A PET-B PET-C

Figure 2.4: Micrographs of PET samples surfaces: (a) PET-A, (b) PET-B, (c) PET-C

Table 2.1: Average diameters <d> of PET-A, PET-B and PET-C samples

Samples	PET-A	PET-B	PET-C
Number of measures	50	50	50
Average diameter <d> (µm)	20.5 ± 0.1	23.3 ± 0.1	21.2 ± 0.1

Tensile tests

Tensile tests are performed on the three different types of samples. A gauge length l_0 of 30mm and a strain rate of 1%/s are used. A uniaxial tensile test on single filaments allows the determination of mechanical properties such as stress and strain at break and Young's modulus.

The nominal stress at break σ_r is obtained by dividing the breaking load F_r for the initial section S_0 of the filament:

$$\sigma_r = \frac{F_r}{S_0}$$

Assuming that the section of filaments is perfectly circular, the initial section S_0 is:

$$S_0 = \pi \cdot \left(\frac{d}{2} \right)^2$$

Where d is the diameter of the single filament obtained by the laser device.

The strain at break ε_r is obtained by dividing the total elongation Δl by the gauge length l_0 of the filament:

$$\varepsilon_r = \frac{\Delta l}{l_0}$$

The value of Young modulus *E* is obtained, instead, by determining the initial slope of the curve stress/strain.

Figure 2.5 shows the typical stress/strain curves of the filaments. The values of initial module of the filaments as well as their elongation and stress at break are similar for the samples PET-A, PET-B and PET-C. The values of mechanical parameters, evaluated from the stress-strain curves of Figure 2.5, are shown in Table 2.2.

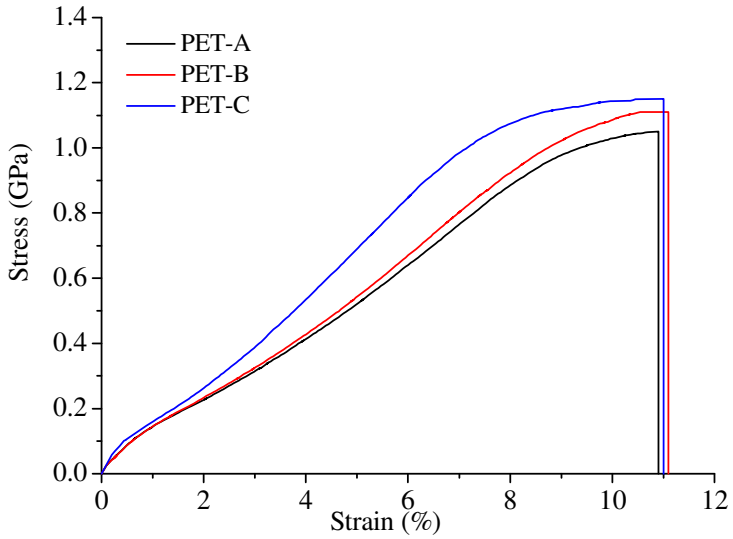

Figure 2.5: The stress-strain curves of the three types of filaments tested: (-) PET-A, (-) PET-B, (-) PET-C

Table 2.2: Young Modulus (*E*) and average values of stress and strain at yeld (σ_y e ε_y) and at break (σ_b e ε_b) of PET-A, PET-B and PET-C samples.

Samples	*E* (GPa)	σ_y (GPa)	ε_y (%)	σ_b (GPa)	ε_b (%)
PET-A	16.9 ± 2.6	0.12 ± 0.01	0.8 ± 0.1	1.05 ± 0.05	10.9 ± 0.6
PET-B	16.8 ± 0.9	0.12 ± 0.01	0.8 ± 0.1	1.11 ± 0.04	11.1 ± 0.8
PET-C	19 ± 1	0.12 ± 0.01	0.6 ± 0.1	1.15 ± 0.06	11.0 ± 0.6

The fracture morphologies of single filaments broken in tension and observed by SEM are shown in Figure 2.6. A two-phase propagation process can be seen; a region of low speed crack propagation, associated with a plastic deformation ahead of the crack tip and, then, a rapid crack propagation perpendicular to the axis. There are not morphological

differences between the tensile fracture surfaces of the PET-A, PET-B and PET-C samples.

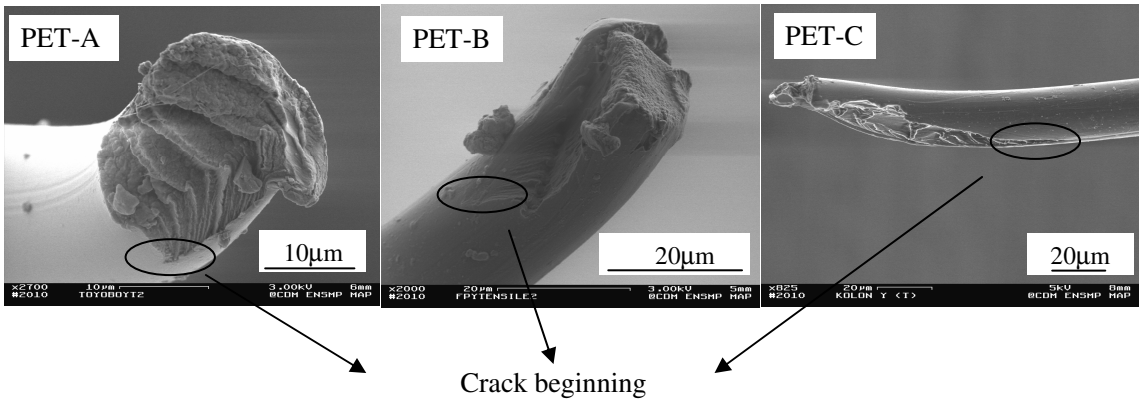

Figure 2.6: Tensile failure morphologies for PET-A, PET-B and PET-C samples.

Fatigue tests

In material science, fatigue is the progressive and localized structural damage that occurs when a material is subjected to cyclic loading.[54]

There are three different ways to conduct a fatigue test[62,63]:
1. The simplest of them is to submit a sample to a cyclic deformation with constant amplitude (Figure 2.7a). The material is inelastic so there is a residual elongation which increases with each cycle, leading to a decrease in the load. In this test the fibre either fails in the first cycle or not at all as the maximum loading levels quickly fall.

2. Another test, designed to avoid the accumulation of plastic deformation, is the cumulative extension cycling (Figure 2.7b). In this test the fibre is held vertically and the plastic deformation produced each strain cycle is removed by opening the bottom grip. A small weight is attached to the bottom end of the fibre and holds it stretched. The grip is closed and the fibre is subjected to another strain cycle. This means that the volume of fibre being tested is progressively decreased so that, although the maximum displacement imposed does not change, the fibre is taken progressively up its stress-strain curve.
With this second type of test, the fibre fails but it can never be clear if the break is due to a fatigue process or just because the end of the stress strain curve has been reached.

3. The third and optimal way of conducting a fatigue test is to apply the maximum load cycling technique. This test has revealed the fatigue process in organic fibres.[64] In this test, the maximum cyclic load on fibre is monitored and maintained constant.[65]

The Universal Fibre Tester machine is capable of adapting the loading conditions on the fibre gradually as it creeps and deforms plastically, as shown in Figure 2.7c. The fibre continue to deform by creep but, during the fatigue test, the fibre is subjected to the maximum load for only a brief part of the cycle, so a failure by creep would be expected to occur after longer times than that observed if the maximum cyclic load is applied constantly.

This third way of conducting fatigue test is applied in this PhD thesis.

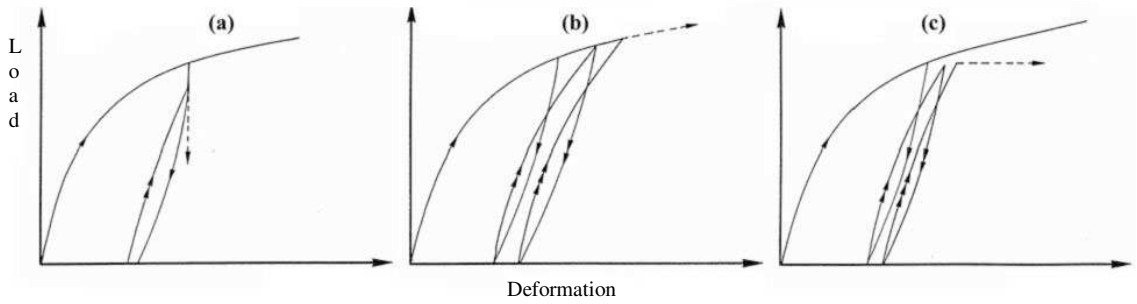

Figure 2.7: Three ways of conducting fatigue tests on fibres: (a) simple extension cycling; (b) cumulative extension cycling; (c) load cycling.[62,63]

Fatigue tests are carried out with a zero minimum load and a maximum load variable from 60% to 80% of the tensile nominal stress at break σ_r obtained by tensile tests. The experiments are performed at 50 Hz, which is within the range of interest for tyre applications. A resume of fatigue tests results is reported in table 2.3.

The fatigue tests indicate that PET-A and PET-C samples do not show break in fatigue, while, only one of PET-B filaments break by fatigue (tests performed over at least 20 specimens). In these experiments a break by fatigue is considered significant only if the filaments break outside the grips, within the gauge length. Several tests, indeed, end up with the

filaments breaking inside the grips. This rupture (inside the grips) is quite common in fatigue tests as loads and the numbers of cycles are increased.

Filaments which have failed outside of the grips are usually found to have failed by tensile or creep and show the classical tensile or creep failure morphology when are inspected by SEM.

Fatigue failure morphology, in fact, is quite different from the similar creep and tensile failure morphologies; it presents a characteristic tongue as shown in the SEM image of a PET-B filament in the Figure 2.8.

As a result of fatigue tests, it seems that all PET samples show improved fatigue properties compared to PET fibres produced by an old technology.[66]

Table 2.3: Results of fatigue tests performed to different percentage of monotonic tensile stress at break σ_r.

SAMPLES	Number of filaments tested				Number of filaments break out of grips				Number of filaments break in fatigure			
	80% of σ_b	70% of σ_b	65% of σ_b	60% of σ_b	80% of σ_b	70% of σ_b	65% of σ_b	60% of σ_b	80% of σ_b	70% of σ_b	65% of σ_b	60% of σ_b
PET-A	20	31	4	1	3	2	none	none	none	none	no test	no test
PET-B	20	10	no test	13	3	2	no test	none	none	1	no test	no test
PET-C	no test	20	no test	no test	no test	1	no test	no test	no test	none	no test	no test

Samples	Filaments break in grips (%)	Filaments break out of grips (%)	Filaments break in fatigue (%)
PET-A	91	9	none
PET-B	88	12	2
PET-C	95	5	none

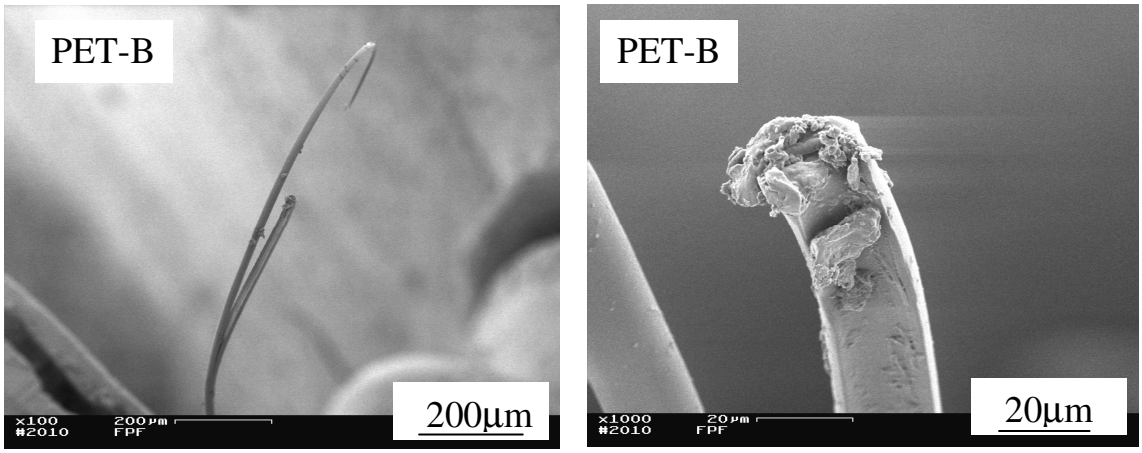

Figure 2.8: Fatigue failure morphology for PET-B sample.

Creep tests

Creep tests are carried out by applying a constant load to a specimen and observing the increase in strain with time.

In this thesis, because of shortage of time, only PET-A and PET-B samples are tested and compared. Creep tests are limited to twenty four hours and the load applied is 80% of tensile stress at break σ_r for each filament.

In figure 2.9a,b creep results are shown as an accumulative failure diagram for PET-A samples (Figure 2.9a) and for PET-B samples (Figure 2.9b). The dotted lines show the median life times, that is the time required for half of the filaments to break, and their values are given in table 2.4.

Creep tests indicate that although there are little difference in tensile strength and initial stiffness (see Figure 2.5 and table 2.2), the PET-A samples fair much better in creep than PET-B samples. In fact, 79% of the PET-B filaments are failed within the twenty four hours period, but, in the same period, only 50% of PET-A fibres is failed.

A resume of creep tests results is reported in table 2.5.

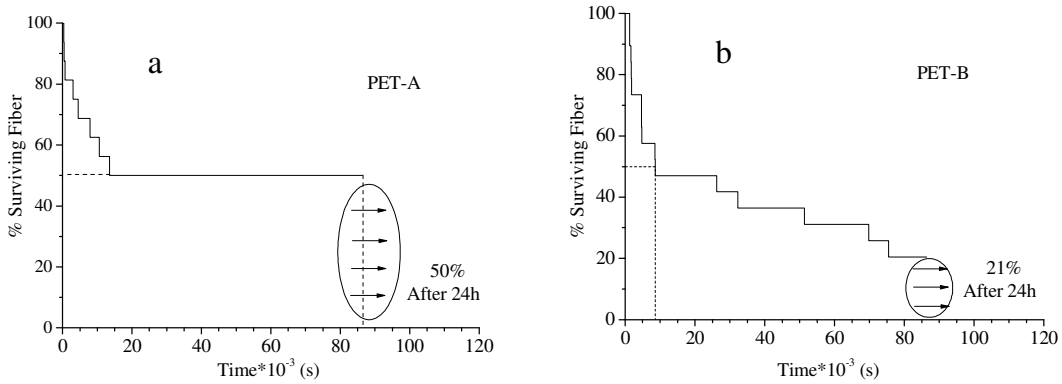

Figure 2.9: Accumulative failure curves for (a) PET-A filaments and (b) PET-B filaments subjected to a loading of 80% of tensile stress at break σ_r.

Table2.4: Median life time of PET-A and PET-B filaments.

Samples	Number of filaments tested	Median life time (h)
PET-A	16	≥24
PET-B	19	2.37

Table 2.5: Results of creep tests performed to 80% of tensile stress at break σ_r.

Samples	Number of filaments tested	Filaments break out of grips in 24h	Filaments no break in 24h
	80% of σ_b	80% of σ_b	80% of σ_b
PET-A	16	8	8
PET-B	19	15	4

Samples	Filaments break in 24h (%)	Filaments no break in 24h (%)
PET-A	50	50
PET-B	79	21

Creep fracture morphologies for both samples are similar and resemble very closely simple tensile fracture morphologies, as is shown in Figure 2.10.

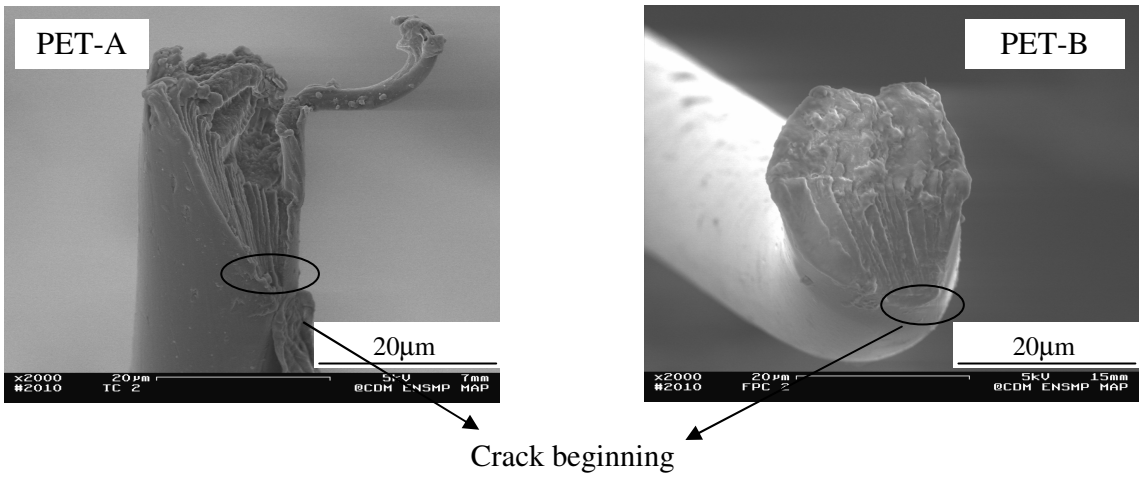

Figure 2.10: Creep failure morphology for PET-A and PET-B samples.

Analysis of creep results: Mechanism of fatigue failure to explain creep failure

Creep tests indicate that although there are little difference in tensile strength and initial stiffness, the PET-A samples fair much better in creep than PET-B samples. In order to explain this result we need to understand the mechanism underlying creep failure. This mechanism can be understood taking into account the mechanism of fatigue failure, and, in particular, assuming that the two mechanisms are practically equal.

It has been observed that fatigue fracture is usually initiated by the presence of foreign particles in the fibres.[67]

In Figure 2.11 optical micrographs, looking down on the fatigue fracture surface of a PET filament are shown.[67] The main fatigue tongue has been removed from the upper left side and a remaining part of that

tongue can be seen on the upper side in the Figure 2.11a,b. Near to one extremity of that tongue, there is an inclusion visible, around 2 µm from the filament surface. An observation of the zone near the inclusion, with polarized light (Figure 2.11c), underlines the perturbations induced by the inclusion in the surrounding polymer. In this and other similar cases, the particle sizes are found to be around 1 µm or less and near the failure surface, so that the association of crack initiation with inclusions seems to be established.

SEM observations in the region of crack initiation, together with Energy-dispersive X-ray spectroscopy (EDS X-ray) mapping of filaments failed in fatigue, have allowed some inclusions to be observed and identified.[67] The nature of these particles in PET samples is attributable to antimony, in particle form, that is used as a catalyst for PET fibres production, and/or to sub-micron TiO_2 particles that can be included to modify the strain-induced crystallisation of the highly stretched polymer. [67,68]

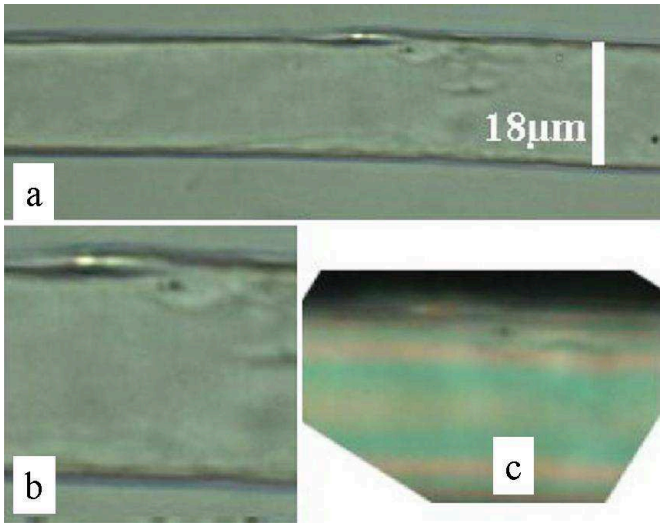

Figure 2.11: Optical microscopy observations with natural light (a,b) of a PET filament failed by fatigue. The tongue is removed from the top left side of the fibre. The final image c is taken with polarized light.[67]

In the Figure 2.12 four optical microscopy images of a microtomized PET filament failed by fatigue are shown.[67]

The first image (Figure 2.12a) is taken under polarized light and reveals the presence of a skin/core structure. In fact, under polarized light, there is a change of birefringence between two zones; the colour of the skin, which is on the side of the fibre section, is different from that of the core. This separation appears at around 1-2 μm from the filament surface. This skin/core structure probably appears during the crystallization of the molten polymer during spinning; the skin seems to result from the plastic deformation of the just crystallized polymer under elongation whilst the core crystallizes subsequently, under or just after flow. The higher orientation induced by plastic deformation seems to be the origin of this skin and of the discontinuity of birefringence along the radius.

The skin has different micro-structural properties from those of the core, so the interface between skin and core is a zone of residual stress that causes a weakening of the filament structure.

From the images collected under natural light, in Figure 2.12b,c,d, is clear that the fatigue failure begins at interface between skin/core and propagates within the filament.

On the basis of these results, it has been clearly demonstrated that the combined effects of a weak interface between skin/core structure and a particle increasing shear stress, in this already weak zone, produces fatigue crack initiation in PET filaments.[67]

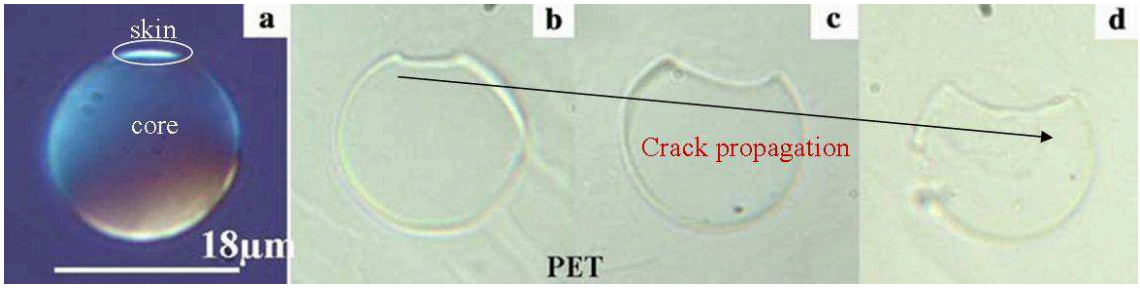

Figure 2.12: Optical microscopy of sections of a PET filament failed by fatigue. The first image (a) is collected under polarisation to reveal a change of birefringence; the three others (b–d) are collected with natural light.[67]

The theory of fatigue failure is assumed to be valid also for the rupture in creep. The particles included in the PET filaments play a crucial role in fatigue crack[67], therefore, it has been hypothesized that the same fundamental role is played in the creep.

As consequence, in order to explain our creep results, we have analyzed, by optical microscopy (OM), if the number of particles in a given length of PET-A and PET-B samples could affect the creep failure of the filaments.

OM analysis shows that PET-A filaments have only a quarter of the number of particles per unit length (μ) as the PET-B filaments, and this clearly justifies the result that PET-A samples fair much better in creep than PET-B samples (Figure 2.9 and Table 2.4). Figure 2.13 shows OM observations made on both filaments.

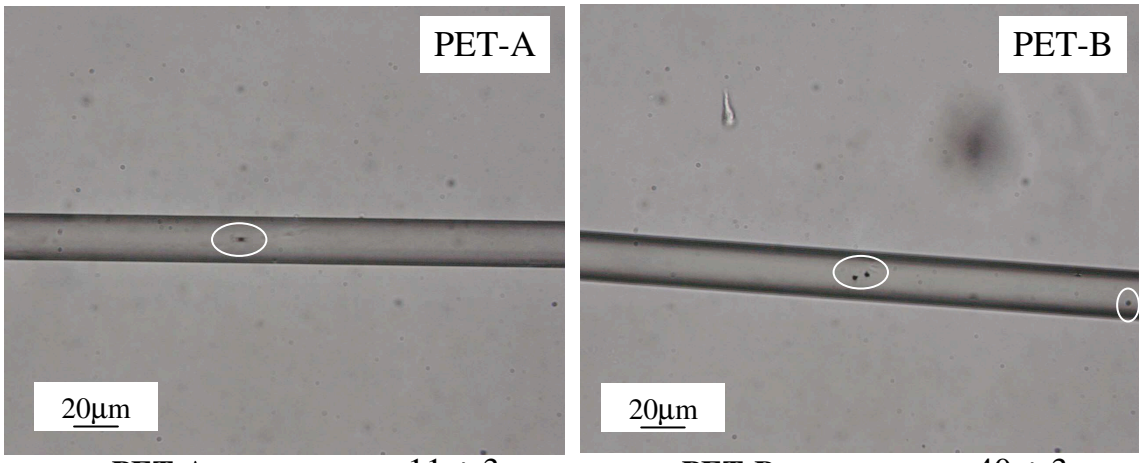

PET-A $\mu_{(N.\ particles/cm)} = 11 \pm 3$ **PET-B** $\mu_{(N.\ particles/cm)} = 40 \pm 3$

Figure 2.13: Optical microscopy (OM) images of the PET-A and PET-B filaments. In white circles we can see the particles. PET-B filaments are seen to have approximately four times the number of particles as the PET-A filaments.

In figure 2.14 optical microscopy images of the region of creep crack initiation in a PET-A filament are shown.

The images reveal the presence of a particle near the failure surface, so the hypothesis that particles play a role not only in fatigue failure but also in creep failure is well verified.

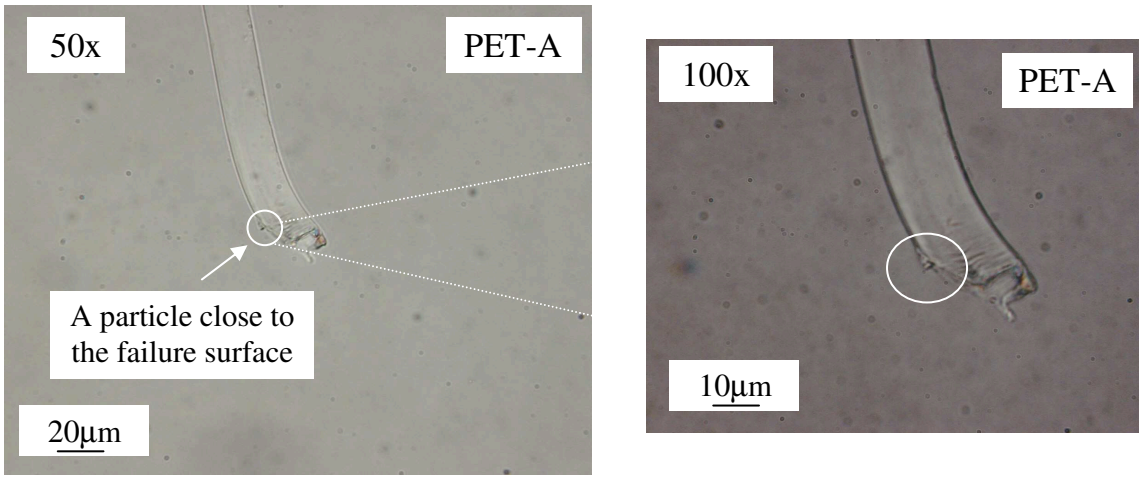

Figure 2.14: OM images of a PET-A filament which have failed in creep. The presence of a particle near the region of crack initiation is revealed.

2.4 Conclusions

A mechanical characterization of monofilaments (PET-A, PET-B and PET-C samples) extracted from PET fibres produced by three different companies have been performed. The filaments show similar tensile properties. All PET samples show unusual breaking in fatigue which reinforces the observation that recent changes in fibres processing have improved tensile fatigue strength of produced fibres. In fact, the tested filaments show great resistance and some of them could be subjected to fatigue tests lasting several hours without failure.

The results of creep tests indicate that failure is initiated not only by fatigue but also by creep in presence of foreign particles placed at the interface between the fibre skin and its core. PET-A samples fair much better in creep than PET-B samples, and an OM analysis shows that the PET-A filaments have only a quarter of the number of particles per unit length (μ) as the PET-B filaments.

On the basis of this study, PET-A fibres have the best mechanical properties and could be subjected to a dipping process and used in a tyre.

Chapter 3

Study of the mechanism of interaction between RF and Latex

3.1 Introduction

Rubber articles such as tyre, hoses and belts are composite materials. They are made using various natural and synthetic rubbers reinforced with different materials such as fibres and other reinforcing fillers. Whit an increasing demand for the longer lasting high performance products, constant improvements are needed in the reinforcing and elastomeric materials.

In the case of tyre applications, higher strength reinforcements can allow the construction of thinner carcass which in turn can reduce the heat build up and enhance the fatigue resistance in the final products. These requirements have resulted in the development of high tenacity fibres such as nylon, polyester and aramid for the reinforcement of tyres.

In general, synthetic fibres have the difficulty of adhering to rubbers because of their smooth surfaces and low reactivity. The low fibre surface activity is due to lower polarity and reactivity of the polymer molecules. Therefore an establishment of physical and/or chemical bonding between fibre and rubber is considerably reduced. Since a direct bond can not be established between the rubber and fibre, an adhesive which can promote the adhesion between these two is necessary.

The first adhesive system developed for rayon, a bland of casein and natural rubber Latex, gives acceptable levels of adhesion for rayon with rubber compounds.

The introduction of synthetic fibres as reinforcements in rubber composites identified the need for an improved adhesives and adhesion promoters for the enhancement of strength between rubbers and fibres.

An improved adhesion requirement for tyre have led to the development of Resorcinol (R)- Formaldehyde (F)- Latex (L) adhesives (RFL-DIP).[16]

Even today it is unclear the precise mechanism by which the RFL-DIP solutions act and, in particular, the role of the Resorcinol-Formaldehyde resin (RF resin) and Latex in ensuring the high performance of a tyre.

The study illustrated in this chapter is centred on the characterization of resorcinol-formaldehyde-Latex (RFL-DIP) adhesives used for tyre application. The aim is to understand the mechanism of interaction between RF resin and Latex by using techniques like Optical microscopy, Raman and Fourier transform infrared (FTIR) spectroscopy.

3.2 Materials and methods

Materials: RFL-DIP production

The ingredients for RFL-DIP solution preparation are materials available on commercial scale. The features of each one are listed below:

- Resorcinol: commercially available in flake shape from INDSPEC;
- Formaldehyde: solution at 37% in water from Sigma Aldrich;
- NaOH: solid pellets from Carlo Erba Reagenti;
- Latex: aqueous dispersion (40-42%) of vinylpyridine (10%) - butadiene (68%) - styrene (22%) copolymer from Polymer Latex.

The RFL-DIP systems can be complex, and many different formulations have been developed to fulfil the needs for various applications. The preparation of a RFL-DIP solution takes place in two stages.

First, an aqueous solution of resorcinol and formaldehyde is matured at room temperature in presence of sodium hydroxide as catalyst. During the maturation process, some degree of condensation takes place.

Second, the RF resin solution is added to a mixture of Latex and water. The components ratio can be varied to achieve the desired RFL-DIP system.

First stage*: *Resorcinol-Formaldehyde Reaction Chemistry

A typical procedure to prepare Resorcinol-Formaldehyde resin (RF resin) solution consists in two fundamental steps:

1. Add sodium hydroxide pellets into water at room temperature.
2. Blend the required amount of resorcinol and formaldehyde into the sodium hydroxide water solution.

In Figure 3.1 a scheme of the reaction between formaldehyde and resorcinol in basic environment is shown:

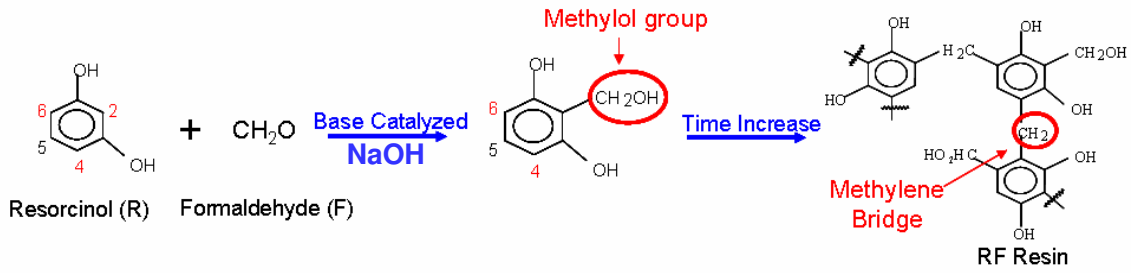

Figure 3.1: Scheme of the reaction between formaldehyde and resorcinol in a basic environment.

As it is illustrated in the figure 3.1, the base catalyzed reaction between resorcinol and formaldehyde lead to the substitution on resorcinol rings in C2, C4, C6 positions by methylol groups. By increasing the reaction time, the methylol groups react by condensation to give methylene bridges which create the typical tri-dimensional cross-linked structure of resorcinol-formaldehyde resins. Then, after reaching a sufficient cross-linked structure, the second stage of reaction can occurs.

Second stage: *RFL System or Final Formulation*

When RF solution has reached a certain level of aging, it can be added to a synthetic rubber Latex (L) solution for the final RFL-DIP formulation. This final solution can be used immediately but the adhesion is improved if the RFL-DIP is aged for at least 12h at 25°C.

The procedure described above has been used to prepare the RFL-DIP adhesives for this study, but the details of RFL-DIP systems preparation will not be reported for reasons of industrial secrecy.

A characterization of RFL-DIP samples in solid state has been performed and reported in this chapter. The aim is to understand the nature and the mechanism of interaction between Latex and RF resin. Solid samples of RFL-DIP are obtained from aqueous solution by casting, and are analyzed using techniques of Optical Microscopy, Raman and FTIR spectroscopy.

Methods

Transmission optical microscopy (OM)

The transmission optical microscope is a type of microscope which uses visible light and a system of lenses to magnify images of small samples.

The modern optical microscope used in this study is a Carl Zeiss Axioskop 40 with an integrated digital camera AxioCam MR, that provides good images and colour quality.

The RFL-DIP solution in liquid state is spread on a glass slide and dried to get solid films. These films are observed by optical microscope and

information about the homogeneous or heterogeneous nature of samples are obtained.

Raman microscopy

A confocal Raman microscope (Jasco, NRS-3100) is used to analyze RFL-DIP system in solid state. The 632.8 nm line of a He–Ne (25 mW) laser is injected into an integrated Olympus microscope and focused to a spot size of approximately 2 mm using a 20x objective. A holographic notch filter is used to reject the excitation laser line. The Raman backscattering is collected at 180° using a 0.1 slit and a 1200 grooves mm^{-1} grating, corresponding to an average spectral resolution of 4 cm^{-1}. It takes 200 s to collect a complete data set using a Peltier-cooled 1024 x 128 pixel CCD photon detector (Andor DU401BVI). Wavelength calibration is performed by using polystyrene and carbon tetrachloride as standards at high and low frequency, respectively.

Fourier transform infrared (FTIR) spectroscopy

FTIR spectroscopy is used to have a detailed analysis of RFL-DIP structure and to point out the possible physical and/or chemical interaction between RF resin and Latex.

The FTIR spectra of RFL-DIP samples are carried out at room temperature by a Jasco FTIR-430 system. The absorption spectra are recorded in the 4000–400 cm^{-1} wavelength range with a spectral resolution of 2 cm^{-1}. The spectrum of each sample represents an average of 64 scans, which is corrected for the spectrum of the air.

3.3 Results and discussions

The study of the interaction between RF resin and Latex in RFL-DIP adhesives is very difficult due to high complex structure of such system.

A previous study of this system shows that spectroscopic techniques, like Ultraviolet-Visible (UV-Vis) and ^{13}C-Nuclear Magnetic Resonance (^{13}C-NMR) in liquid state, are not useful. UV-Vis spectroscopy is not good due to the high overlapping of the absorption band caused by the presence of the Latex. ^{13}C-NMR spectroscopy, instead, is ineffective because of broad band observed in the spectra due again to the presence of Latex which is a solid suspension in water.[38]

In this thesis a study of the RFL-DIP system by Optical microscopy, Raman and FTIR spectroscopy helps to have an overview on the nature of the interaction among RF resin and Latex.

In figure 3.2a,b optical microscopy images of RF films, obtained by casting of a resorcinol-formaldehyde solution without Latex, are shown.

RF films are substantially homogeneous on micrometer scale. The visible black spots in Figure 3.2a are mainly due to impurities.

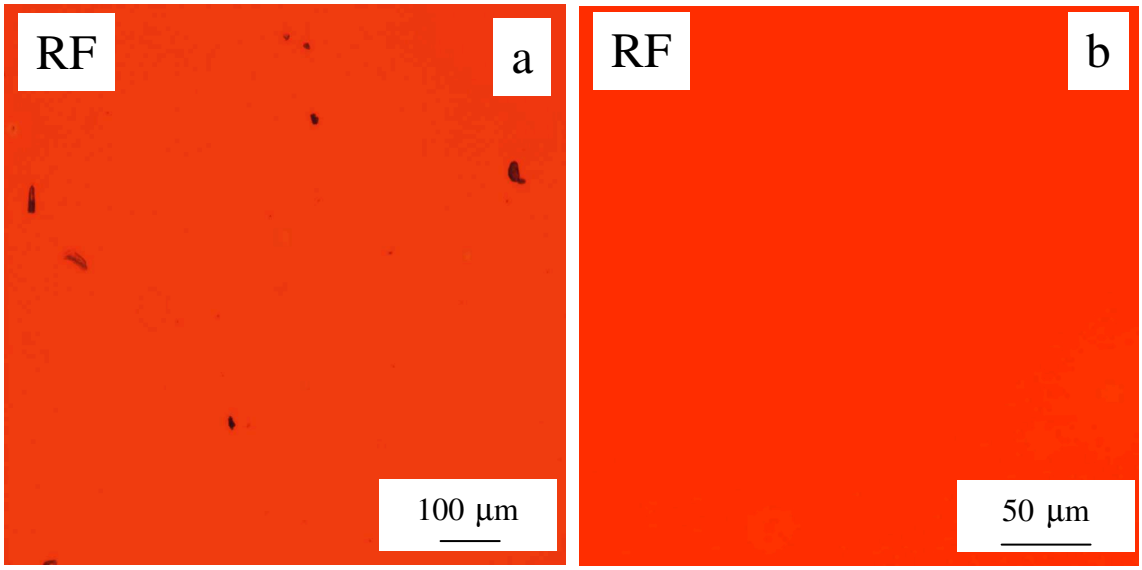

Figure 3.2: Optical microscopy images of RF resin films.

In figure 3.3a,b optical microscopy images of standard RFL films, obtained by casting of a RFL-DIP standard solution with F/R molar ratio = 1.75 and a content of Latex = 42w% of the total solution weight, are shown.

RFL films are heterogeneous on micrometer scale. A large number of black spots are visible in Figure 3.3a,b. This result indicates that a phase separation occurs in this system.

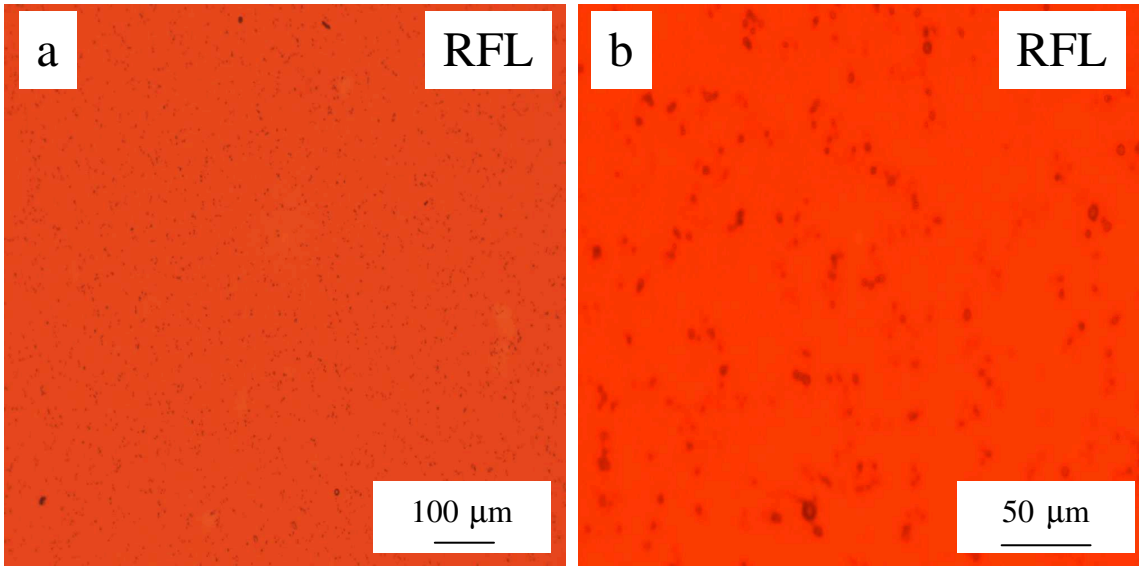

Figure 3.3: Optical microscopy images of RFL-DIP films.

The observation of a phase separation in RFL systems is certainly something never previously observed, and for this reason worthy to be clarified.

For this purpose, a study aimed to understand how the content of heterogeneities varies with the content of Latex has been performed.

In figure 3.4 a comparison of optical microscopy images of RFL films with different content of Latex: (a) 26w% (RFL-L26%), (b) 42w% (RFL-L42%) and 59w% (RFL-L59%) of the total RFL solution are shown.

In figure 3.4, it is possible to observe that heterogeneities decrease with increasing of the content of Latex.

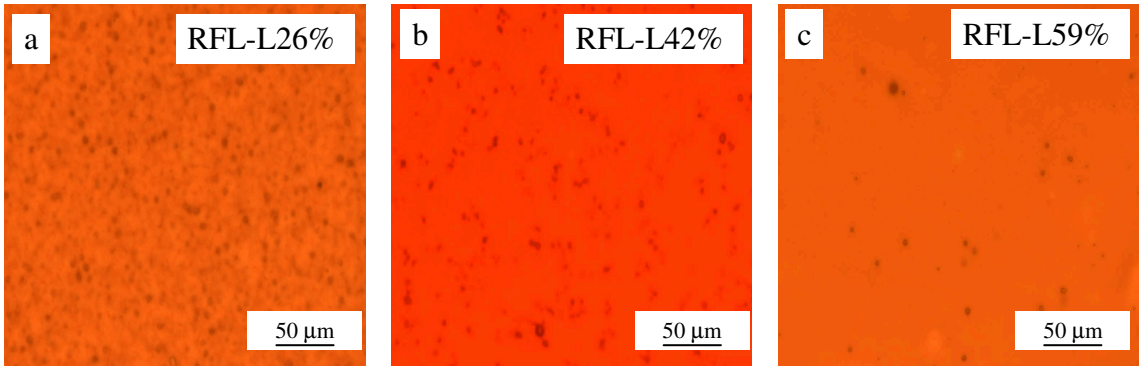

Figure 3.4: Optical microscopy images of RFL-DIP films with different content of Latex: (a) 26w%, (b) 42w% and (c) 59w% of the total RFL solution.

A quantitative analysis to establish the size and the concentration of heterogeneities in RFL samples with different content of Latex has been performed.

The number and size of the dark heterogeneities have been measured by ORMA Micro-image analyzer software assuming that the black spots are circular and independent.

Figure 3.5 shows the size distribution of the diameters of the heterogeneities obtained measuring more than 100 black spots of the RFL-L26%, RFL-L42% and RFL-L59% samples.

In the table 3.1 the average value of the diameter (<d>) for the RFL samples analyzed is reported. This value is approximately constant independently from the RFL samples considered.

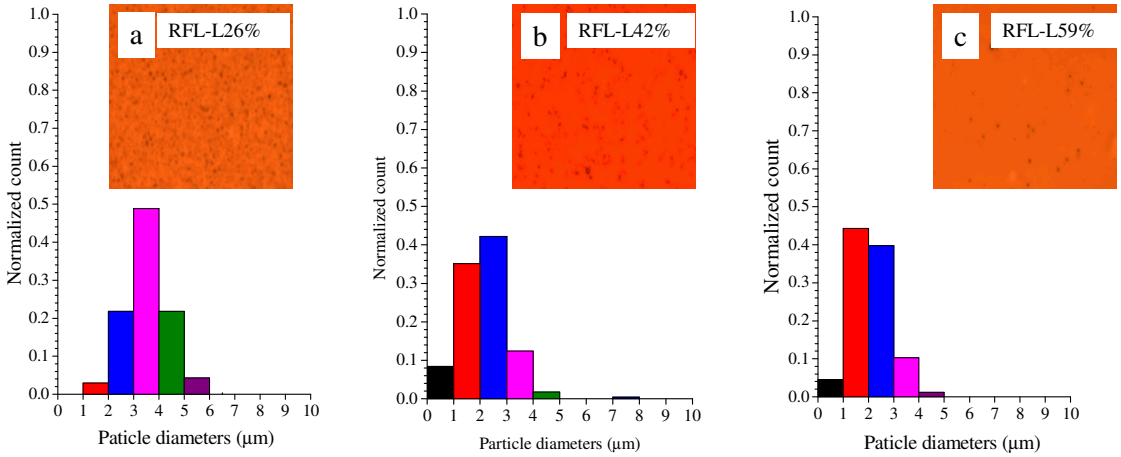

Figure 3.5: Size distribution of the diameters of the heterogeneities, obtained measuring more than 100 black spots of the RFL samples with different content of latex: (a) 26w%, (b) 42w% and (c) 59w% of the total RFL solution.

Table 3.1: Average value of diameter (<d>) for the RFL samples analyzed.

Samples	<d> (µm)
RFL-L26%	3.5 ± 0.8
RFL-L42%	2.3 ± 0.7
RFL-L59%	2.1 ± 0.7

The concentration of heterogeneities in RFL samples (RFL-L26%, RFL-L42% and RFL-L59%) has been evaluated. The calculus has been performed on 3 films of each RFL samples as follows.

For each RFL film four random zone of equal area (162.5 μm x 127.5 μm) have been selected. The number and average diameters of the dark heterogeneities in this selected area have been measured. The percentage of the total area filled by black spots, assuming that particles are circular and independent, has been obtained as follows:

$$\frac{\sum_{i=1}^{N} n_i \pi (R_i)^2}{A_f} \times 100$$

Where:

R_i = radius of black spot i

n_i = number of black spots with a diameter R_i

A_f = area of a selected zone (162.5 μm x 127.5 μm)

The total area filled by particles has been mediate over the four random zones and a standard deviation of ± 1 has been estimated.

Figure 3.6 shows the average area filled by black spots (<A>) as a function of the latex content. In table 3.2 the average values of the area filled by particles (<A>) for each RFL sample is reported.

The area decreases with increasing of the content of Latex, so it is quantitatively demonstrated that the increase of content of Latex lead to a decrease of the heterogeneities in the samples.

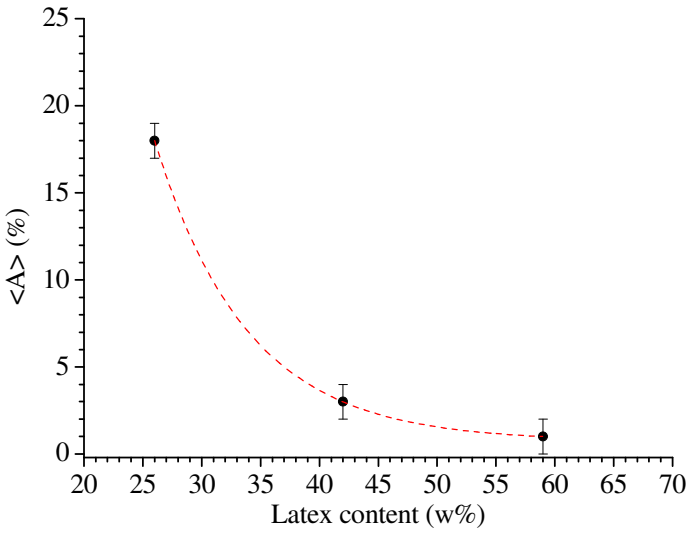

Figure 3.6: Average area <A> filled by black spots as a function of the content of Latex.

Table 3.2: Average values of the area filled by black particles (<A>) for each RFL sample analyzed.

Samples	<A> (%)
RFL-L26%	18 ± 1
RFL-L42%	3 ± 1
RFL-L59%	1 ± 1

To interpret the optical microscopy results reported above, a hypothesis has been advanced.

RFL system is a system in which the reactants resorcinol (R) and formaldehyde (F) are initially well mixed with the Latex dispersion (L). As the reaction proceeds, a phase separation occurs into a phase rich in Latex and in a phase rich in RF resin. This hypothesis is in agreement with a mechanism denominated Polymerization Induced Phase Separation (PIPS).[69]

On the basis of this hypothesis, the red matrixes of the RFL samples (Figure 3.2 and Figure 3.3) is considered substantially Latex, while the black spots, which decrease with increasing of the Latex content (Figure 3.3 and Figure 3.6), are essentially made of RF resin.

To confirm this hypothesis a study of the matrix and of the black spots in RFL films by Raman microscopy and FTIR spectroscopy has been done.

In figure 3.7 Raman spectra of the pure Latex (a) and RF resin (b), of the matrix (c) and black spot (d) of a standard RFL film (RFL-L42%) are reported. The spectra are shifted arbitrarily along the vertical axis.

The spectrum of the Latex (a) shows clear peaks at shifts of approximately 1700, 1400, 1300, 1200 and 1000 cm^{-1}.

The spectrum of the RF resin (a) is very noisy and shows some shoulders at approximately 600, and in the zone 1300-1600 cm^{-1}. The spectrum of the RFL matrix (c) is so noisy that is difficult to establish any correlation with the pure Latex and RF resin spectra; in fact, it does not show the Latex peaks or the resin shoulders clearly anymore. Finally, the spectrum of the RFL black spot (d) is also noisy but seems to reproduce the RF spectrum.

The results of Raman microscopy analysis seem to confirm the hypothesis that the heterogeneities observed by optical microscopy (Figure

3.3 and Figure 3.4) are mainly composed of resin, but the quality of the spectra is very low so the certainty of the result can not be clearly ensured.

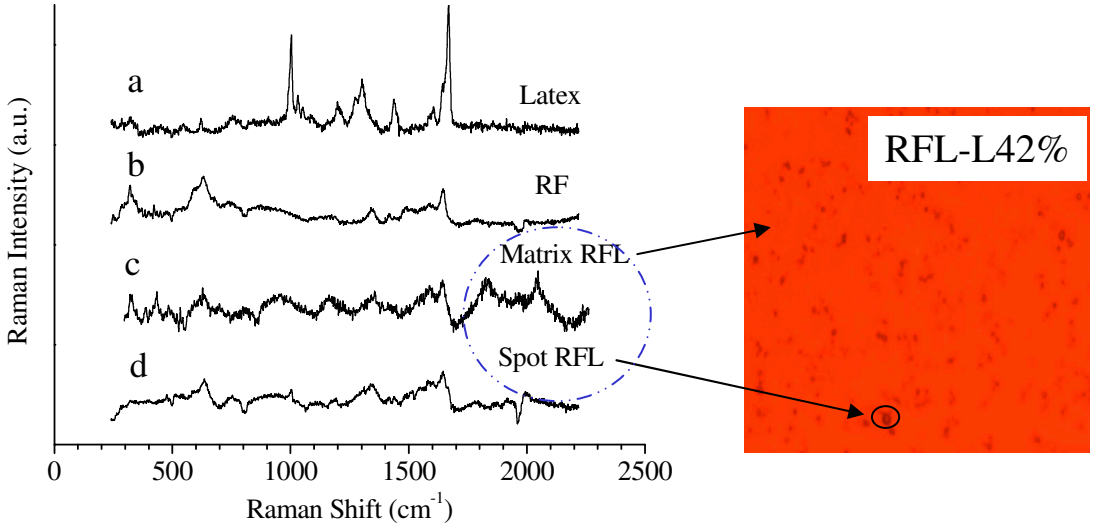

Figure 3.7: Raman spectra of the two pure components of RFL system: Latex (a) and RF resin (b), and of the matrix (c) and black spot (d) of a RFL standard film.

In order to receive more information about the matrix and the heterogeneities of RFL films and about the nature of interaction between RF resin and Latex, a further analysis is carried out using FTIR spectroscopy.

In Figure 3.8 FTIR spectra of the pure RF resin (a), Latex (b) and of a standard RFL film (RFL-L42%) (c) are reported.

RF resin spectrum (a) presents some distinctive peaks in the zone 1000-1600 cm^{-1} that are essentially due to the aromatic ring and a large shoulder in the zone 3200-3600 cm^{-1} that is due to hydrogen-bonded hydroxyl groups.[70]

The spectra of the pure Latex (b) and RFL (c) show a strong resemblance and have the same main peaks, which are assigned and reported in Table 3.3.[70-75]

The contribution of RF resin to the RFL spectrum can be observed in the large shoulder at 3200-3600 cm^{-1}, but is almost negligible compared to the Latex contribution. The analogy between Latex and RFL spectra is a clear indication that RFL system consists almost entirely of Latex.

This result is in agreement with the hypothesis that the matrix of RFL systems is essentially composed by Latex.

In addition, RFL spectrum shows no additional bands as effect of chemical reaction between Latex and RF resin and this suggests that the nature of the interaction among the components is solely physical.

In particular, the broad band in RFL spectrum at 3200-3600 cm^{-1} can suggest possible hydrogen bonds between hydroxyl-hydroxyl groups of RF resin and hydroxyl groups of RF resin and pyridine groups of Latex.[76]

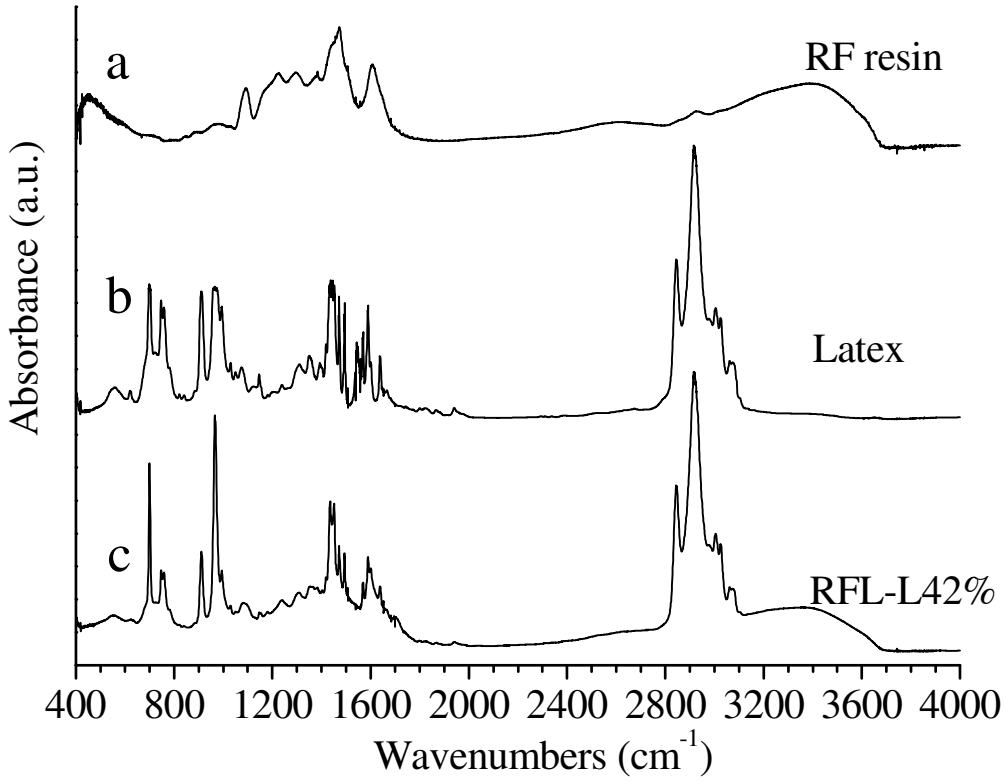

Figure 3.8: FTIR spectra of the pure RF resin (a), Latex (b) and of a standard RFL system RFL-L42% (c).

Table 3.3: Main vibrational groups in Latex and RFL samples.[70-75]

Vibrational groups	**Wavenumbers (cm^{-1})**
polystyrene group	700
cis-1,4 structure polybutadiene	746
polystyrene group	757
cis-1,2 structure polybutadiene	910
trans-1,4 structure polybutadiene	964
polystyrene and vinylpyridine group	1436-1447-1470-1490
vinylpyridine group	1569-1590
stretching CH group	2800-2900

A further study by FTIR spectroscopy has been conducted on RFL films to evaluate the effects of the content of Latex and of the temperature on the interaction between RF resin and Latex.

In figure 3.9 FTIR spectra of pure RF resin (a), of RFL films with a different content of Latex: RFL-L26% (b), RFL-L42% (c), RFL-L59% (d) and of pure Latex (e) are reported.

RFL spectra (b,c,d) do not show differences among themselves and with Latex spectrum (e). There are not additional bands as an evidence of a possible chemical reaction between RF resin and Latex.

In figure 3.9a-e, the intensity and the band center of hydrogen-bonded hydroxyl group (3200-3600 cm^{-1}) respectively decreases and slightly shifts with the increasing of latex content.

This result reflects a new distribution of hydrogen bonding in RFL samples with the hydroxyl-pyridine interactions favorites on hydroxyl-hydroxyl interactions with the increase of the content of Latex.[76]

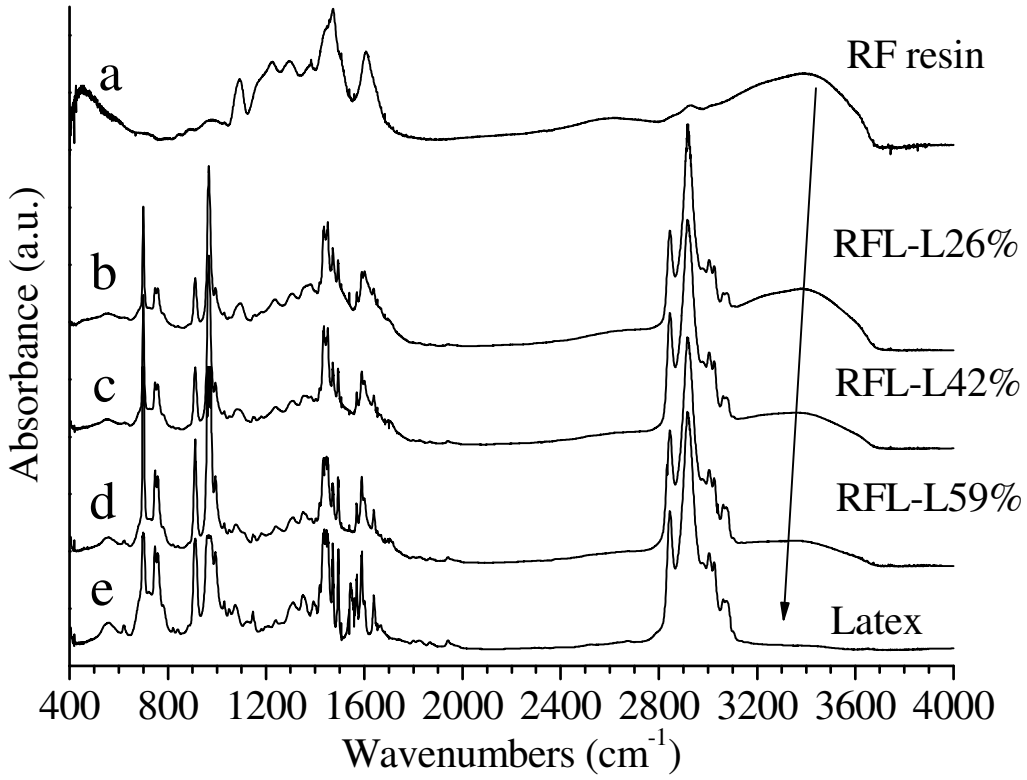

Figure 3.9: FTIR spectra of pure RF resin (a), of RFL films with a different content of Latex: RFL-L26% (b), RFL-L42% (c), RFL-L59% (d), and of pure Latex (e).

In figure 3.10 FTIR spectra of RFL films with a different content of Latex and cured at T=200°C for a day under a nitrogen flux (RFL-L26% (a), RFL-L42% (b), RFL-L59% (c)) are reported.

The temperature of 200°C is the temperature at which RFL system is approximately treated in a standard dipping process.

RFL spectra do not show differences between themselves, furthermore we do not have additional bands linked to chemical reaction between resin and Latex. This result indicates that interaction between RFL components is essentially physical even when the system is treated to temperature typical for an industrial dipping process.

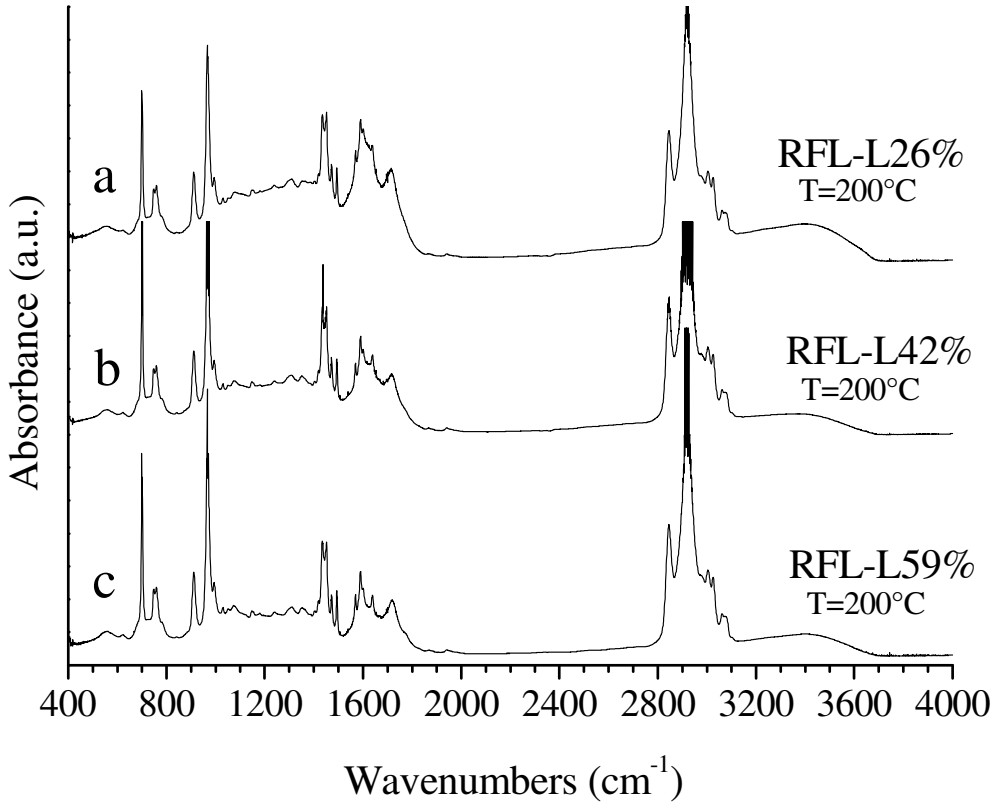

Figure 3.10: FTIR spectra of RFL films with different Latex content and cured at T=200°C for a day under a nitrogen flux: RFL-L26% (a), RFL-L42% (b), RFL-L59% (c).

3.4 Conclusion

In this chapter RFL-DIP systems in solid state are characterized in order to clarify the nature and mechanism of interaction between Latex and RF resin.

Solid samples of RFL, obtained by casting, are analyzed using techniques of Optical Microscopy (OM), Raman and Fourier transform infrared (FTIR) spectroscopy.

Optical microscopy shows, in line with the Polymer Induced Phase Separation (PIPS) mechanism, that these systems are heterogeneous on micrometer scale.

The concentration of such heterogeneities has been critically and dimensionally evaluated in RFL systems with different content in Latex. The concentration of the heterogeneities decreases with increasing of the content in Latex, for this we guess that these RFL systems are essentially made by RF resin particles dispersed in a latex matrix.

In order to confirm this hypothesis, the same systems are studied by Raman and FTIR spectroscopy. FTIR spectroscopy confirms that the matrix of the RFL systems is mainly Latex, while, Raman microscopy seems to confirm that the heterogeneity are substantially particles of RF resin.

FTIR spectroscopy analysis shows that the interaction between Latex and RF resin has a physical nature, even when RFL samples are cured at a typical dipping process temperature. The physical interactions could be mainly hydrogen bonds between hydroxyl groups of RF resin and pyridine groups of Latex.

Chapter 4

Study of the mechanism of interaction of the systems: RFL/reinforcing fibres and RFL/rubber

4.1 Introduction.

Although the RFL-treatment of tyre-cords has been invented in 1938 and since then has not changed, the exact mechanism of rubber to cord bonding through RFL adhesive is still unclear. There are numerous conflicting opinions concerning the nature of the fibre to rubber interactions, but only a few papers have tackled about this problem. It is generally recognized that there are two primary factors to be considered, i.e. the nature of the RFL to fibre interactions and the nature of the RFL to rubber interactions.[29]

The nature of fibre plays an important role in RFL treatment of tyre cords. In practice it has been recognized that Rayon and Nylon tyre-cords are easy to bond to rubber by RFL treatment, but with polyester cord this is extremely difficult. This should be attributed to the nature of polyester structures. Rayon and Nylon contain reactive groups such as hydroxyl group –OH and amide groups –CONH–. Polyester, instead, has a less reactive structure, and it has not groups able to form effective hydrogen bonds. The ability for hydrogen bonding of polyester indeed is lower than that of polyamide.[77]

There are many opinions on how RFL interacts with Rayon and Nylon: hydrogen bonding between phenolic hydroxyl groups in RF resin and electronegative groups in fibres,[77] condensation reaction between methylol group of RF resin and active hydrogen in the fibre,[31,78] molecular entanglements,[78] dipole-dipole interaction.[79]

Some results supports the chemical reaction theory between RFL and cords and some denies it suggesting that the nature of the interaction is only physical.

However, the evidence has been insufficient for any of these bonding mechanisms to give wide acceptance.

Also the mechanism of interaction between RFL and rubber is extremely complex. Many and controversial opinions have been presented to explain it: co-vulcanization of carbon-carbon double bonds in rubber,[32] chemical reaction between RF resin and rubber,[78] inter-diffusion between RFL and rubber,[80] ionic interaction.

The study illustrated in this chapter is focused on understanding the nature of the RFL to fibre interaction and nature of the RFL to rubber interaction. Raman, FT-IR/ATR, ^{13}C-NMR spectroscopy and mechanical and thermogravimetric (TGA) analysis are used to clarify RFL/Nylon interaction. FT-IR/ATR is instead used to clarify RFL/rubber interaction.

4.2 Materials and methods

Materials

The ingredients and the preparation procedure for RFL solution have already been reported in the paragraph 3.2 of the chapter 3. The samples of Nylon 6,6 and natural rubber (NR) used in this PhD activity have been supplied by Bridgestone Technical Centre Europe. The material specifications are omitted for reasons of industrial secrecy. Nylon 6,6 has been chosen because it is easy to bond to rubber by RFL treatment.[29]

The RFL/Nylon samples are prepared by immerge the fibres in the RFL solution for 30 seconds and then treating at 220°C to allow the solution to adhere to the cords. The temperature of 220°C is the temperature for a standard dipping process of Nylon cord.

The samples for the study of interface between RFL/rubber are prepared as follow. Nylon cords, covered by RFL solution, are included in a rubbery matrix of natural rubber. A vulcanization process occurs about at 160°C for 20 min and then the cords are extracted from the rubbery matrix. FT-IR/ATR analysis at the interface between the rubber residue on the cords and the RFL solution has been performed.

Methods

Raman microscopy

A confocal Raman microscope (Jasco, NRS-3100) is used to analyze the interface between RFL and Nylon fibres.

The specifications of the instrument have already been widely described in the paragraph 3.2 of the chapter 3.

Attenuated total reflectance (FT-IR/ATR) spectroscopy

Attenuated total reflectance (ATR) is a sampling technique, used in conjunction with an infrared spectroscopy (IR), which enables samples to be examined directly in the solid state.

FT-IR/ATR spectroscopy is used to point out the possible physical and/or chemical interaction between Nylon/RFL and RFL/rubber.

FT-IR/ATR spectra of samples are collected using a Thermo-Nicolet system equipped with a diamond crystal. The absorption spectra are recorded in a wavenumbers range of 400–4000cm-1 with a spectral resolution of 2 cm^{-1}. The spectrum of each sample represents an average of 64 scans, which is corrected for the spectrum of the air.

13C-Nuclear Magnetic Resonance (13C-NMR)

^{13}C-NMR spectra have been obtained by a Bruker 400 MHz spectrometer, and the operating parameters are listed below:

- Probe temperature = 25°C
- Pulse width = 4.30 μs (≈ 30°)
- Pulse delay = 1 sec
- Line broadening = 2 Hz

^{13}C-NMR spectra on Nylon samples are obtained using a procedure found in an article.[81] This procedure involves the use of two solvents, a 2,2,2-trifluoroethanol (TFE) to dissolve Nylon fibres and a deuterated chloroform ($CDCl_3$) to obtain a deuterium lock, in a ratio 4:1.

The number of scans is about 3000 in order to obtain a good signal-to-noise ratio.

Mechanical properties

The study of mechanical properties of Nylon samples has been performed by using a dynamometer Zwicki by Zwick Roell according to ASTM D 885M-85 procedure, which covers the testing of tyre cords, tyre cords fabrics and industrial filament yarns made from man-made organic base fibres.

The specimens of Nylon cords with a length of around 50 mm have been stretched by using a rate of crosshead travel in mm/s of 10% of the initial gauge length in millimeters of the specimen and applying a pretension load of 5 ± 1 mN/tex.

The Young modulus (expressed in N/tex) has been calculated according the equation:

$$E = (10 \times L) / K$$

Where:

L = load for 10% elongation (expressed in N), determined from the intersection point between the tangent to the initial straight-line portion of load-elongation curve and the line perpendicular to the abscissa corresponding to 10% of elongation.

K = nominal linear density (expressed in tex).

The nominal linear density for the samples analyzed is 280 tex.

The values of elongation at break (ε_b) and load at break ($Load_b$) have been determined in correspondence of specimen break.

The values reported for tensile properties represent the average of at least ten tests.

Thermogravimetric analysis (TGA)

Thermogravimetric analysis or thermal gravimetric analysis (TGA) is a type of testing performed on samples that determines changes in weight in relation to change in temperature.

TGA is commonly employed in research to determine characteristics of materials such as polymer (in this case Nylon), degradation temperatures, absorbed moisture content of materials, the level of inorganic and organic components in materials, decomposition points of solvents residues.

TGA spectra are obtained using a TA-SDT 2960 simultaneous DSC-TGA instrument under a flux of nitrogen. The spectra are collected in a range of temperature between 25-800°C.

4.3 Results and discussion

As already stated in the paragraph 4.1 of this chapter, the mechanism of interaction between RFL and reinforcing fibres, and RFL and rubber is extremely complex.[31,32,77-80]

The aim of this chapter is to understand the mechanism of these interactions by Raman, FT-IR/ATR, ^{13}C-NMR spectroscopy and mechanical and thermogravimetric (TGA) analysis.

The analysis has been divided in two parts:

1. Study of RFL/Nylon interaction.
2. Study of RFL/rubber interaction.

Study of RFL/Nylon interaction

According to the current literature[29,31,78] the interactions between RFL resin and reinforcing fibres have been explained postulating the formation of bonds between RF resin and reactive groups of fibres. In order to probe formation of such bonds we have used Raman microscopy.

In figure 4.1A,B Raman spectra of pure Nylon (a) and RF resin (b), and of a Nylon cord covered by RF resin and cured at 220°C (Nylon/RF) (c) are shown.

Raman spectra, performed in the range of frequencies 400-2200 cm^{-1}, are reported in Figure 4.1A. Nylon/RF spectrum is similar to pure RF spectrum. In Nylon/RF spectrum, nylon peaks[82] are completely covered by RF signals and this is due to RF absorbance that is ten times Nylon absorbance in this range of frequencies.

Raman analysis in this zone does not give information about chemical or physical interactions between Nylon and RF.

Raman spectra, performed in the range of frequencies 2500-4000 cm^{-1}, are reported in Figure 4.1B. The spectrum of RF appears very noisy. Nylon/RF and pure Nylon spectra, instead, are quite similar, but a difference must be emphasized. Nylon spectrum shows –NH group at 3300 cm^{-1}, while Nylon/RF spectrum seems to show a decrease of this peak (black circle in Figure 4.1B) and a formation of a new peak (red circle in Figure 4.1B) at a lower frequency of 3200 cm^{-1}.

This difference can be interpreted as a possible hydrogen bond involving Nylon amide group –CONH– and RF resin –OH group.[83]

However, the zone among 3000-3500 cm^{-1} in Nylon/RF spectrum is so noisy that it is impossible to reveal by Raman the nature of interaction between Nylon and RFL.

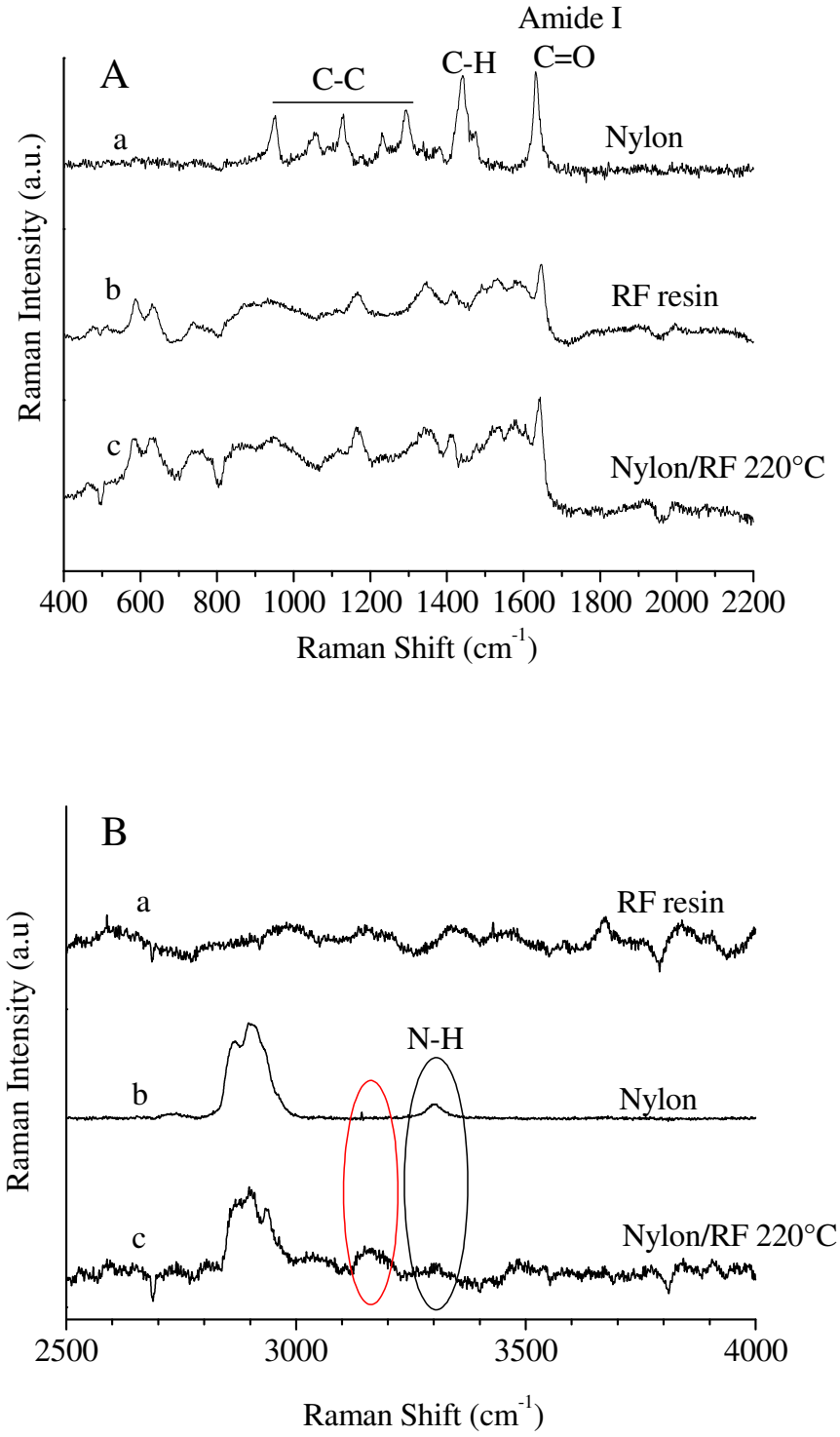

Figure 4.1: Raman spectra of pure Nylon and RF resin, and of a Nylon cord covered by RF resin and cured at 220°C (Nylon/RF): **A**) spectra collected in the range of frequencies 400-2200 cm^{-1}, **B**) spectra collected in the range of frequencies 2500-4000 cm^{-1}.

In order to obtain better information about the nature of interaction between RFL and Nylon fibres, a further analysis is carried out using FT-IR/ATR spectroscopy.

In Figure 4.2 ATR spectra of pure RF resin (a) and Nylon (b), and of a Nylon cord covered by RF resin and cured at 220°C (Nylon/RF) (c) are reported.

Nylon/RF spectrum is similar to pure Nylon spectrum, and does not show shift or additional bands as a result of a possible physical and/or chemical interaction between Nylon and RF resin.

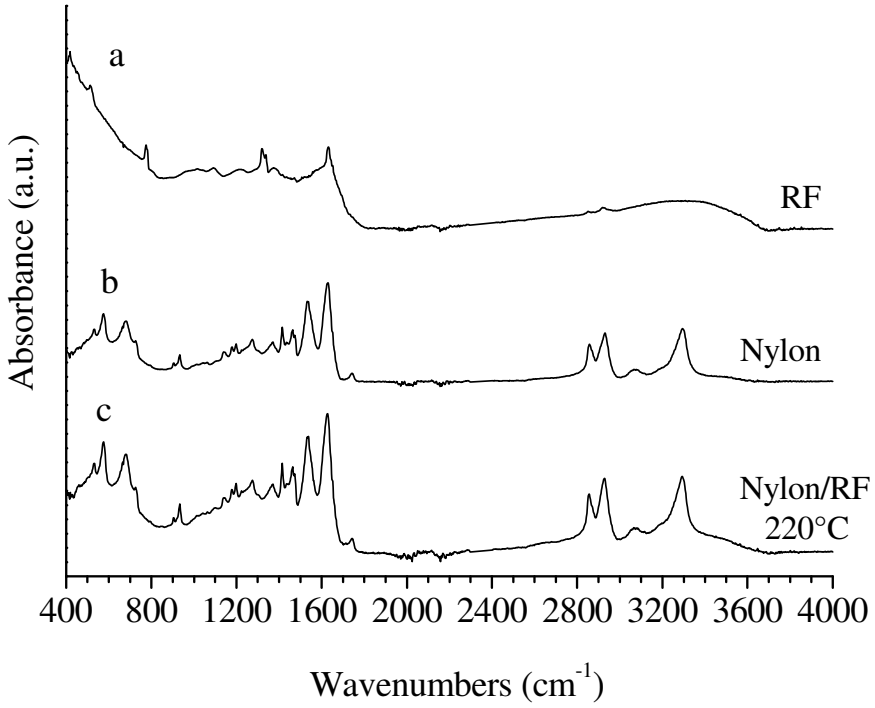

Figure 4.2: ATR spectra of pure RF resin (a) and Nylon (b), and of a Nylon cord covered by RF resin and cured at 220°C (Nylon/RF) (c).

A study of the behavior of the Nylon/RF system changing the curing temperature from 25°C to 230°C has been also made.

In particular, in Figure 4.3, ATR spectra of pure Nylon, and Nylon/RF systems cured at different temperature are reported.

There are not differences between the spectra of Nylon and Nylon/RF systems, and this result seems to confirm the absence of interaction between Nylon and RF at any temperature.

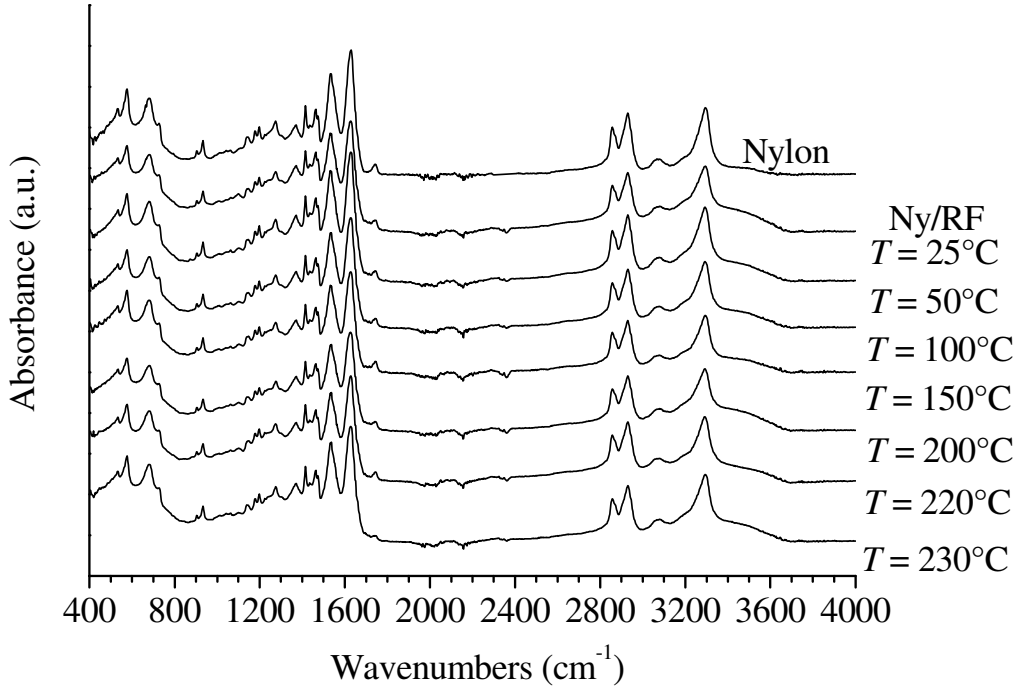

Figure 4.3: ATR spectra of pure Nylon and Nylon/RF systems cured at different temperature from 25°C to 230°C.

In figure 4.4, instead, ATR spectra of pure RFL system (a) and Nylon (b), and of a Nylon cord covered by RFL (Nylon/RFL) (c) and by Latex (Nylon/Latex) (d) and cured at 220°C are shown.

In this case, it is clear that a decrease of intensity of Nylon amide group bands[83-87] at 1532, 1631, 3297 cm^{-1} in Nylon/Latex and Nylon/RFL spectra (c,d), compared to pure Nylon spectrum (b), occurs.

The decrease of intensity of these Nylon amide group bands is indicative of a possible physical and/or chemical interaction between Nylon and RFL components, and more specifically with the Latex component of RFL system. However, Nylon/Latex and Nylon/RFL spectra show no additional bands as a result of a clear chemical reaction between Nylon and RFL, and this probably suggests that the nature of the interaction among them is only physical.

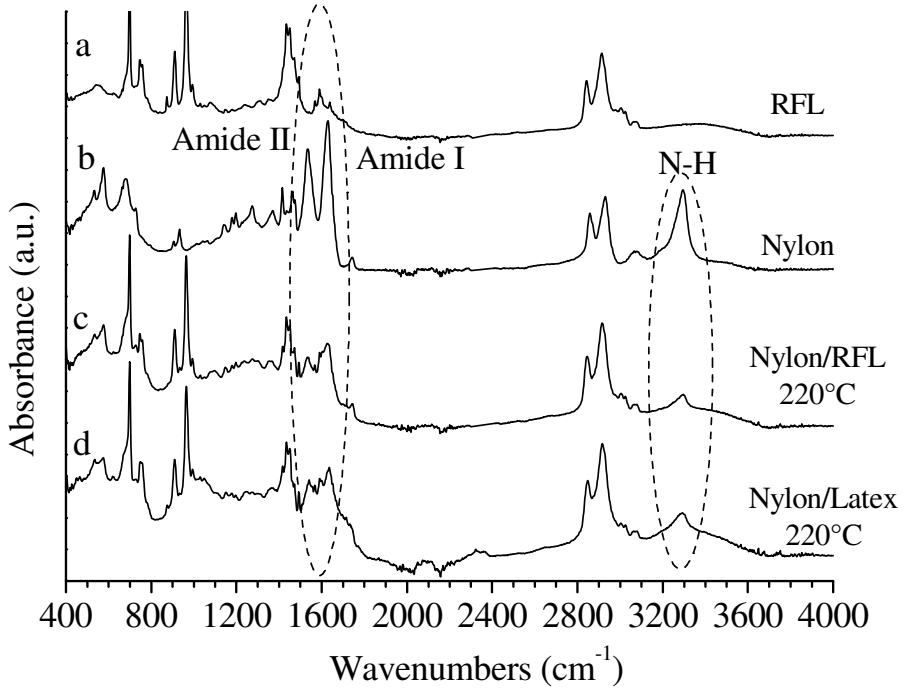

Figure 4.4: ATR spectra of pure RFL system (a) and Nylon (b), and of a Nylon cord covered by RFL (Nylon/RFL) (c) and by Latex (Nylon/Latex) (d) and cured at 220°C.

A study of the behavior of the Nylon/RFL and Nylon/Latex systems changing the curing temperature from 25°C to 230°C has been also made.

In particular, in Figure 4.5, ATR spectra of pure Nylon and Nylon/RFL systems cured at different temperature are reported.

In Figure 4.6, the ratio between the heights of the Nylon amide group bands at 1532, 1631, 3297 cm^{-1} in pure Nylon and Nylon/RFL systems and the constant height of the –CH group band at 2929cm^{-1} is reported as a function of temperature.

The intensity decrease of Nylon amide group bands in Nylon/RFL spectra occurs in the range of temperature between 25-50°C and it remains constant with increasing of the temperature. The interaction between RFL and Nylon already occurs at 25-50°C.

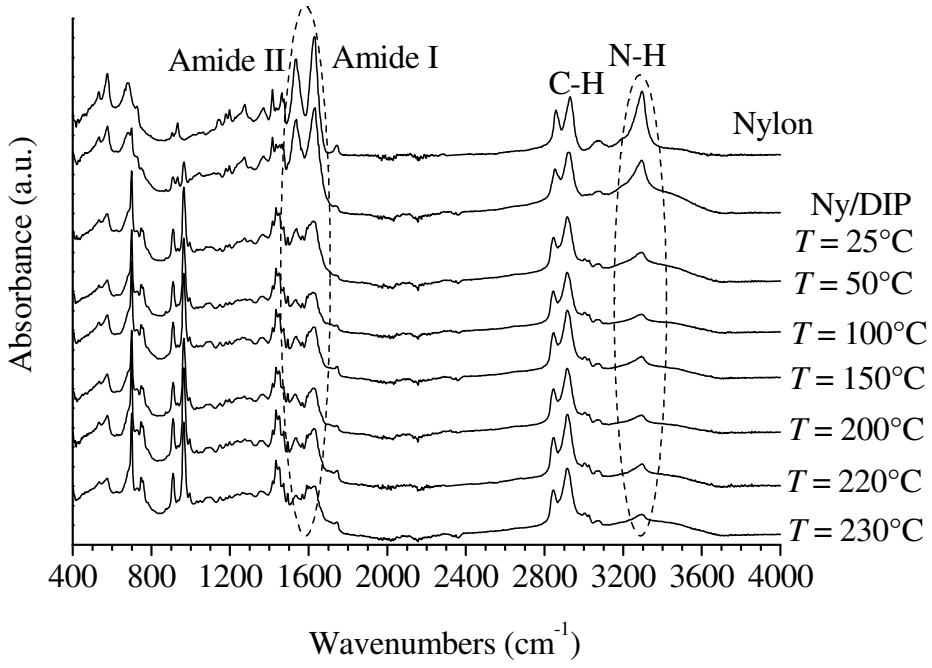

Figure 4.5: ATR spectra of pure Nylon and Nylon/RFL systems cured at different temperature from 25°C to 230°C.

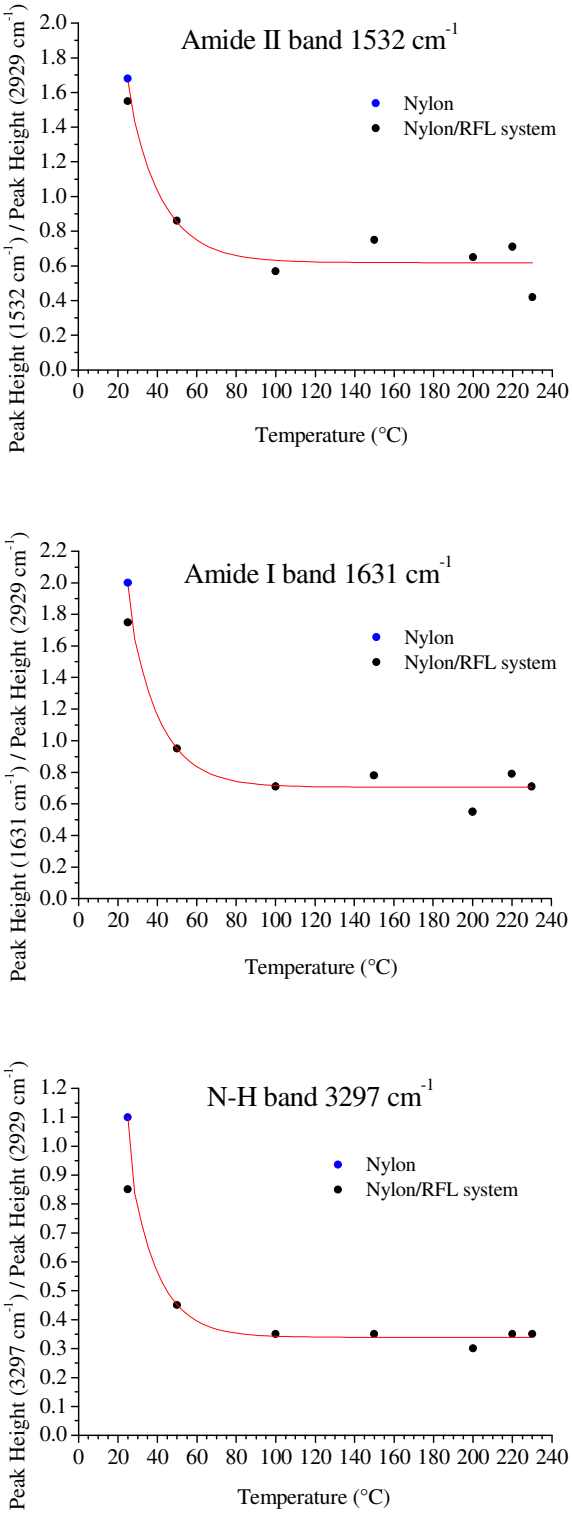

Figure 4.6: Ratio between the heights of the Nylon amide group bands at 1532, 1631, 3297 cm^{-1} in pure Nylon (●) and Nylon/RFL (●) systems and the height of the –CH group band at 2929cm^{-1} is reported as a function of temperature.

In Figure 4.7 ATR spectra of pure Nylon and Nylon/Latex systems cured at different temperature are reported.

In Figure 4.8, the ratio between the heights of the Nylon amide group bands at 1532, 1631, 3297 cm^{-1} in pure Nylon and Nylon/Latex systems and the constant height of the –CH group band at 2929cm^{-1} is reported as a function of temperature.

Also in this case, as for Nylon/RFL systems, the decrease of Nylon amide groups occurs in the range of temperature between 25-50°C and remains constant with increasing of the temperature. This result seems to confirm that interaction between RFL and Nylon involves essentially Latex components and Nylon amide groups and already occurs at 25-50°C.

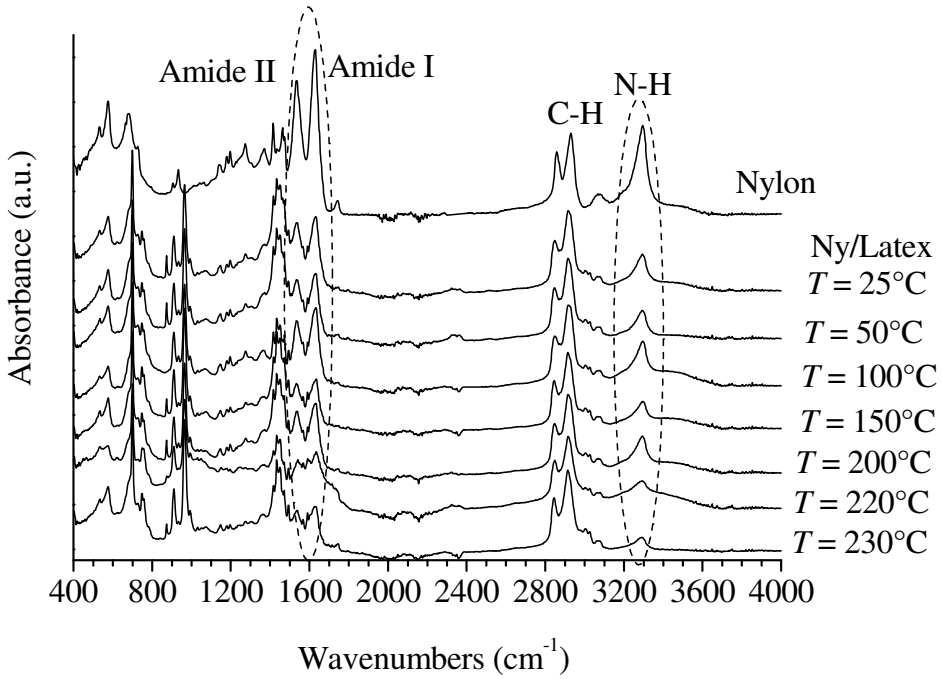

Figure 4.7: ATR spectra of pure Nylon and Nylon/Latex systems cured at different temperature from 25°C to 230°C.

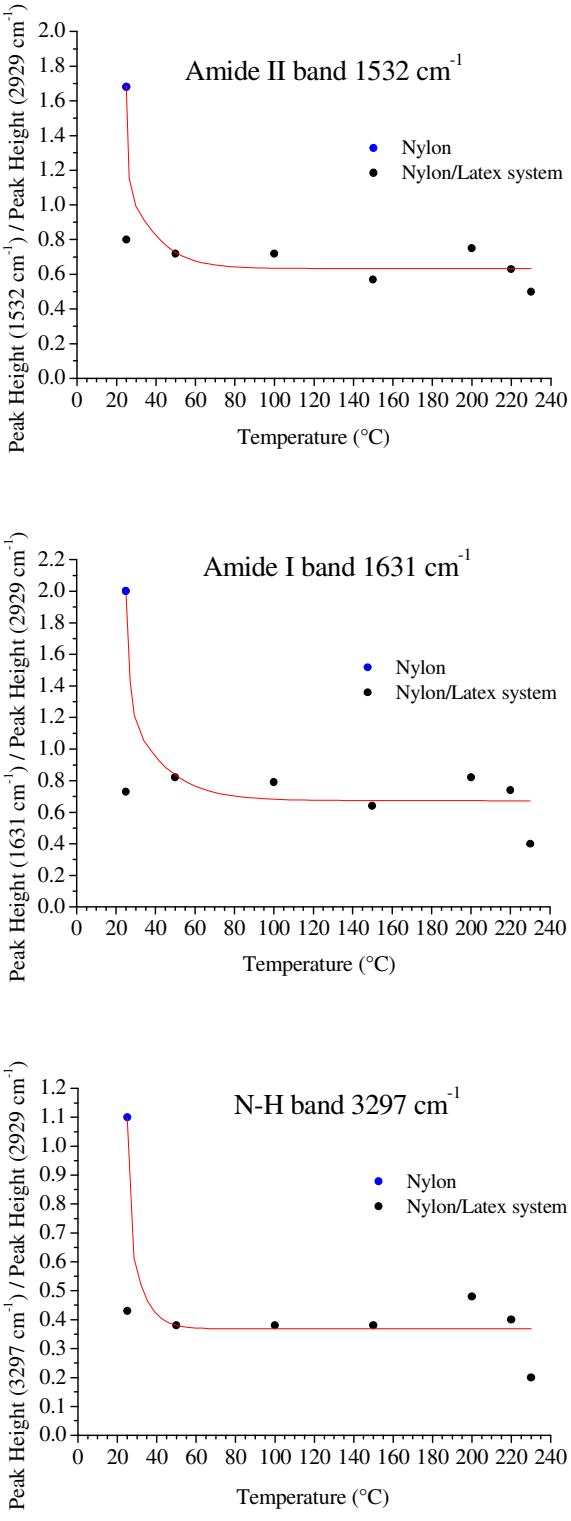

Figure 4.8: Ratio between the heights of the Nylon amide group bands at 1532, 1631, 3297 cm^{-1} in pure Nylon (●) and Nylon/Latex (●) systems and the height of the –CH group band at 2929cm^{-1} is reported as a function of temperature.

ATR results show that interaction between RFL and Nylon involves essentially Latex components and Nylon amide groups. In order to understand which part of Latex interact with Nylon, we have treated Nylon fibres with the components of Latex, namely styrene-butadiene latex (SBR latex) and with 2-vinylpyridine (2VP).

In Figure 4.9 ATR spectra of pure Nylon (a), SBR latex (b), and the calculated spectrum of Nylon/SBR system (c) are reported. The calculated spectrum has been obtained by the sum of Latex and SBR latex spectra in a 1:1 ratio. The experimental spectrum of a Nylon cord covered by SBR latex and cured at 220°C (Nylon/SBR 220°C) (d) is also reported.

Nylon/SBR 220°C and Nylon/SBR calculated spectra are similar. The decrease of Nylon amide groups and a formation of new additional bands as a result of a chemical interaction between Nylon and SBR in Nylon/SBR 220°C spectrum are not observed. The data of Figure 4.9 suggest that the Nylon fibres and the components of SBR latex have scarce or not interactions.

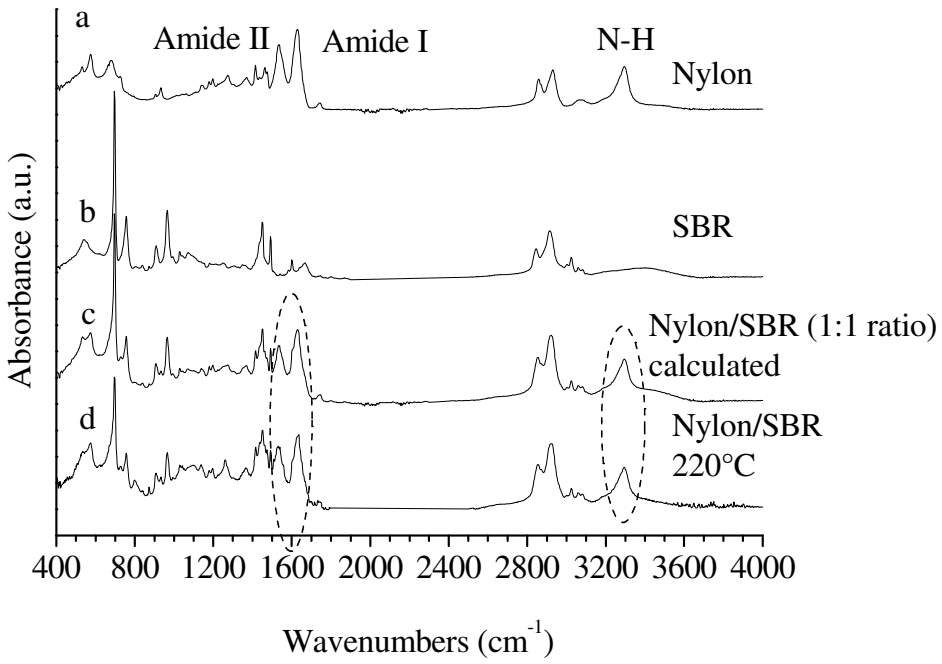

Figure 4.9: ATR spectra of pure Nylon (a), SBR latex (b), calculated spectrum of Nylon/SBR system (c) and experimental spectrum of a Nylon cord covered by SBR latex and cured at 220°C (Nylon/SBR 220°C) (d). The calculated spectrum has been obtained by the sum of Latex and SBR latex spectra in a 1:1 ratio.

In Figure 4.10 ATR spectra of pure Nylon (a), and of Nylon fibres covered by 2-vinylpyridine and dried at 25°C (Nylon/2VP 25°C) (b) and 60°C (Nylon/2VP 60°C) (c) are reported.

Pure Nylon (a) and Nylon/2VP (b,c) spectra are similar. Also in this case, as for Nylon/SBR latex system, the decrease of Nylon amide groups and a formation of new additional bands as a result of a chemical interaction between Nylon and 2VP in Nylon/2VP spectra are not observed.

The treatment of the Nylon fibres with liquid 2VP is probably not sufficient to establish any interaction.

On the basis of these results, ATR analysis performed on Nylon fibres treated with Latex components (SBR latex and 2-vinylpyridine) does not

give clear information about which part of Latex interacts with Nylon and on the nature of this interaction.

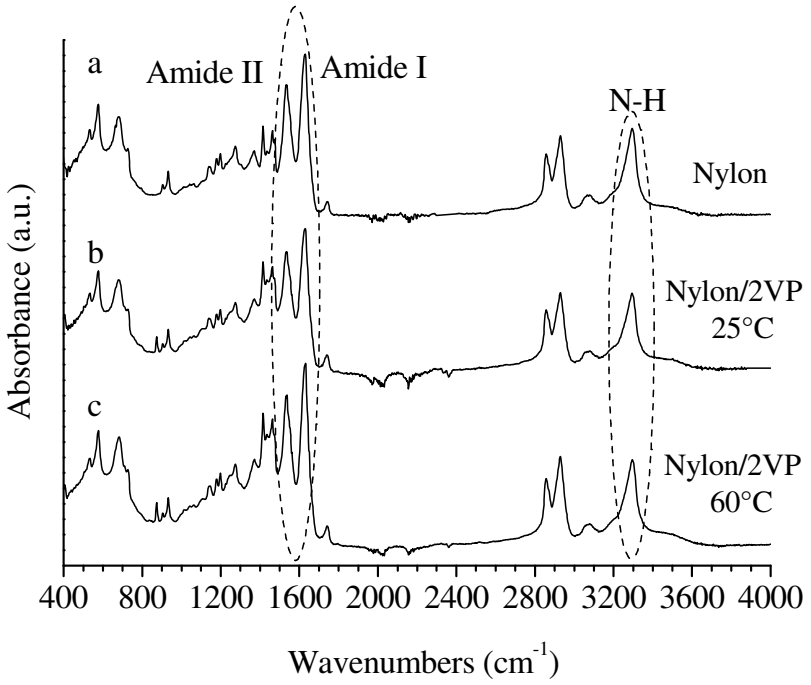

Figure 4.10: ATR spectra of pure Nylon (a) and of Nylon fibres covered by 2-vinylpyridine and dried at 25°C (Nylon/2VP 25°C) (b) and 60°C (Nylon/2VP 60°C) (c).

ATR analysis seems to highlight a physical interaction between RFL, in particular Latex, and Nylon. However, ATR does not dissolve the doubts about a chemical reaction between RFL and Nylon. For this reasons, we have thought about how confirm the result of the ATR analysis and how to exclude completely the possibility of a chemical reaction between RFL and Nylon.

After a careful analysis of the system, we have hypothesized that chemical reaction between Nylon and RFL can occur by means of Nylon hydrolysis, which leads to the formation of reactive groups like amine and carboxyl. If we induce the hydrolysis of Nylon in presence of RFL

components, we can obtain the reaction among these reactive groups and RFL chemicals.

First of all, we have treated the Nylon fibres with H_2O and RFL components in a flask under reflux at 100°C for 1h. We have observed the changes in mechanical properties trying to associate these to a Nylon structural variation.

In Figure 4.11 the load-strain curves of a pure Nylon (–), Nylon treated by H_2O and not dried (Nylon/H_2O_wet) (–) and Nylon treated by H_2O and dried in an oven at 80°C for one day (Nylon/H_2O_dried80°C) (–) are shown. In these figures the values of the Young modulus (*E*), breaking strength ($Load_b$), and strain at break (εb) are also indicated.

Nylon/H_2O_wet curve, compared to a pure Nylon curve, shows a decrease of the Young modulus, an increase of the strain at break, and a constant breaking strength. Nylon/H_2O_dried80°C curve shows a little increase in modulus compared to the modulus of Nylon/H_2O_wet samples, but always lowers than pure Nylon curve, and a strain at break and a breaking strength comparable to those of Nylon/H_2O_wet.

On the basis of these observations, Nylon/H_2O_wet and Nylon/H_2O_dried80°C samples show more ductility and less stiffness than pure Nylon sample.

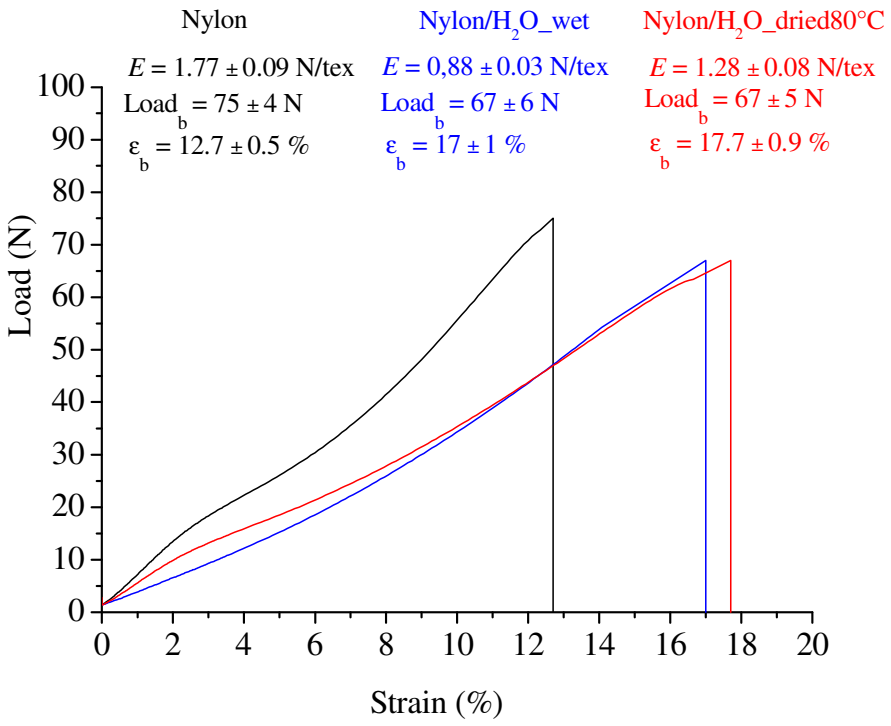

Figure 4.11: Load-strain curves of a pure Nylon (–), Nylon treated by H_2O and not dried (Nylon/H_2O_wet) (–) and Nylon treated by H_2O and dried in a oven at 80°C for a day (Nylon/H_2O_dried80°C) (–).

In Figure 4.12 the load-strain curves of a pure Nylon (–), Nylon treated by H_2O and not dried (Nylon/H_2O_wet) (–) and Nylon treated by H_2O and NaOH (0.12M, PH≈10 as standard RFL preparation) and not dried (Nylon/H_2O/NaOH_wet) (–) are shown.

Nylon/$H_2$0/NaOH_wet curve is similar to Nylon/H2O_wet curve, so the effect of treatment of Nylon with NaOH (Nylon/H_2O/NaOH_wet) induces, as already seen in samples treated with only H_2O, a loss in mechanical strength and an increase in ductility compared to pure Nylon.

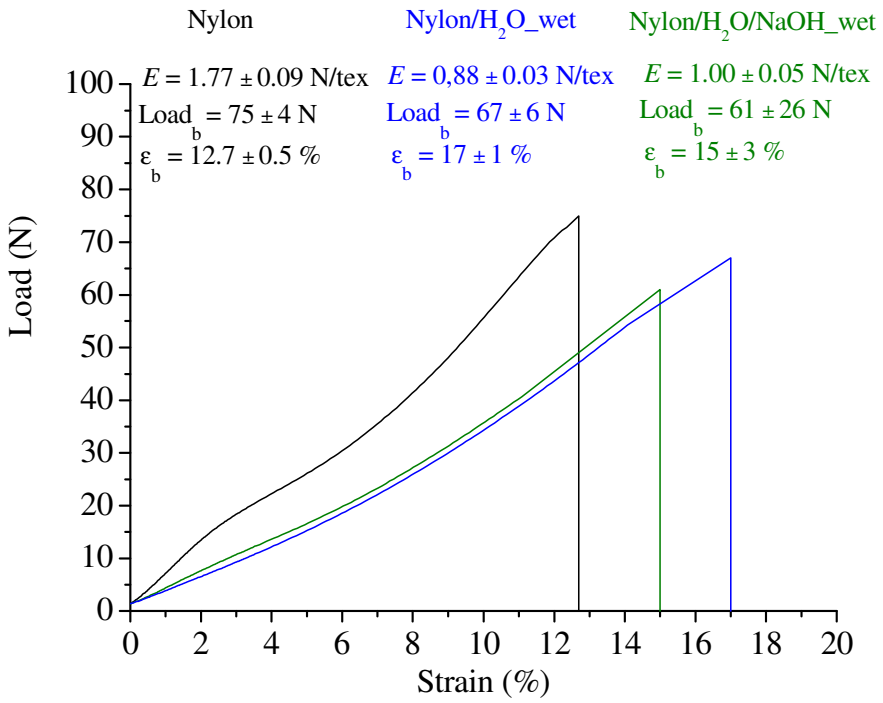

Figure 4.12: Load-strain curves of a pure Nylon (–), Nylon treated by H_2O and not dried (Nylon/H2O_wet) (–) and Nylon treated by H_2O and NaOH (0.12M, PH≈10 as standard RFL preparation) and not dried (Nylon/H_2O/NaOH_wet) (–)

After that, we have tried in Figure 4.13A,B,C to further complicate the system by treating Nylon cords with RFL components in the amount used for a standard RFL preparation (F/R molar ratio = 1.75 and a content of Latex = 42w% of the total solution weight).

In particular, in Figure 4.13A the load-strain curves of a pure Nylon (–), Nylon treated by RF components (Resorcinol and Formaldehyde) and not dried (Nylon/RF_wet) (–) and Nylon treated by RF components and dried in an oven at 80°C for a day (Nylon/RF_dried80°C) (–) are shown.

Instead, in Figure 4.13B the load-strain curves of a pure Nylon (–), Nylon treated by Latex and not dried (Nylon/Latex_wet) (–) and Nylon treated by Latex and dried in a oven at 80°C for a day (–) are reported.

Finally, in Figure 4.13C the load-strain curves of a pure Nylon (–), Nylon treated by the complete RFL system and not dried (Nylon/RFL_wet) (–) and Nylon treated by RFL and dried in an oven at 80°C for a day (Nylon/RFL_dried80°C) (–) are shown.

The treatment of Nylon cords with RFL components in Figure 4.13A,B,C produces the same result observed for Nylon/H_2O and Nylon/H_2O/NaOH systems in Figure 4.11 and Figure 4.12, with a loss of mechanical strength and an increase of ductility compared to pure Nylon.

A summary of the value of the mechanical properties of all samples analyzed is shown in Table 4.1.

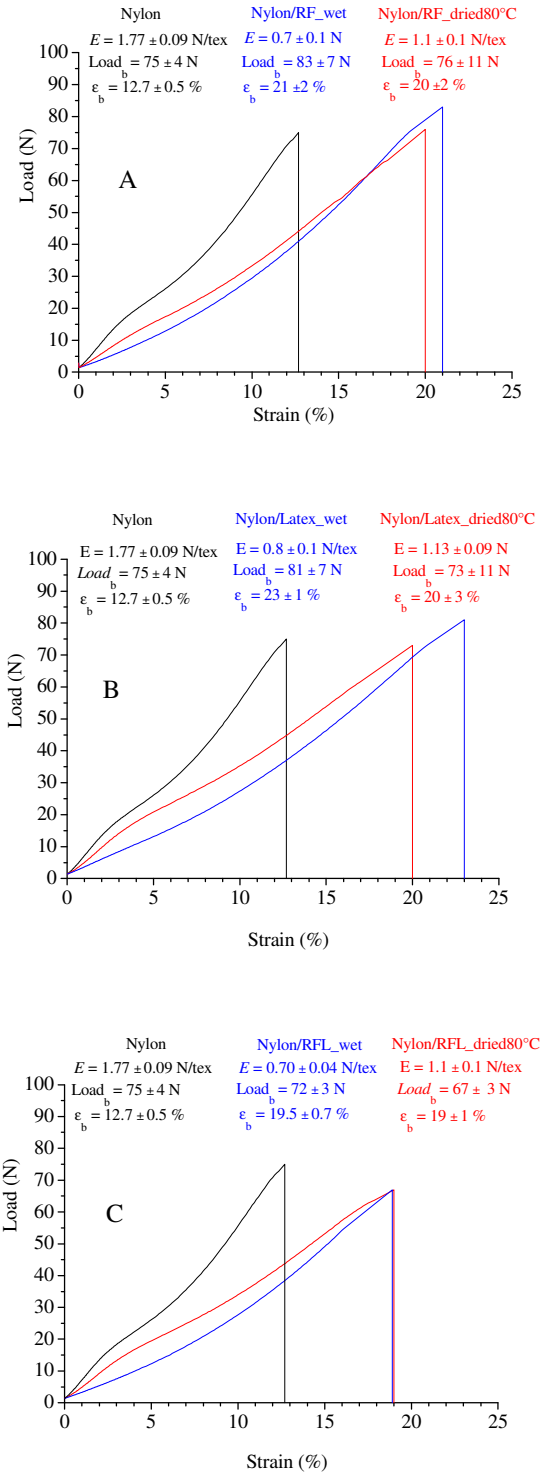

Figure 4.13: Load-strain curves of: **A**) pure Nylon (–), Nylon treated by RF and not dried (Nylon/RF_wet) (–) and Nylon treated by RF and dried (Nylon/RF_dried80°C) (–). **B**) pure Nylon (–), Nylon treated by Latex and not dried (Nylon/Latex_wet) (–) and Nylon treated by Latex and dried (Nylon/Latex_dried80°C) (–). **C**) pure Nylon (–), Nylon treated by RFL and not dried (Nylon/RFL_wet) (–) and Nylon treated by RFL and dried (Nylon/RFL_dried80°C) (–).

Table 4.1: Values of Young modulus (*E*), breaking strength ($Load_b$) and strain at break (ε_b) for all Nylon samples analyzed.

Samples	*E* (N/Tex)	$Load_b$ (N)	ε_b (%)
Nylon_raw	1.77 ± 0.09	75 ± 4	12.7 ± 0.5
Nylon/H_20_wet	0.88 ± 0.03	67 ± 6	17 ± 1
Nylon/H_20_dried80°C	0.8 ± 0.1	80 ± 8	18.5 ± 0.7
Nylon/H_20/NaOH_wet	1.00 ± 0.05	61 ± 26	15 ± 3
Nylon/RF_wet	0.7 ± 0.1	83 ± 7	21 ± 2
Nylon/RF_dried80°C	1.1 ± 0.1	76 ± 11	20 ± 2
Nylon/Latex_wet	0.8 ± 0.1	81 ± 7	23 ± 1
Nylon/Latex_dried80°C	1.13 ± 0.09	73 ± 11	20 ± 3
Nylon/RFL_wet	0.70 ± 0.04	72 ± 3	19.5 ± 0.7
Nylon/RFL_dried80°C	1.1 ± 0.1	67 ± 3	19 ± 1

Mechanical tests on Nylon cords treated with H_2O and RFL components show a loss of mechanical strength and an increase of ductility compared to pure Nylon.

This variation in mechanical properties can be associated with two phenomena; a plasticizing effect of water and/or a hydrolysis of the Nylon chains and possible reaction with RFL chemicals.

^{13}C-NMR spectroscopy analysis can give us precise indication of which of the two phenomena really occurs.

^{13}C-NMR spectra are obtained using a procedure suggested in an article.[81] This procedure involves the use of two solvents, a 2,2,2-trifluoroethanol

(TFE) to dissolve Nylon fibres and a deuterated chloroform ($CDCl_3$) to obtain a deuterium lock, in a ratio 4:1.

In Figure 4.14A ^{13}C-NMR spectrum of pure Nylon is reported. The regions where the resonance of Nylon[81,88] occur are comprised between 20-45 ppm (region of -CH2 backbone groups) and 170-180 ppm (region of Nylon amide group –CONH–). These regions are reported in an enlarged scale in Figure 4.14B,C.

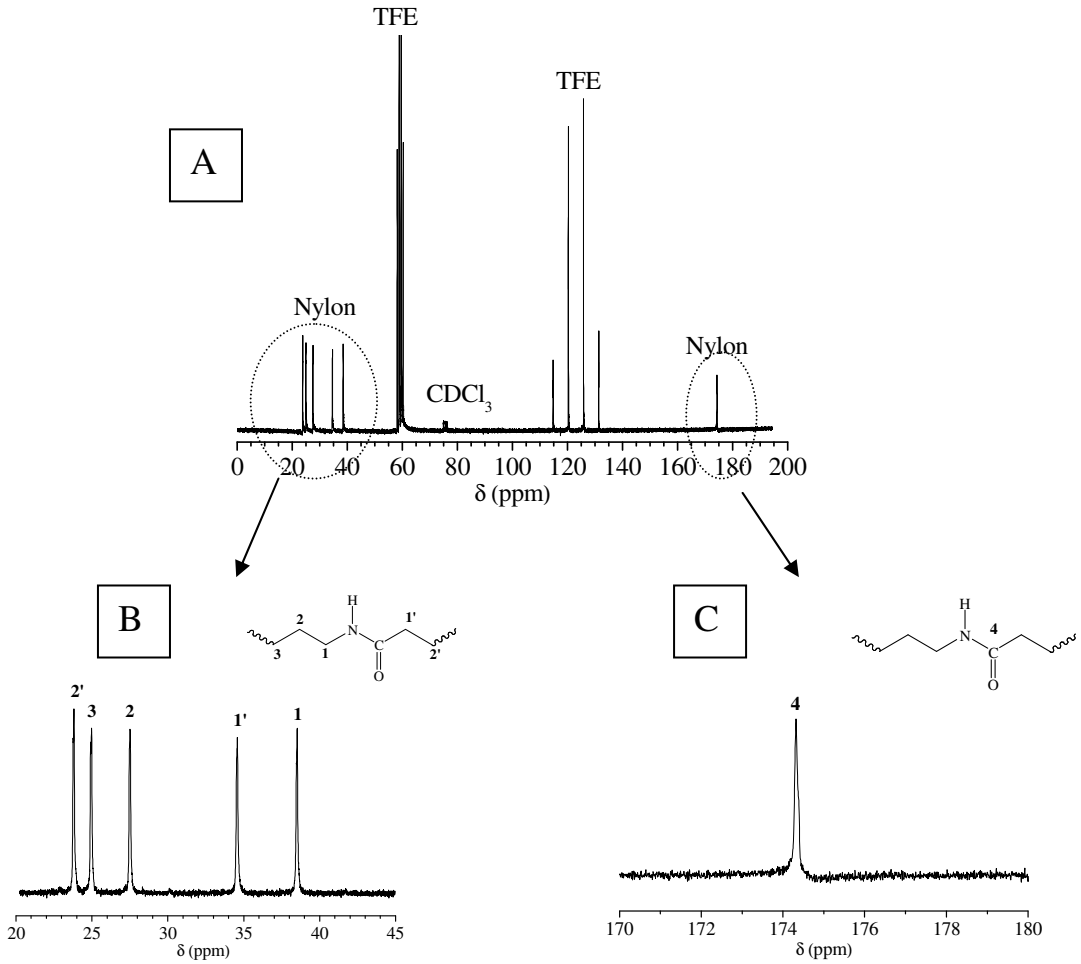

Figure 4.14: ^{13}C-NMR spectrum of pure Nylon (A). The regions where the resonance of Nylon[81,88] occur are comprised between 20-45 ppm (region of -CH2 backbone groups) and 170-180 ppm (region of Nylon amide group –CONH–). These regions are reported in an enlarged scale (B,C).

In the case of hydrolysis of nylon chains, amide bond is broken to form amine and carboxyl groups. This would involve, in terms of ^{13}C-NMR spectroscopy, a variation of the position of C=O Nylon peak (≈174ppm in Figure 4.14C). In fact, this C would be more shielded, as a result of breaking, and would resonate at lower values of the chemical shift by several ppm.

In Figure 4.15A,B a comparison between ^{13}C-NMR spectra of pure Nylon (a), Nylon/H_2O_wet (b) and Nylon/H2O/NaOH_wet (c) is shown. The region between 20-45 ppm is reported in Figure 4.15A, while the region between 170-180 ppm in Figure 4.15B.

In Figure 4.15B, a shift of C=O peak in Nylon/H_2O_wet and Nylon/H2O/NaOH_wet systems, as an effect of hydrolysis, is not observed. The hydrolysis does not occur in these systems and the change in mechanical properties observed in Figure 4.11 and Figure 4.12, such as a decrease of mechanical strength and an increase of ductility compared to pure Nylon, can be only attributed to a plasticizing effect of H_2O.

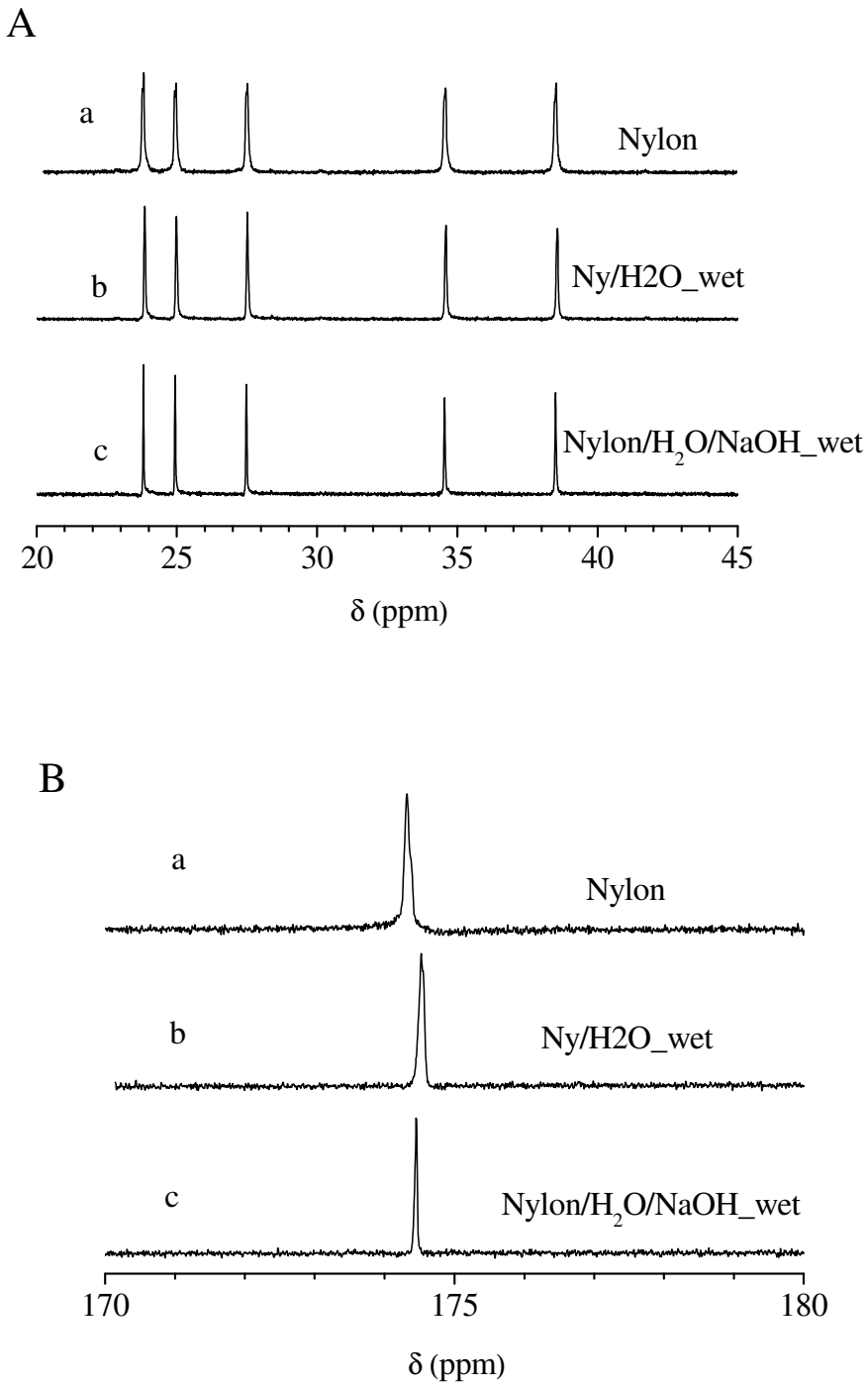

Figure 4.15: Comparison between ^{13}C-NMR spectra of pure Nylon (a), Nylon/H_2O_wet (b) and Nylon/H_2O/NaOH_wet (c). **A**) Region between 20-45 ppm. **B**) Region between 170-180 ppm.

At this point, we have tried to force the hydrolysis of the nylon chains using drastic conditions. In particular, nylon cords are treated, at first by only H_2O and then by H_2O and NaOH, in a steel mini-reactor at 220°C for 2 min and 30 min respectively.

In Figure 4.16A,B a comparison between ^{13}C-NMR spectra of pure Nylon (a), Nylon treated by H_20 at 220°C for 2 min (Nylon/H_2O_reactor2min) (b) and Nylon treated by H_2O and NaOH at 220°C for 2 min (Nylon/H_2O/NaOH_reactor2min) (c) is reported. The region between 20-45 ppm is reported in Figure 4.16A, while the region between 170-180 ppm in Figure 4.16B.

In Figure 4.17A,B, instead, a comparison between ^{13}C-NMR spectra of pure Nylon (a), Nylon treated by H_2O at 220°C for 30 min (Nylon/H_2O_reactor30min) (b) and Nylon treated by H_2O and NaOH at 220°C for 30 min (Nylon/H_2O/NaOH_reactor30min) (c) is shown. The region between 20-45 ppm is reported in Figure 4.17A, while the region between 170-180 ppm in Figure 4.17B.

In the Figure 4.16B and Figure 4.17B, even treating Nylon cords under drastic conditions, a substantial shift of C=O Nylon peak is not observed, so it is clear that the hydrolysis of Nylon chains does not occur even using these conditions.

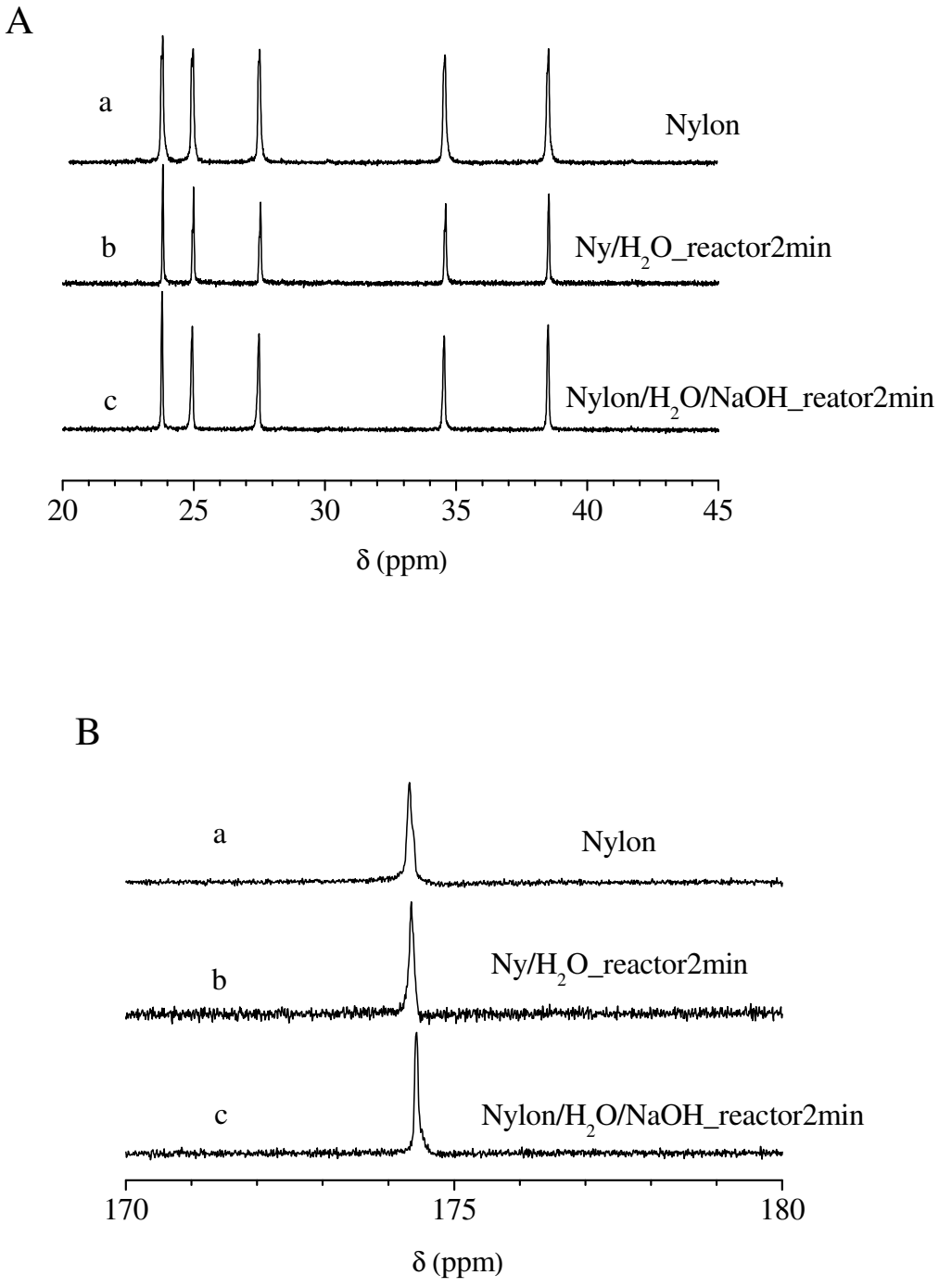

Figure 4.16: Comparison between ^{13}C-NMR spectra of pure Nylon (a), Nylon treated by H_2O at 220°C for 2 min (Nylon/H_2O_reactor2min) (b) and Nylon treated by H_2O and NaOH at 220°C for 2 min (Nylon/H_2O/NaOH_reactor2min) (c). **A**) Region between 20-45 ppm. **B**) Region between 170-180 ppm.

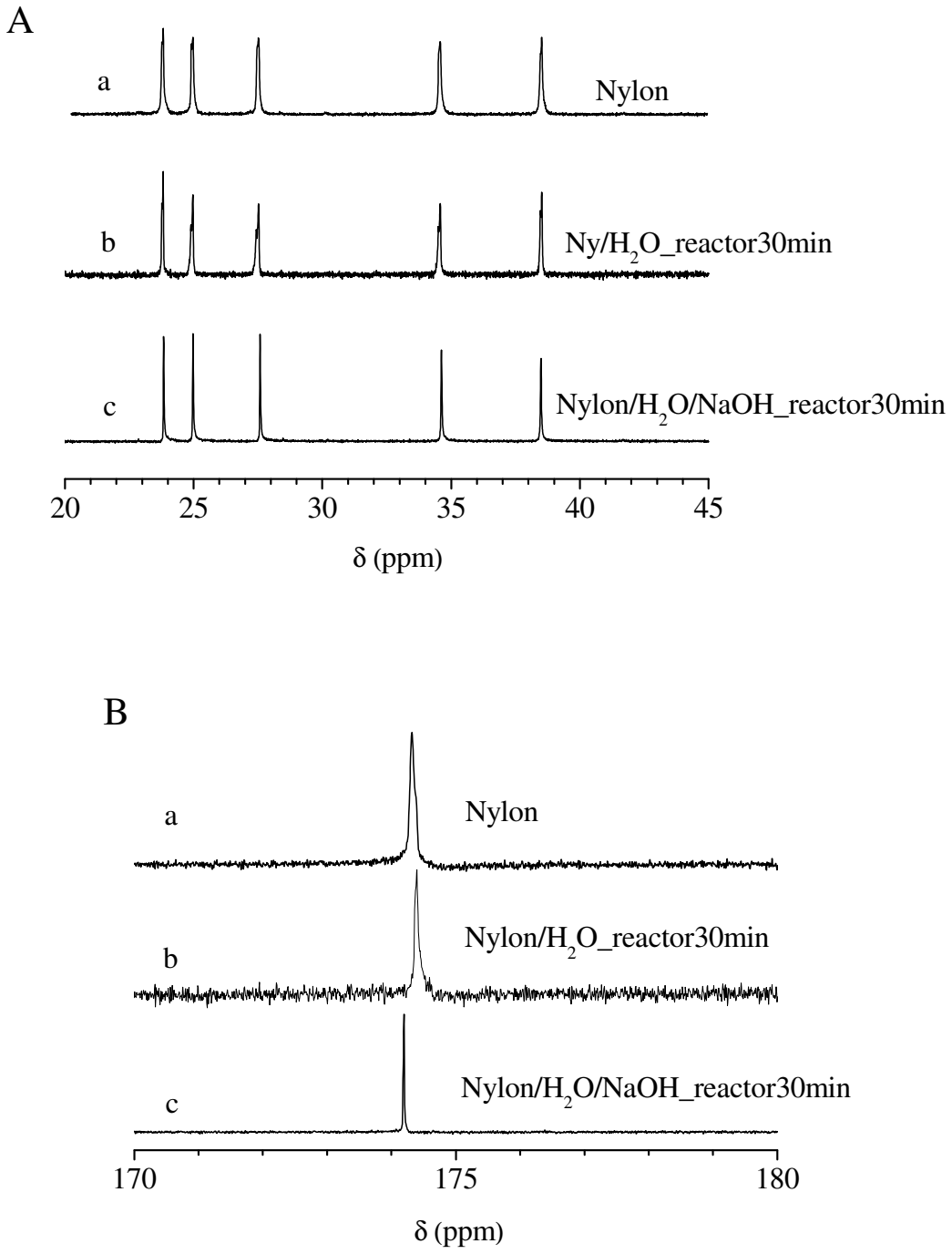

Figure 4.17: Comparison between ^{13}C-NMR spectra of pure Nylon (a), Nylon treated by H_2O at 220°C for 30 min (Nylon/H_2O_reactor30min) (b) and Nylon treated by H_2O and NaOH at 220°C for 30 min (Nylon/H_2O/NaOH_reactor30min) (c). **A**) Region between 20-45 ppm. **B**) Region between 170-180 ppm.

To further confirm that the hydrolysis of the nylon chains does not occurs even using drastic conditions, a thermogravimetric analysis (TGA) has been performed on the systems treated in these conditions.

In the case of hydrolysis of Nylon chains, a weight loss in TGA thermograms due to the oligomers formed for effect of breaking of the Nylon chains is expected.

In Figure 4.18 TGA thermograms of pure Nylon (–), Nylon/H_2O_reactor2min (–) and Nylon/H_2O/NaOH_reactor2min (–) are reported.

TGA thermograms show a weight loss of 5w% up to 400°C (due to the loss of H_2O), and than samples degradation which start after 400°C. The weight loss due to the possible presence of oligomers in Nylon/H_2O_reactor2min and Nylon/H_2O/NaOH_reactor2min systems is never observed, so hydrolysis does not occur and this confirms the result of ^{13}C-NMR analysis in Figure 4.16.

In Figure 4.19 TGA thermograms of pure Nylon (–), Nylon/H_2O_reactor30min (–) and Nylon/H_2O/NaOH_reactor30min (–) are reported.

Also in this case, as for samples in Figure 4.18, there is no weight loss due to the presence of oligomers, so hydrolysis does not occur and the result of ^{13}C-NMR analysis in Figure 4.17 is confirmed.

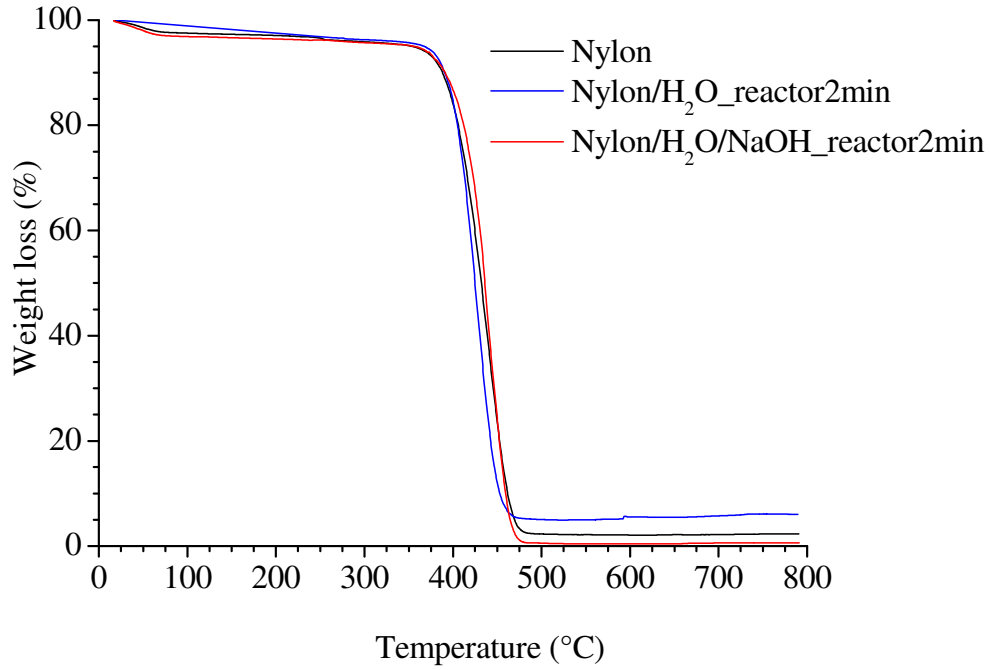

Figure 4.18: TGA thermograms of pure Nylon (–), Nylon/H_2O_reactor2min (–) and Nylon/H_2O/NaOH_reactor2min (–).

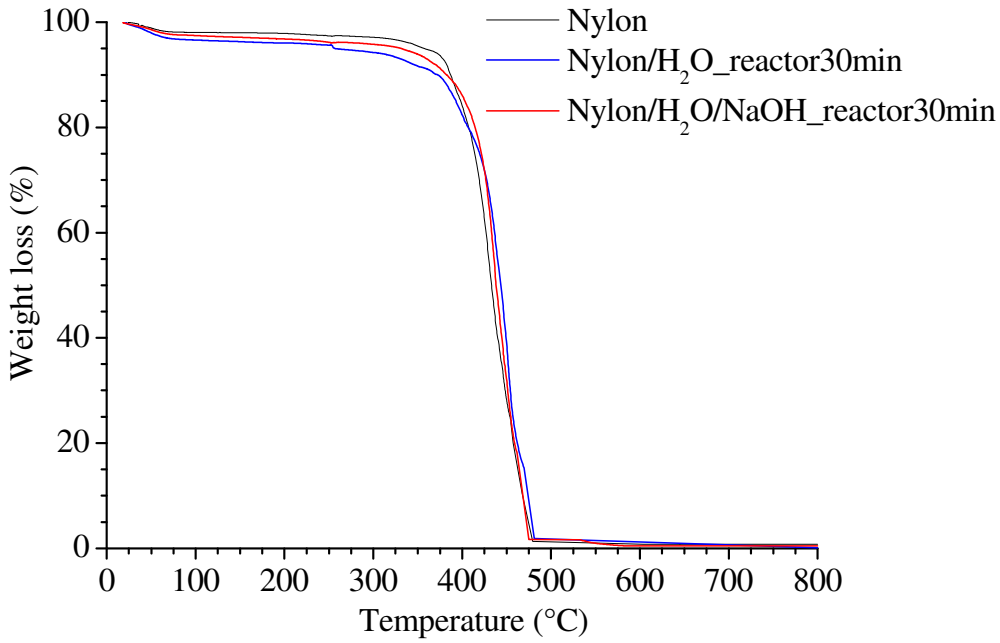

Figure 4.19: TGA thermograms of pure Nylon (–), Nylon/H_2O_reactor30min (–) and Nylon/H_2O/NaOH_reactor30min (–).

^{13}C-NMR spectroscopy and TGA analysis show that the hypothesis of a chemical reaction between Nylon and RFL by means of hydrolysis of Nylon chains is not realistic. Based on these results and on the basis of the results obtained from ATR, we can conclude that the interactions between Nylon and RFL, in particular Latex component of RFL, are probably purely physical.

Several physical interactions can occur between RFL and Nylon, such as Van der Waals forces, dipole-dipole interactions and hydrogen bonds. The physical interactions could be mainly hydrogen bonds between amide groups of Nylon and pyridine groups of Latex. In figure 4.20 is reported a scheme of a possible hydrogen bond between Nylon amide group and 2-vinylpyridine of Latex system.

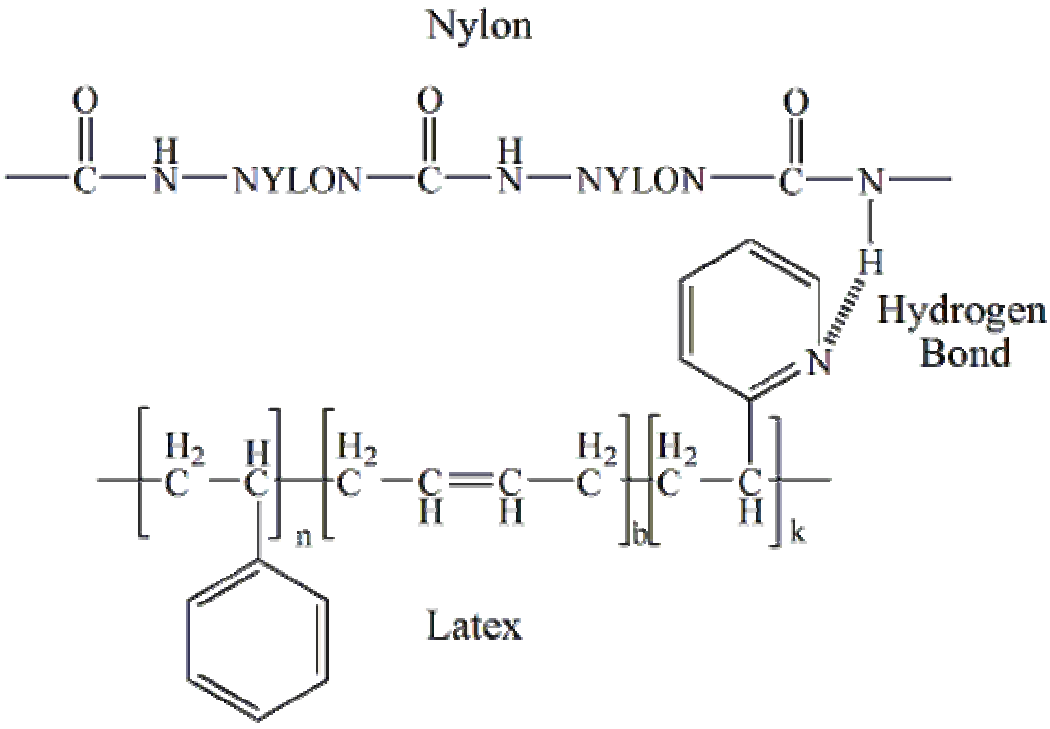

Figure 4.20: Scheme of a possible hydrogen bond between Nylon amide group and 2-vinylpyridine of Latex system.

Study of RFL/rubber interaction

The mechanism of interaction between RFL and rubber is extremely complex and still today is not very clear.

As already seen in paragraph 4.1 of this chapter, many opinions have been presented to clarify the nature of this interaction,[32,78,80] but none of these seem to give clear and unambiguous results.

In this section, a possible explanation of the nature of this interaction is given by FT-IR/ATR spectroscopy.

Samples for the study of interface between RFL/rubber are prepared as follow. Nylon cords, covered by RFL solution, are included in a rubbery matrix of natural rubber. A vulcanization process occurs about at 160°C for 20 min and then the cords are extracted from the rubbery matrix. FT-IR/ATR analysis at the interface between the rubber residue on the cords and the RFL solution has been performed.

In Figure 4.21A,B ATR spectra of pure Nylon (a), RFL (b), Natural Rubber (NR)(c), Nylon/RFL/NR calculated (d) are reported. The calculated spectrum has been obtained by the sum of Nylon, RFL and NR spectra in a 1:1:1 ratio. The experimental spectrum of Nylon/RFL/NR system (e) is also reported.

In Figure 4.21A, ATR spectra in the range of wavenumbers among 400-4000 cm^{-1} are reported. A magnification of these spectra in the zone among 400-1200 cm^{-1} is instead reported in Figure 4.21B.

In Figure 4.21B, it is possible to observe that there are some differences between ATR spectra.

In particular, the peak of $–CH_2\text{-}CH_2–$ group at 871 cm^{-1} present in NR[89] and Nylon/RFL/NR calculated spectra, disappears in Nylon/RFL/NR experimental system (red circle).

Also the peak of polystirene group (PS) at 700cm^{-1} and the peaks of polybutadiene groups (PB) at 910 and 964cm^{-1} present in RFL$^{70\text{-}75}$ and Nylon/RFL/NR calculated spectra substantially decrease in Nylon/RFL/NR experimental system (blue circles).

This result can be due to the vulcanization process occurring not only between natural rubber chains and sulphur (CH groups of NR and S), but also between CH groups of NR, sulphur and Latex components (principally involving polybutadiene units) of RFL.

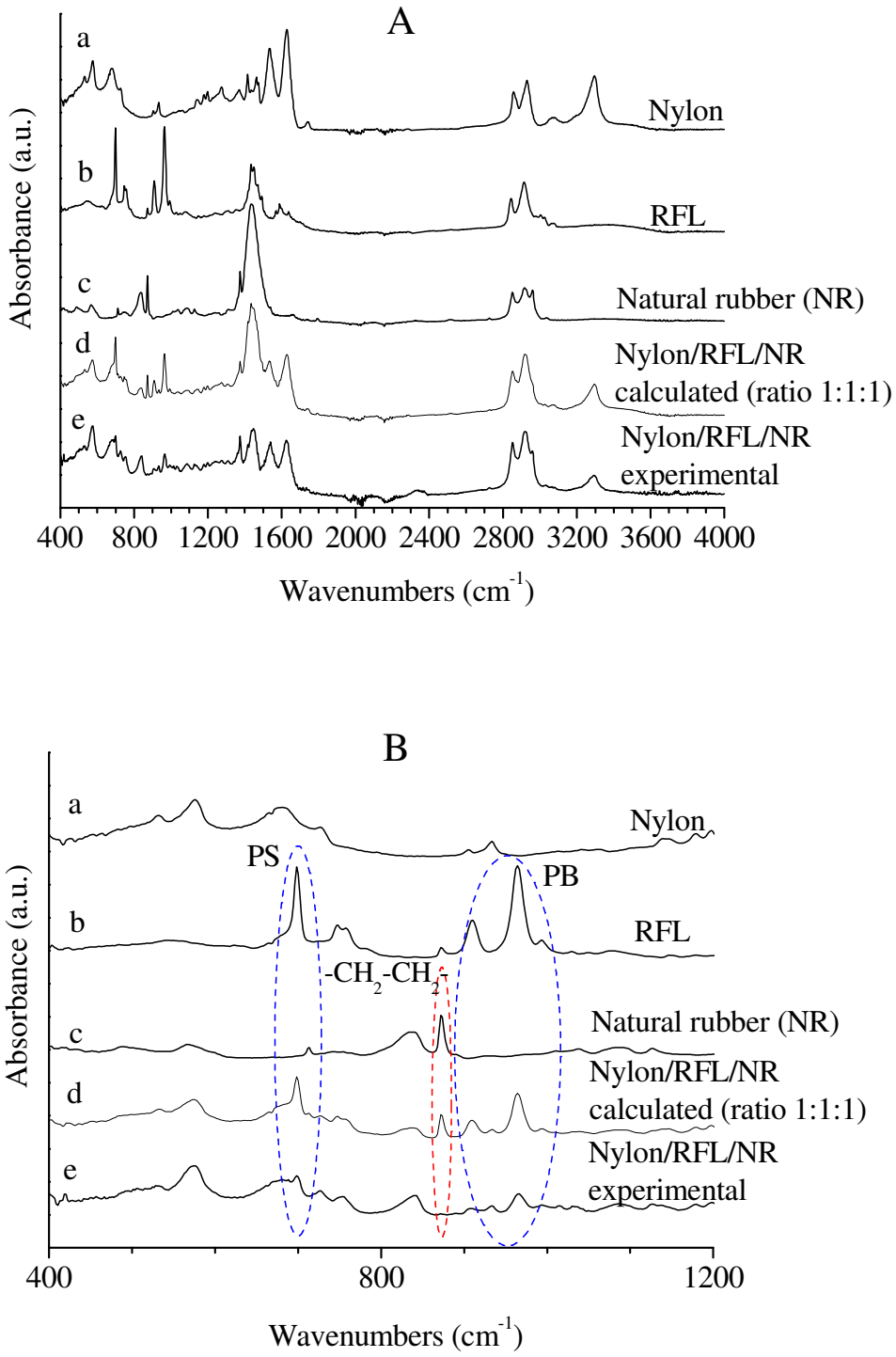

Figure 4.21: ATR spectra of pure Nylon (a), RFL (b), Natural Rubber (NR) (c), Nylon/RFL/NR calculated (d), and of a Nylon/RFL/NR experimental system (e). The calculated spectrum is obtained by the sum of Nylon, RFL and NR spectra in a 1:1:1 ratio. **A)** Spectra in the range of wavenumbers among 400-4000cm^{-1}. **B)** Spectra in the range of wavenumbers among 400-1200cm^{-1}.

4.4 Conclusion

The mechanism of interaction between RFL and reinforcing fibres, and RFL and rubber is extremely complex.

Many and controversial opinion have been presented in the past to explain these interactions but, unfortunately, none of theme give clear and unambiguous results.

In this chapter we have tried to elucidate these interactions by means of spectroscopic techniques such as Raman, FT-IR/ATR, ^{13}C-NMR spectroscopy, and by mechanical and thermogravimetric (TGA) analysis.

As for as Nylon/RFL interface, Raman spectroscopy does not give clear results. ATR analysis seems instead to highlight a physical interaction between RFL, in particular Latex, and Nylon. However, ATR does not dissolve the doubts about a chemical reaction between RFL and Nylon, so we have thought about how confirm the result of the ATR analysis and how to exclude completely the possibility of a chemical reaction between RFL and Nylon.

After a careful analysis of the system, we have hypothesized that chemical reaction between Nylon and RFL can occur by means of Nylon hydrolysis, which leads to the formation of reactive groups like amine and carboxyl. If we induce the hydrolysis of Nylon in presence of RFL components, we can obtain the reaction among these reactive groups and RFL components.

^{13}C-NMR spectroscopy and TGA analysis show that the hypothesis of a chemical reaction between Nylon and RFL by means of hydrolysis of Nylon chains is not realistic, so we can conclude that the interactions between Nylon and RFL, in particular Latex component of RFL, are

probably purely physical. The physical interactions could be mainly hydrogen bonds between amide groups of Nylon and pyridine groups of Latex.

As for as RFL/rubber interface, ATR spectroscopy shows that the vulcanization process probably occurs not only between natural rubber chains and sulphur (CH groups of NR and S), but also between CH groups of NR, sulphur and Latex components (principally involving polybutadiene units) of RFL.

Chapter 5

Eco-friendly (formaldehyde-free) alternative DIP

5.1 Introduction: Formaldehyde - human and environmental poison

Formaldehyde is a colourless, flammable, toxic, strong-smelling chemical that is used in building materials and to produce many household products.

It is used in many articles, such as: particleboard, plywood, and fibreboard, glues and adhesives, permanent-press fabrics, paper product coatings, and certain insulation materials. In addition, formaldehyde is commonly used as an industrial fungicide, germicide, and disinfectant.

Formaldehyde also occurs naturally in the environment. It is produced in small amounts by most living organisms as part of normal metabolic processes.

The sources of exposure to formaldehyde in indoor and outdoor are many. According to a 1997 report by the U.S. Consumer Product Safety Commission, formaldehyde is normally present in both indoor and outdoor air at low levels, usually less than 0.03 parts of formaldehyde per million parts of air (ppm). Materials containing formaldehyde can release formaldehyde toxic gas or vapour into the air with consequent environmental and health problems.

Pressed-wood products containing formaldehyde resins are often a significant source of formaldehyde in homes. Other potential indoor sources of formaldehyde include cigarette smoke and the use of fuel-burning appliances, such as: gas stoves, wood-burning stoves, and kerosene heaters.

Industrial workers who produce formaldehyde or formaldehyde-based resin could be exposed to higher levels of formaldehyde than the general public. Exposure occurs by inhaling formaldehyde gas or vapour from the air or by absorbing liquids containing formaldehyde through the skin.

The short-term health effects of formaldehyde exposure are widely known. When formaldehyde is present in the air at levels exceeding 0.1 ppm, some individuals could experience adverse effects such as: watery eyes, burning sensations in the eyes, nose, and throat, coughing, wheezing, nausea, and skin irritation. Some people are very sensitive to formaldehyde, whereas others have no reaction to the same level of exposure.

Although the short-term health effects of formaldehyde exposure are well known, less is known about its potential long-term health effects.

In 1980, some studies show that exposure to formaldehyde can cause nasal cancer in rats. Based on these studies, scientists have tried to understand whether formaldehyde exposure can also cause cancer in humans. In 1987, the U.S. Environmental Protection Agency (EPA) classifies formaldehyde as a probable human carcinogen under conditions of unusually high or prolonged exposure.[90]

Since that time, some studies of humans have suggested that formaldehyde exposure is associated with certain types of cancer.

In 2006, the International Agency for Research on Cancer (IARC) definitively classifies formaldehyde as a human carcinogen.[46]

In 2011, the National Toxicology Program, an interagency program of the Department of Health and Human Services, names formaldehyde as a known human carcinogen in its 12th Report on Carcinogens.[91]

Over the last thirty years scientists have learned a lot about the relationship between formaldehyde and cancer.

Since the 1980s, the National Cancer Institute (NCI), a component of the National Institutes of Health (NIH), has conducted studies to determine whether there is an association between occupational exposure to formaldehyde and an increase in the risk of cancer. The results of this research have provided EPA and the Occupational Safety and Health Administration (OSHA) with information to evaluate the potential health effects of workplace exposure to formaldehyde.

The long-term effects of formaldehyde exposure have been evaluated in epidemiologic studies (studies that attempt to uncover the patterns and causes of disease in groups of people).

One type of epidemiologic study is called a cohort study. A cohort is a group of people who could vary in their exposure to a particular factor, such as formaldehyde, and are followed over time to see whether they develop a disease.

Another kind of epidemiologic study is called a case-control study. Case-control studies begin with people who are diagnosed as having a disease (cases) and compare them to people without the disease (controls), trying to identify differences in factors, such as exposure to formaldehyde, that could explain why the cases develop the disease but the controls does not. Several of these epidemiologic studies on people, who are potentially exposed to formaldehyde in their work, have suggested that these individuals are an increased risk of leukaemia, nasopharyngeal and brain cancer compared with the general population.[92-97]

From the moment it is understood the real problems that formaldehyde can cause, a series of initiatives in support of workers have been adopted.

In 1987, OSHA has been established a standard that reduced the amount of formaldehyde to which workers can be exposed over an 8-hour workday from 3 ppm to 1 ppm. In May 1992, the standard has been

amended, and the formaldehyde exposure limit was further reduced to 0.75 ppm.

Based on these described issues, in recent years, research is moving to eliminate as much as possible formaldehyde and formaldehyde-based products in favour of ‘green’ formaldehyde-free products.

In particular, the desire of Bridgestone T.C.E. is to develop an eco-friendly (formaldehyde-free) alternative DIP. The strategy is to search for a synthetic biodegradable resin, which can replace resorcinol-formaldehyde resin, and combined it with latex to form an innovative DIP.

In this thesis two possible systems have been identified: soy-based DIP and starch-based DIP. These systems will be tested, in the future, as potential substitutes of traditional RFL-DIP systems. This could be the first step toward a tyre seen as a completely ‘green’ composite.

5.2 'Green' composites

Fibre reinforced polymeric composites have been used for a variety of structural applications because of their high specific strength and modulus compared to metals. Initially developed for the aerospace industry, high-performance or 'advanced' composites are now found in applications from automotive parts to circuit boards, and from building materials to specialty sporting goods.

Most composites currently available on the market are designed with long-term durability and are made using non-degradable polymeric resins, such as epoxies and polyurethane, and high-strength fibres, such as graphite, aramids, and glass.

Many of these polymers and fibres are derived from petroleum, a non-replenish able commodity. The push now is to use composites in place of common plastics in consumer products to improve performance and reduce weight and cost.

With increasing numbers of applications and mass volume uses, in particular, recording double-digit growth worldwide, disposal of composites after their intended life is already becoming critical, as well as expensive. Because composites are made using two dissimilar materials, they cannot be easily recycled or reused. Most composites end up in landfills, while some are incinerated after use, although there are some efforts to recycle and/or reuse them. Both these disposal alternatives are expensive and wasteful, and could contribute to pollution. In addition, landfills are decreasing in number, making less space available to discard waste. For example, between 1988 and 1998 the number of landfills in the US dropped from 8000 to 2314.[98]

Since many of the fibres and resins are made using non-degradable, mostly petroleum-based materials, once discarded they do not degrade for several decades under normal environmental conditions. This exacerbates the existing ecological and environmental problems.

In recent years, the ever-growing worldwide litter problem has raised environmental consciousness among consumers, manufacturers, and governments. Further, it is estimated that we are currently consuming petroleum at an 'unsustainable' rate, 10^5 times faster than nature can create it.

To alleviate these problems, governments in many countries have established laws to encourage the use of recycled and/or bio-based 'green' products.[99]

Some governments have enforced strict laws requiring manufacturers to take back packaging and products after their intended use. The growing global environmental awareness and societal concern, high rate of depletion of petroleum resources, concepts of sustainability, and new environmental regulations have together triggered the search for new products and processes that are compatible with the environment.

Sustainability, 'cradle-to-grave' design, industrial ecology, eco-efficiency, and 'green' chemistry are not just newly coined buzzwords, but form the principles that are guiding the development of a new generation of 'green' materials. Composite materials are no exception to this new paradigm. In fact, most major manufacturers have plans to make their products 'green' or recyclable to the maximum possible extent and are working vigorously towards that goal. Undoubtedly, environment-friendly, fully biodegradable 'green' composite materials will play a major role in greening the products of the future.

'Greener' composite alternatives

The use of biodegradable and environment-friendly plant-based 'lignocellulosic' fibres has been a natural choice for reinforcing (or filling) polymers to make them 'greener'. The availability of inexpensive plant-based fibres in every part of the world has fed their use in the past few years. These fibres offer several other advantages as well. They are nonabrasive to processing equipment, can be incinerated, are CO_2 neutral (when burned), and, because of their hollow and cellular nature, perform well as acoustic and thermal insulators. The hollow tubular structure also reduces their bulk density, making them lightweight.

Plenty of examples can be found of the use of plant-based fibres for reinforcing non-degradable thermoplastic polymers.[100-104]

Examples can also be found of plant-based fibres that have been used with thermosetting resins such as epoxy and polyurethane.[105-108]

Longer plant-based fibres such as abaca, bamboo, flax, henequen, hemp, jute, kenaf, pineapple, ramie, and sisal with good mechanical properties are being evaluated as low-cost alternative reinforcements to commonly used glass fibres in composites. These fibres, obtained from the plant stems or leaves, are renewable annually as compared to wood, which takes 20-25 years to grow before it can be cut and used. Some plants such as bamboo grow so fast that they can be harvested every few months. As a result, their supply could be virtually endless.

These fibres could not be as strong as graphite or aramids, but have higher stiffness than glass fibers.[108]

Panels made from such fibres and PP or other thermoplastics are already in use in many automotives. All major automotive manufacturers are exploring their use in other interior applications as well.

Besides natural fibres, manufactured cellulose fibres such as high-tenacity viscose rayon could also be used as reinforcement in 'green' composites. Although viscose rayon production traditionally involves a complex, polluting process, Tencel® fibres developed recently by UK Company Courtaulds Fibres are produced via a non-polluting method.[109]

Some oils have been chemically modified to yield inexpensive resins for a different class of 'greener' composites. Soybean oil based resins were used by Henry Ford in 1938 to make the first fibre reinforced car body panel.[110] Since soybeans contain about 20% oil, efforts are now under way to use genetic modification to increase the oil content and thus provide an inexpensive source of resins.

The Affordable Composites from Renewable Resources (ACRES) has also developed a series of maleinized hydroxylated triglycerides derived from safflower, olive, and other genetically engineered oils from DuPont.[111]

Although most of these resins were found to be non-degradable, it could be possible to chemically modify them to make them biodegradable. Since these so-called 'greener' composites combine non-degradable resins with degradable fibres, at the end of life they can neither return to an industrial metabolism nor to a natural metabolism. Unfortunately, they cannot be food stock for either system. They can only be down-cycled because of property degradation in reprocessing or incinerated to recover the energy value.

Fully 'green' composites

Significant research efforts are currently being spent in developing a new class of fully biodegradable 'green' composites by combining natural fibres with biodegradable resins.[112-118]

Most of the current technology is still in the research and development stage, but, however, few companies have begun producing some products on a commercial scale. These composites are environment-friendly, fully-degradable, and sustainable. At the end of their life they can be easily disposed of or composted without harming the environment (Figure 5.1).[119]

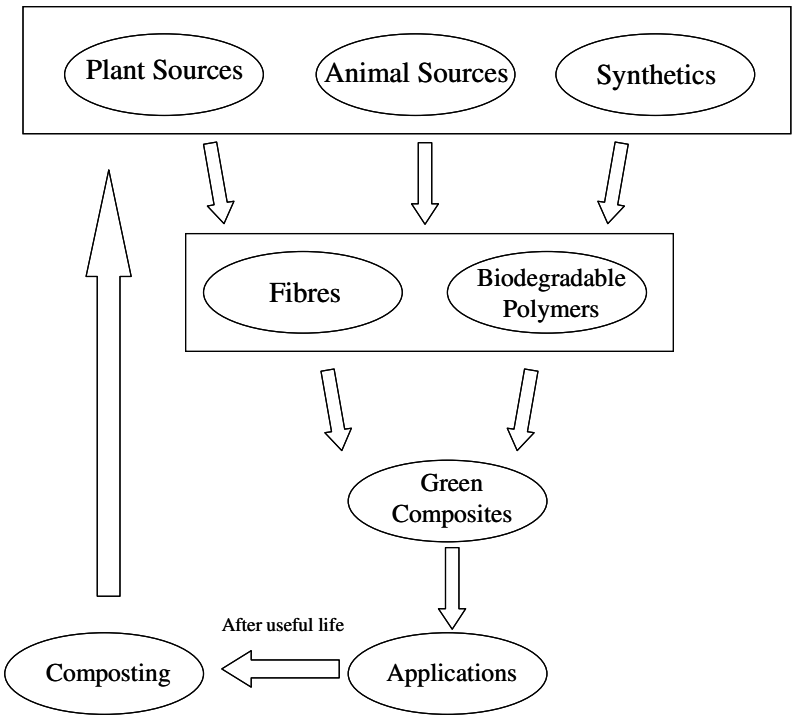

Figure 5.1: Typical life cycle of green composites.[119]

These green composites could be used effectively in many applications such as mass-produced consumer products with short life cycles of one to two years (nondurable) or products intended for one-time or short-term (few times) use before disposal.

The challenge of the researcher is to find green composites with a useful life of several years for outdoor application.

However, nowadays, most green composites could be used for indoor applications with a life of several years. A variety of natural and synthetic biodegradable resins are available for use in such green composites.[98,119]

A partial list of such resins is provided in Table 5.1.[119]

Table 5.1: Biodegradable polymer resin.[119]

Natural	Synthetic
1. Polysaccharides	1. Poly(amides)
Starch	2. Poly(anhydrides)
Cellulose	3. Poly(amide-enamines)
Chitin	4. Poly(vinyl alcohol)
Pullulan	5. Poly(ethylene-co-vinyl alcohol)
Levan	6. Poly(vinyl acetate)
Konjac	7. Polyesters
Elsinan	Poly(glycolic acid)
2. Proteins	Poly(lactic acid)
Collagen/Gelatin	Poly(caprolactone)
Casein, albumin, fibrogen, silks, elastins	Poly(ortho esters)
Protein for grains	8. Poly(ethylene oxide)
3. Polyesters	9. Some Poly(urethanes)
Polyhydroxyalkanoates	10. Poly(phosphazines)
4. Other Polymers	11. Poly(imino carbomates)
Lignin	12. Some Poly(acrylates)
Lipids	
Shellac	
Natural Rubber	

Most of these resins degrade through enzymatic reactions when exposed to a compost environment. Many also degrade in moist/wet outdoor environments through similar microbial/bacterial attack.

Luo and Netravali use Biopol® (poly(hydroxybutyrate-co-hydroxyvalerate) or PHBV resin from Monsanto Company) with pineapple and henequen fibres to make green composites. The tensile and flexural strengths of green composites are reported to be significantly higher in the grain direction than many wood-varieties, even at a low fibre content of 28%. With higher fibre content and better processing, the mechanical performance can improve further for use in non-critical applications, such as secondary structures in housing and transportation.[112-114]

Other researchers have developed jute fabric/Biopol composites. In these cases, chemical of fibre surfaces and alkali treatment of fibres are carried out to increase the fibre/resin interface bonding and improve the strength of the composites.[120,121]

Jute fabrics, with various surface treatments, have been used to form green composites with polyester amide resin (BAK 1095 from Bayer).[122] These composites are shown to degrade rapidly with composting.

Hermann and others have reported the tensile properties of unidirectional laminates from ramie, hemp, and flax fibers in Sconacell A (starch modified resin by Buna Sow Leuna). Some of these composites had properties comparable to glass fibre/epoxy composites and are found to be suitable for a variety of structural applications.[123]

Significant work has been done on soy protein polymers, which could be available in the form of soy flour (SF), soy protein isolate (SPI), or soy protein concentrate (SPC).[115-118,124-133]

Bio-absorbable polyphosphate fillers are blended with SPI and compression molded to obtain relatively water-resistant and stiff composites.[125-127]

Thames and his group reported wood fibre-filled soy protein composites by hot compression molding. The mechanical properties of these composites are reported to be comparable to or better than composites made using polystyrene and wood fibres.[129,130]

Phenix Biocomposites has commercialized the decorative composite board, Environ®, made using recycled wastepaper and SF. Environ can be used for furniture and architectural non-structural applications. Being fully degradable, Environ can also be composted.

Recently, Drzal et al. reported composites made using hemp fibres and SF. They find increased strength and a higher heat deflection temperature compared with the soy polymer as a result of adding hemp.[131]

Netravali and co-workers have reported work on plant-fibre based soy protein composites.[115-117,132,133]

Lodha and Netravali have prepared composites containing chopped ramie fibres and SPI polymer by hot pressing. Significant improvement in strength is reported after adding ramie fibres with lengths above 5 mm.[116]

Chabba and Netravali have reported chopped henequen fibre/SPC composites with similar properties. These composites with moderate strength would be useful in packaging applications as well as in nondurable consumer goods.[132]

Nam and Netravali[118] have reported unidirectional ramie fibre/SPC composites (65% fibre content) with strength in the range of 275 MPa. This strength is twice that of many wood varieties such as walnut, bass, and cherry and is comparable to some varieties of steel. These composites are

also found to be many times tougher than wood and also have superior flexural properties.[133]

By optimizing the processing conditions and better fibre lay up, the strength, stiffness, and flexural properties of these composites can be improved further.

Starch and modified starch blends have also been used as resin to form 'green' composites.[134-137]

Takagi and coworkers[134-136] have reported composites based on modified starch resin and mao, hemp, and bamboo fibres. The high stiffness of the bamboo fibres results in composites with excellent flexural properties.[134]

Unidirectional composites of hemp fibre and starch-based resin have tensile strengths in the range of 200 MPa, close to steel, making them useful for structural applications.[135]

Goda et al. used ramie fibres in the form of low-twist yarns and starch-based resin to obtain green composites. These composites also have strengths in the range of 250 MPa and would be suitable for structural applications. [137]

Many such examples can be found in the open literature. However, many hurdles to the commercialization of green composites remain.

One of the major problems is the cost of the resins. However, as green composites gain acceptance and production increases, the cost is expected to come down as it does with most materials. Inexpensive production of oils for resins through biotechnology would certainly be of help in expediting their commercialization. Faster, better, and more efficient processing will also reduce manufacturing costs.

Besides the resin costs, there are other problems as well. Diameters and strengths of plant-based fibres vary significantly depending on factors

such as source, age, retting and separating techniques, geographic origin, rainfall during growth, and cellulose/hemicellulose/lignin content. Most cellulosic fibres also swell and lose strength when they absorb moisture and shrink when they lose moisture. Repeated moisture absorption/desorption can significantly lower their strength and affect their bonding to the resin.

The future developments

Most of the research on green composites to date has used plant-based fibres because of their ready availability. However, opportunities exist for using high-strength protein fibres, such as dragline silk obtained from the golden orb spider.

These fibres are five to ten times stronger than steel and can form the basis of 'advanced' green composites. Unfortunately, 'silking' the golden orb spider is a difficult and time-consuming process. These small creatures are only capable of producing about 1 mg of dragline silk for day. As a result, many research groups have been studying the structure and chemistry of spider silk in an effort to synthesize polypeptide molecules with similar chemistry and produce fibres in the lab.[138-139]

Since continuous filaments are produced, there is the possibility of using these fibres for many applications, such as body armour, sports gear, and aerospace materials.

Research into solvent spinning of liquid crystalline cellulose, chitosan, and other materials also looks promising for producing high-strength fibers.[140,141]

Biotechnology is used to modify and/or increase the yield of specific triglycerides and oils in beans for producing resins.[111]

These resins will also be inexpensive compared with those available today and, if suitably modified, could be biodegradable. Research is also being conducted at various research laboratories to develop new pathways to synthesize inexpensive biodegradable resins with better mechanical properties, as well as thermal stability using nanotechnology.[142,143]

Once fully developed, these resins and high strength fibres have great promise for replacing many of the non-degradable advanced composites currently in use. With these and other significant developments, the future for ‘green’ composites looks both promising and exciting.

5.2 Soy and Starch-based DIP

The stringent regulations in terms of safety and environmental pollution have led Bridgestone T.C.E. to look for an eco-friendly (free of formaldehyde) alternative DIP. The strategy is to search for a synthetic biodegradable resin, which can replace resorcinol-formaldehyde resin, and combined it with latex to form an innovative DIP.

Studies in recent years, especially in the wood industry, are focused on the potential use of soy and starch-based resins as potential substitutes of formaldehyde-based resins.

Our idea is to add such innovative resins to Latex and form new DIP systems. The goodness of the adhesion of these alternative DIP solutions to the reinforcing fibres of the tyre will be tested in the future by adhesion test (CRA-ST test).

Soy-based adhesives

Soybean is primarily an industrial crop cultivated for oil and protein. Despite the low oil content of the seed (20% on moisture free basis) soybeans are the largest single source of edible oil and account for 52% of the total oil seed production of the world. With each ton of crude soybean oil, approximately 4.5 tons of soybean meal (protein content 44%) is produced. For each ton of soybean processed, the commercial value of the meal obtained usually exceeds that of the extracted oil. Despite considerable public and commercial interest in soybean products as food, the proportion of soy protein consumed directly in human nutrition and

other industrial uses is really small and there is a need to look for the new industrial uses of soy protein.

U.S. and Brazil account for most of the soybean production. According to FAO estimates over 160 million tonnes of soybean is produced worldwide in the year 2000. The leading producer is the USA, which accounts for 49%; Latin America and the Caribbean produce 34%, Asia 14% and Africa less than 1%.[144]

Soy-based plastics, adhesives, films and coatings are being considered for applications such as agricultural equipment, automobiles, plywood, marine infrastructure and civil engineering.[145-148]

Industry needs environment-friendly adhesives from renewable resources because petroleum resources are finite and are becoming limited, whereas the demand for adhesives is increasing. On the other hand, abundant proteins are available from renewable resources and agricultural processing by-products such as soybean proteins from oil processing. Utilisation of these protein by-products as biodegradable adhesives and resins will help to overcome environmental problems and add value to agricultural by-products.

Soy protein based adhesives have been first developed in 1923 when a patent is granted for soybean meal-based glue.[149]

By the late 1920s, soy proteins are used in many industrial products, such as adhesives for wood and paper, binders in coatings and paints and as emulsifiers in colloidal rubber products.

Other industrial soy-based products that came in the 1930s and 40s included textile fibres, foams for fire extinguishers, plastics and lubricants.

However, the availability of petroleum at a lower cost and biochemical inertness of petroleum-based products has proved disastrous for the industrial use of soy. It is only after the lapse of almost 50 years that

the significance of eco-friendly material has been realised and once again, the polymer scientists are looking at nature for developing adhesives, plastics, composites, elastomers from soybean.

The bulk of soy proteins are globulins, characterised by their solubility in salt solutions. The solubility of soy proteins in water is strongly affected by the pH. About 80% of the protein in raw seeds or unheated meal can be extracted at neutral or alkaline conditions. As the acidity is increased, solubility drops rapidly and a minimum is observed at pH 4.2–4.6. Ultracentrifugation, gel filtration and electrophoresis can also be used for more precise fractionation.[150]

The soy protein fractions have also been characterised by their sedimentation constants. Two major fractions, known as 11S and 7S have been studied extensively (S stands for Svedberg units). The numerical coefficient is the characteristic sedimentation constant in water at 20 °C. The content of 11S is around 52% and of 7S is 35%. The other minor fractions have been designated as 2S (8%) and 15S (5%).[150]

The 11S fraction consists of glycinin, the principal protein of soybeans. Glycinin has a molecular mass of 320–360 kDa.

The 7S fraction is highly heterogeneous. Its principal component is beta-conglycinin, a sugar containing globulin with a molecular mass in the order of 150–190 kDa. The fraction also comprises enzymes (beta-amylase and lipoxygenase) and hemagglutinins.

The 2S fraction consists of low molecular mass polypeptides (in the range of 8000–20,000 Da) and comprises mainly the soybean trypsin inhibitors.

The 15S protein is probably a dimer of glycinin. Soy protein consists mainly of the acidic amino acids (aspartic and glutamic acids) and their corresponding amides (asparagine and glutamine), non-polar amino acids

(alanine, valine and leucine), basic amino acids (lysine and arginine), uncharged polar amino acid (glycine) and approximately 1% of cystine.

Soybean protein materials, which are useful for forming protein adhesives, are soy flour, protein concentrate, and, most preferably soy protein isolate. The soybean starting material is either soybean meal, flakes, cake or chips. The processing of soybean seeds includes cleaning, drying, cracking, dehulling, flaking and extraction of oil by using hexane (Figure 5.2).[124,151]

The residual soybean meal, which contains some hexane, is then used for the production of defatted soybean meal that is treated to give soy flour (SF), soy protein concentrates (SPC) and soy protein isolates (SPI).[152]

The composition of all the three soybean products is given in Table 5.2.[124,150]

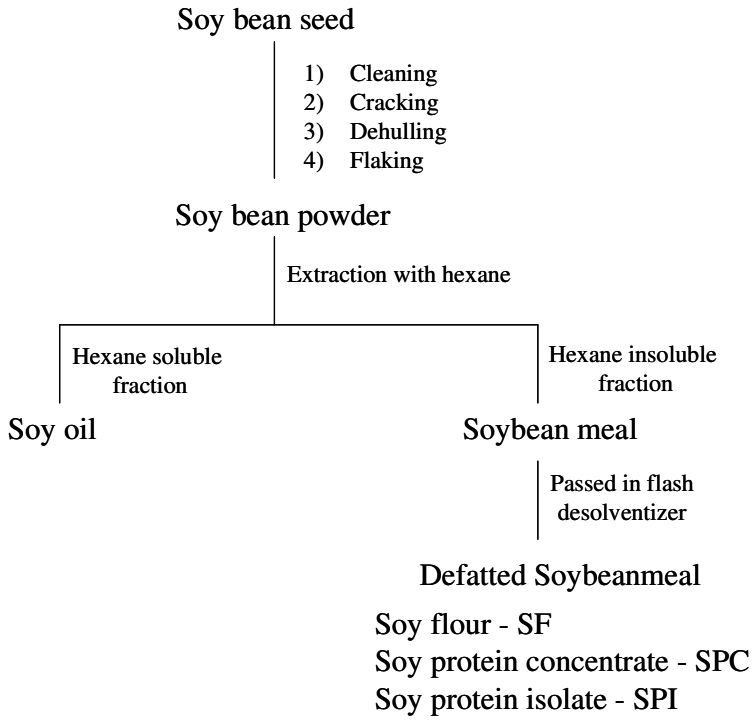

Figure 5.2: Flow diagram for the production of soy.[124,151]

Table 5.2: Composition of different soy protein products. [124,150]

g/100g product	Soy Flour (SF)	Soy protein Concentrate (SPC)	Soy protein Isolate (SPI)
Protein (as is)	48	64	92
Fat (min)	0.3	0.3	0.5
Moisture (max)	10	10	<5
Fibre (crude)	3	4.5	<1
Ash	7	7	4
Carbohydrate	31-32	14-15	-

The adhesive performance of soybean proteins is dependent upon the particle size, nature of surface, structure of protein, its viscosity and pH Other factors, which can affect their performance, are the processing parameters such as press temperature, pressure and time.[153]

The particle size of the soybean meal used for adhesive has a significant effect on its suitability and performance. Fineness of the grind is often expressed in terms of specific surface area (cm^2/g according to standard test) than mesh size. A specific surface area of 3000–6000 cm^2/g is considered to be satisfactory for adhesive grade or in other words, at least 97% should pass through a 325-mesh screen.[154]

Adhesive properties are also dependent upon the nature of surface to be bonded. If the surface is too rough, it will cause a cohesive failure and if the surface structure is too smooth, it will cause an adhesive failure.[154]

Viscosity is an important property, which largely governs the adhesive behaviour. The operating viscosity limits of soybean glues are very large ranging from 500 to 75000 cP upon the application and the nature of the materials to be glued. A viscosity of 500–5000 cP is needed for gluing materials which are highly absorbing, and over 50000 cP for poor absorbing materials.[153]

The high viscosity soybean proteins result from increased intermolecular interactions due to unfolded protein molecules. The major forces that facilitate such interactions are electrostatic and covalent

disulphide bonding. Ionic environments have been known to weaken the electrostatic interactions between protein molecules. Thus the viscosity of protein can be varied by treating with salts or by using reducing agents without affecting the adhesive strength or water resistance. Enzymatic or alkaline hydrolysis also reduces the viscosity. Higher the pH, higher will be the rate of hydrolysis, better adhesive strength and water resistance but short storage life. At higher pH, viscosity decreased with storage time and adversely affects the adhesive properties.

A moderate pH/temperature combination (pH= 10°C and T=50°C) has been recommended for better performance.[155]

The adhesive strength of protein glue depends on its ability to disperse in water and on the interaction of apolar and polar groups of the protein with material to be adhesive.

In a native protein, the majority of polar and apolar groups are unavailable due to the internal bonds resulting from Van der Waals forces, hydrogen bonds and hydrophobic interactions. For this reason a simple paste of soy flour is a poor adhesive and a chemical change is required to break the internal bonds and uncoil or disperse the polar protein molecules. Dispersion and unfolding of protein are enhanced by hydrolysis or by increasing the pH to about 11 or higher.[153]

Treatment with sodium hydroxide unfolds the protein molecules exposing the polar and apolar groups which in turn can interact with the material to be adhesive leading to an improvement in the adhesive strength and improve water resistance but at the same time shortens the useful life.

For the production of a good soy-based adhesive must therefore take into account the observed variables.

Netravali and his co-workers are nowadays the greatest researchers of soy-based adhesive systems. [115-117,132,133,156-158]

Their studies, some of them already analyzed in detail in the paragraph 5.2 of this chapter, can be very useful for develop of an innovative soy-based adhesive to be applied in tyres.

Starch-based adhesives

Starch is a carbohydrate consisting of a large number of glucose units joined together by glycosidic bond.

Starch has an intricate structure. It consists of two varieties of molecules: linear and helical amylose and the branched amylopectin. Starch usually encloses 20-25% of amylose and about 75-80% of amylopectin. The exact percentages of amylose and amylopectin for each starch are largely responsible for its working properties.

During the adhesive production, in fact, the amylose and amylopectin areas of the molecule behave very differently. The amylose fraction, for example, is responsible for the internal strength of a starch, for its degree of stiffening upon cooling, and for gelatinization.[159]

Starch appears as a white, tasteless, odourless powder consisting of tiny granules that vary among starch types in form, size, range of size, and marking.

Starch is finding in potatoes, rice, corn, wheat, cassava, and many other vegetables. The plant material is processed by a variety of means including treatment with acids, bases, enzymes, and oxidizers. These processes modify the viscosity of starch. Depending on the starch type, and the processing method, a vast range of viscosities and adhesive strengths can be produced.

The adhesive qualities of vegetable starches are recognized in early history. The first recorded use of a starch adhesive dates from the first

century A.D. in a description of papyrus manufacture by Pliny the Elder using a paste made from wheat flour.

Starch adhesive, or glues were first used in large scale industrial application approximately in the 1910s. The starch industry extracts and refines starches from seeds, roots and tubers, by wet grinding, washing, sieving and drying. The main commercial refine starches are: cornstarch, tapioca flour, wheat flour and potato starch.

Adhesives pastes are generally prepared by first soaking the starch in water and then curing it in additional water. Longer curing time, higher temperatures, and agitation promote the necessary separation of the granules.

Each starch has its characteristic gelatinization range which extends from approximately 55-80°C. Curing procedure, as well as origin of the starch, affects the characteristics of the resulting adhesive. Starches do not form true solutions, but rather colloidal dispersions. Starches swell in cold water and are partially dispersed in hot water. Curing starch paste is a mixture of swollen granules, little fragments of granules and dissolved starch.[160]

The pH of either the starch water slurry or the curing paste can be adjusted easily. The use of alkaline water (pH>8) to prepare pastes can improve the adhesion promoting ready dispersal and slow settling of the granules.[161]

Starch is one of the most abundant natural polymers and it is nowadays widely studied as a potential substitute of formaldehyde-based adhesives.[162]

Starch yields adhesives with excellent affinity for polar materials such as cellulose and rayon. Ideally, the contact angle between the adhesive and the substrate should be small. This allows the adhesive to wet the surface

and spread uniformly in a thin film with a minimum of voids. In this regard, starch based-adhesives wet the polar surface of cellulose, penetrate crevices and pores and, thus, form strong adhesive bonds.[162]

Imam et al. studied an adhesive prepared by crosslinking starch and polyvinylalcohol (PVOH) with hexamethoxymethylmelamine in the presence of citric acid as a catalyst. The effects of variable humidity and temperature on bonding and the effect of added latex (a copolymer of acrylic and methacrylic acids and their derivates) on viscosity and moisture resistance are investigated.[162]

Several studies have been also carried out where bio-composites were developed using starch in combination with tunicin whiskers, wood pulp, sisal and jute fibres and gluten with wood fibre. [163-166]

Corradini et al. studied starch/gluten/glycerol as a biodegradable matrix reinforced with lingocellulosic fibres. In this study the use of this combined Starch/gluten matrix improves noticeably the adhesion with coconut, sisal and jute fibres.[167]

Moubarik et al. studied the mechanical and physical properties of a new formaldehyde-free adhesive based on cornstarch and tannins with hexamine as hardener.[168]

The studies mentioned above[162-168], and the studies[134-137] already mentioned in paragraph 5.2 of this chapter, can be helpful for develop of an innovative Starch-based adhesive to be applied in tyres.

5.3 Conclusions

In recent years, research is moving to eliminate as much as possible formaldehyde and formaldehyde-based products in favour of 'green' formaldehyde-free products.

Formaldehyde-based adhesives are not renewable. Moreover, formaldehyde is considered a priority pollutant by the United States Environmental Protection Agency. Its emission into the environment and exposure of workers at manufacturing facilities continues to be a major safety concern.

The desire of Bridgestone T.C.E. is to develop an eco-friendly (formaldehyde-free) alternative DIP. The strategy is to search for a synthetic biodegradable resin, which can replace resorcinol-formaldehyde resin, and combined it with latex to form an innovative DIP.

In this thesis two possible systems have been identified: soy-based DIP and starch-based DIP. These systems will be tested, in the future, as potential substitutes of traditional RFL-DIP systems. This could be the first step toward a tyre seen as a completely 'green' composite.

Chapter 6
Conclusions

Textile cords used in rubber applications are commonly treated with the so-called Resorcinol-Formaldehyde-Latex (RFL-DIP). Despite the relevance of good adhesion between cords and rubber, and although this system dates back as far as 1938 and is still commonly used for rubber reinforcement till today, the mechanism by which the adhesion is obtained has remained unclear.

The level of knowledge of adhesion between RFL-treated cords and rubber today is empirical rather than scientific. With the introduction of new material in recent years, it is considered appropriate to revisit the physical and/or chemical processes at the basis of the interactions between latex and resin in the RFL-DIP traditional systems and to define also the nature of interactions among the RFL components and the reinforcing fibers and the RFL components and rubber.

Based on the results obtained from the understanding of these interactions, a study on the possibility of developing alternative DIP systems formaldehyde-free has been performed. Currently, in fact, there are restrictions on the industrial use of formaldehyde based on the proven carcinogenic properties.

In **chapter 2** a mechanical characterization of PET fibers produced by three different suppliers has been performed. The aim was to establish the fibre with the best properties in terms of tensile, creep and fatigue strength at break and that can be subjected to the treatment of dipping.

The monofilaments (PET-A, PET-B and PET-C samples) extracted from PET fibres produced by three different companies have been analyzed.

The filaments show similar tensile properties. Moreover, all PET samples analyzed show unusual breaking in fatigue which reinforces the observation that recent changes in fibres processing have improved tensile fatigue strength of produced fibres. In fact, the tested filaments show great resistance and some of them could be subjected to fatigue tests lasting several hours without failure.

The results of creep tests indicate that failure is initiated not only by fatigue but also by creep in presence of foreign particles placed at the interface between the fibre skin and its core. PET-A samples fair much better in creep than PET-B samples, and an OM analysis shows that the PET-A filaments have only a quarter of the number of particles per unit length (μ) as the PET-B filaments.

On the basis of this study, PET-A fibres have the best mechanical properties and could be subjected to a dipping process and used in a tyre.

In **Chapter 3** RFL-DIP traditional systems are characterized in the solid state in order to understand the nature and mechanism of interaction between latex and RF resin. Solid samples of RFL-DIP, obtained by casting of an aqueous solution, are analyzed using techniques of Optical Microscopy (OM) and Raman and FT-IR attenuated total reflection (ATR) spectroscopies.

Optical microscopy shows, in line with the Polymer Induced Phase Separation (PIPS) mechanism, that these systems are heterogeneous on micrometer scale.

The concentration of such heterogeneities has been critically and dimensionally evaluated in RFL systems with different content in Latex.

The concentration of the heterogeneities decreases with increasing of the content in Latex, for this we guess that these RFL systems are essentially made by RF resin particles dispersed in a latex matrix.

In order to confirm this hypothesis, the same systems are studied by Raman and FTIR spectroscopy. FTIR spectroscopy confirms that the matrix of the RFL systems is mainly Latex, while, Raman microscopy seems to confirm that the heterogeneity are substantially particles of RF resin.

FTIR spectroscopy analysis shows that the interaction between Latex and RF resin has a physical nature, even when RFL samples are cured at a typical dipping process temperature. The physical interactions could be mainly hydrogen bonds between hydroxyl groups of RF resin and pyridine groups of Latex.

In **Chapter 4** the study of the mechanism of interaction between RFL and reinforcing fibres, and RFL and rubber is reported.

Many and controversial opinion have been presented in the past to explain these interactions but, unfortunately, none of theme give clear and unambiguous results.

In this chapter we have tried to elucidate these interactions by means of spectroscopic techniques such as Raman, FT-IR/ATR, ^{13}C-NMR spectroscopy, and by mechanical and thermogravimetric (TGA) analysis.

As for as Nylon/RFL interface, Raman spectroscopy does not give clear results. ATR analysis seems instead to highlight a physical interaction between RFL, in particular Latex, and Nylon. However, ATR does not dissolve the doubts about a chemical reaction between RFL and Nylon, so we have thought about how confirm the result of the ATR analysis and how to exclude completely the possibility of a chemical reaction between RFL and Nylon.

After a careful analysis of the system, we have hypothesized that chemical reaction between Nylon and RFL can occur by means of Nylon hydrolysis, which leads to the formation of reactive groups like amine and carboxyl. If we induce the hydrolysis of Nylon in presence of RFL chemicals, we can obtain the reaction among these reactive groups and RFL components.

^{13}C-NMR spectroscopy and TGA analysis show that the hypothesis of a chemical reaction between Nylon and RFL by means of hydrolysis of Nylon chains is not realistic, so we can conclude that the interactions between Nylon and RFL, in particular Latex component of RFL, are purely physical. The physical interactions could be mainly hydrogen bonds between amide groups of Nylon and pyridine groups of Latex.

As for as RFL/rubber interface, ATR spectroscopy shows that the vulcanization process probably occurs not only between natural rubber chains and sulfur (CH groups of NR and S), but also between CH groups of NR, sulfur and Latex components (principally involving polybutadiene units) of RFL.

In **Chapter 5** a bibliographic study of eco-friendly (formaldehyde-free) alternative DIP systems is reported.

In recent years, research is moving to eliminate as much as possible formaldehyde and formaldehyde-based products in favour of 'green' formaldehyde-free products.

Formaldehyde-based adhesive are not renewable. Moreover, formaldehyde is considered a priority pollutant by the United States Environmental Protection Agency. Its emission into the environment and exposure of workers at manufacturing facilities continues to be a major safety concern.

The desire of Bridgestone T.C.E. is to develop an eco-friendly (formaldehyde-free) alternative DIP. The strategy is to search for a synthetic biodegradable resin, which can replace resorcinol-formaldehyde resin, and combined it with latex to form an innovative DIP.

In this PhD thesis two possible systems have been identified: soy-based DIP and starch-based DIP. These systems will be tested, in the future, as potential substitutes of traditional RFL-DIP systems. This could be the first step toward a tyre seen as a completely ‘green’ composite.

References

1. R.W. Thomson, *"Carriage wheels"*. 1845, U.K. patent no° 10990.
2. T. French, *"Tyre Technology"*. 1988, New York: Adam Hilger.
3. P.M. Cross and E.J. Bevan, (GB9676) *Abel & Imray*, 1895.
4. W.H. Carothers, (US2071253) *DuPont*, 1935. C.F.
5. P. Schlack, (US2142007) *I.G. Farbenindustrie*, 1938.
6. J.R. Whinfield and J.T. Dickson, (US2465319) *DuPont*, 1941.
7. T.I. Bair and P.W. Morgan, (CA928440) *DuPont*, 1973.
8. S.L. Kwolek, (FR2010753) *DuPont*, 1969.
9. H. Blades, (DE2219703) *DuPont*, 1971.
10. H. Blades, (DE2219646) *DuPont*, 1971.
11. L. Vollbracht, (DE2605531) *Akzo Nobel*, 1976.
12. P. Smith and P.J. Lemstra, (NL7900990) *Stamicarbon B.V.*, 1979.
13. H. Brody, *"Synthetic fibre materials"*. 1st ed. 1994, Essex: Longman Scientific & Technical.
14. Private communication Teijin Twaron company.
15. W.B. Wennekes**,** Ph.D. thesis, University of Twente, 2008
16. W.H. Charch, N.Y. Buffalo, and D.B. Maney, (US2128635) *DuPont*, (1938)
17. C. Hepburn and Y.B. Aziz, *Ind. Eng. Chem.*, **5**, 153-159 (1985).
18. A. Garton and J.H. Daly, *J. Polym. Sci., Part A: Polym. Chem.*, **23**, 1031-1041 (1985).
19. P.J.D. Lange, P.G. Akker, A.J.H. Maas, A. Knoester, and H.H. Brongersma, *Surf. Interface Anal.*, **31**, 1079-1084 (2001).
20. P.J.D. Lange, E. Mader, K. Mai, R.J. Young, and I. Ahmed, *Composites*, **32**, 331-342 (2001).
21. D.B. Wootton, *"the Present Position of Tyre Cord Adhesives"*, in *"Developments in Adhesives"*, W.C. Wake, Editor. Appl. Sci. Publ. LTD., London. (1977).
22. Y. Iyengar, *Rubber World*, **197**, 24-29 (1987).
23. G. Gillberg and L.C. Sawyer, *J. Appl. Polym. Sci.*, **28**, 3723-3743 (1983).
24. D.B. Rahrig, *J. Adhes.*, **16**, 179-216 (1984).
25. D.B. Wootton, *"The Application of Textiles in Rubber"*. Shawbury: Rapra technology LTD. (2001).

26. W. Hupjé, *"Hechting van Textiel aan Rubber"*, in *De Nederlandse Rubber Industrie*. 1970.
27. N.K. Porter, *J. Coat. Fabrics*, **21**, 230-239 (1992).
28. R.V. Uzina, I.L. Schmurak, M.S. Dostyan, and A.A. Kalinia, *Sovjet Rubber Technology*, **20**, 18-22 (1961).
29. T. Takeyama and J. Matsui, *Rubber Chem. Technol.*, **42**, 159-257 (1969).
30. N.K. Porter, *J. Coat. Fabrics*, **23**, 34-45 (1993).
31. A.L. Miller and S.B. Robison, *Rubber World*, **137**, 397 (1957).
32. M.I. Dietrick, *Rubber World*, **136**, 847-851 (1957).
33. W.H. Hupjé, *De Tex*, **29**, 267-271 (1970).
34. R.T. Murphy, L.M. Baker, and R. Reinhardt, *Ind. Eng. Chem.*, **40**, 2292-2295 (1948).
35. T.S. Solomon, *Rubber Chem. Technol.*, **58**, 561-577 (1985).
36. H.M. Wenghoefer, *Rubber Chem. Technol.*, **47**, 1066-1073 (1974).
37. T.W.G. Solomons, *"Organic Chemistry"*. 1996, New York: John Wiley & Sons, Inc. p. 1218.
38. L. Caliano**,** Ph.D. thesis, University of Naples, 2009.
39. T.S. Solomon, *"Tire Cord Adhesion - I. Resorcinol Formaldehyde Latex (RFL) Cord Dips"*. 2000: BFGoodrich R&D center.
40. D.B. Wootton, *"the Present Position of Tyre Cord Adhesives"*, in *"Developments in Adhesives"*, W.C. Wake, Editor. 1977, Appl. Sci. Publ. LTD., London.
41. N.K. Porter, *J. Coat. Fabrics*, **25**, 268-275 (1996).
42. T. Takeyama and J. Matsui, *Rubber Chem. Technol.*, **42**, 159-256 (1969).
43. T.S. Solomon, *in Meeting of the Rubber Division ACS*, 1983. Houston, Texas.
44. G. Xue, *J. Macromol. Sci., Part A: Chemistry*, **24**, 1107-1120 (1987).
45. Y. Iyengar, *Rubber World*, **197**, 24-29 (1987).
46. World healt organization, International agency for research on cancer, IARC monographs on the evaluation of cancerogenic risks to umane, vol. 88 (2006).
47. D.B. Wootton, *Textile reinforcement of elastomers*. Chapter 2 (1982).
48. A.R. Bunsell, *Reinforcing fibers in: Encyclopedia of Applied Physics*, VCH publishers, 343-368 (1996).
49. X.C.Hu, H.H. Yang, *Polyamide and polyester fibers, in: Comprehensive Composite Materials*, ed. A. Kelly, 1, p. 327-344 (2000).

50. J.Brandrup, E.H. Immrgut, E.A. Grulke, *Polymer handbook*, 4th ed., Wiley, (1999).

51. R.W. Cahn, *Structure and properties of polymers, Materials Science and Technology*, **12**, VCH, (1993).

52. M.F. Culpin, K.W. Kemp, *Proceedings of the Physical Society*, **69**, 1301-1308 (1957)

53. G.T. Davis, H.S. Taylor, *Textile Research Journal*, 35, 405-411 (1965).

54. H.H. Kausch, N. Heymans, C.J. Plummer, P. Decroly, *Matériaux Polymères: Propriétés mécaniques et physiques,* Presses Polytechniques et Universitaires Romandes, **14**, 658, (2001).

55. A. Marcellan, A. Bunsell, R. Piques, P.Colomban, *Journal of Materials Science*, 38, 2117-2123 (2003).

56. B. Wunderlich, *Macromolecular physics*, **3**, 69 (1980).

57. A.R. Bunsell, J.W.S. Hearle, R.D. Hunter, *An apparatus for fatigue-testing of fibres, Journal of Physics E – Scientific Instruments*, **4**, 868-872 (1971).

58. J.W.S. Hearle, P.M. Cross, *Journal of Materials Science*, **5**, 507-516 (1970).

59. J.W.S. Hearle, *Textile Manufacturer*, no. 1177, p. 24-25 (1973).

60. J.W.S. Hearle, B. Lomas, A.R. Bunsell, *Applied Polymer Symposia*, **23**, p. 147-156 (1974).

61. J.W.S. Hearle, B. Lomas, W.D. Cooke, *Atlas of fibre fracture and damage to textiles*, Woodhead publishing, 2nd ed., (1998).

62. A.R.Bunsell, *Chemtech*, p. 292-299 (1974).

63. J.M. Herrera Ramirez**,** Ph.D. thesis, Ecole des Mines de Paris, 2004

64. A.R. Bunsell, J.W.S. Hearle, *Journal of Materials Science*, **10**, 1303-1311 (1972).

65. A.R. Bunsell, *Handbook of tensile properties of fibres*, Woodhead Publishers, Cambridge, (2009).

66. A.R. Bunsell, *private communication*.

67. C. Le Clerc, A.R. Bunsell, A. Piant, B. Monasse, *Journal of Materials Science,* vol. **41**, num. 20, 6830-6842 (2006).

68. A. Taniguchi, M. Cakmak, *Polymer*, **45**, 6647 (2004).

69. R.J.J. William, B.A. Rozenberg, J.P. Pascault, *Advances in Polymer Science: Polymer Analysis, Polymer Physics*. Springer, vol. **128**, p. 95 (1997).

70. Hummel/Scholl, *Infrared analysis of polymers, Resins and additives An atlas*, vol.1 part.1/2, Wiley, (1969)

71. P. Zhang, J. He, X. Zhau, *Polymer testing*, **27**, 153-157 (2008).
72. Xu-Dong Li, S.H. Goh, J. W. Zheng, *Journal of Applied Polymer Science*, Vol.**87**, 1137-1143 (2003).
73. E. Groppo, M.J. Uddin, O. Zavorotynska, A. Damin, J.G. Vitillo, G. Spoto, A. Zecchina, *J.Phis. Chem. C*, **49**, 112 (2008).
74. G. Martinez-Barrera, H.Lopez, V.M. Castano, R. Rodriguez, *Radiation physics and Chemistry*, **69**, 155-162 (2004).
75. R.M. Silverstein, *Spectrometric identification of organic compounds*, Wiley, (1962).
76. Shiao-Wei Kuo, Cheng-Lung Lin, Feng-Chih Chang, *Polymer*, **43**, 3943-3949 (2002).
77. H. Patterson, *Adhesive Age*, **6**(9), 38 (1963).
78. H. Moult, in "Handbook of adhesives", I. Skeist , Reinhold Publishing Corp., New York, 495 (1962).
79. M.W. Wilson, *Tappi*, **43**(2), 129 (1960).
80. V.E. Basin, A.A. Berlin, and R.V. Uzina, *Soviet Rubber and technology*, **21**(9), 12 (1962).
81. R.D. Davis, S.J. Steadman, W.L. Jarrett, and L.J. Mathias, *Macromolecules*, **33**, 7088-7092 (2000).
82. E. Smith and G. Dent, *Modern Raman spectroscopy-A pratical approach*, Wiley, (2005).
83. G.Socrates, *Infrared and Raman characteristic group frequencies: tables and charts*, Wiley, (2001).
84. H. Matsui et al., *Polymer*, **42**, 5625-5632 (2001).
85. N. Perkas et al., *Journal of Applied Polymer Science*, **104**, 1423-1430 (2007).
86. R.A. Nyquist, *Interpreting Infrared, raman and nuclear magnetic resonance spectra*, Elsevier, (2001).
87. Li-Ling Cho, *Forensic Science journal*, **6** (1), 55-62 (2007).
88. K. De Vries, H. Linssen., G. Van der Velden, *Macromolecules*, **22**, 1607, (1989).
89. M.A. Healey, J.H. Patrick, and D.W. Yvonne, *Polymer*, **37**(18), 4009-4024, (1996).
90. U.S. Environmental Protection Agency, Office of Air and Radiation. *Report to Congress on Indoor Air Quality, Volume II: Assessment and Control of Indoor Air Pollution*, (1989).

91. National Toxicology Program (June 2011). *Report on Carcinogens, Twelfth Edition.* Department of Health and Human Services, Public Health Service, National Toxicology Program. Retrieved June 10, 2011.
92. M. Hauptmann, P.A. Stewart, J.H. Lubin et al., *Journal of the National Cancer Institute*, **101(24)**, 1696–1708 (2009).
93. M. Hauptmann, J.H. Lubin, P.A. Stewart, R.B. Hayes, A. Blair, *Journal of the National Cancer Institute*, **95(21)**, 1615–1623 (2003).
94. L. Beane Freeman , A. Blair, J.H. Lubin, *Journal of the National Cancer Institute*, **101(10)**, 751–761 (2009).
95. L.E. Pinkerton, M.J. Hein, L.T. Stayner, *Occupational Environmental Medicine*, **61**, 193–900 (2004).
96. D. Coggon, E.C. Harris, J. Poole, K.T. Palmer, *Journal of the National Cancer Institute*, **95(21)**, 1608–1615 (2003).
97. M. Hauptmann, J.H. Lubin, P.A. Stewart, R.B. Hayes, A. Blair, *American Journal of Epidemiology* , **159(12)**, 1117–1130 (2003).
98. E. S. Stevens, *Green Plastics*, Princeton University Press, Princeton, (2002).
99. M. M. Nir et al., *Plastics Engineering*, 75 (1993).
100. S. Peterson et al., *Composite*, *Part A*, **33**, 1123 (2002).
101. L.T. Drzal et al., *Polymer Preprints*, **42**, 31 (2001).
102. K. Joseph, *J. Appl. Polym. Sci.*, **47,** 1731 (1993).
103. S. J. Eichhorn et al., *J. Mater. Sci.*, **36**, 2107 (2001)
104. G. Canche-Escamilla et al., *Composite*, *Part A*, **33**, 539 (2002).
105. P. Flodin and P. Zadorecki, *Composite Systems from Natural and Synthetic Polymers*, Elsevier Science, 59 (1986)
106. P. Zadorecki et al., *Compos. Sci. Technol.*, **27**, 291 (1986).
107. L. Hua et al., *Polym. Compos.*, **8**, 203 (1987).
108. D.N. Saheb and J.P. Jog, *Advances in Polymer Technology*, **18**, 351 (1999).
109. Courtaulds Fibers, Coventry, UK, Tencel Technical Overview.
110. D.L. Kaplan, *Biopolymers from renewable resources*, Springer, NY, (1998).
111. R.P. Wool, Proc. of ICCE-6, B45 (1999).
112. S. Luo and A. N. Netravali, *Polym. Compos.*, **20**, 367 (1999).
113. S. Luo and A. N. Netravali, *J. Mater. Sci.*, **34**, 3709 (1999).
114. S. Luo, Ph.D. thesis, Cornell University, NY, (2000).
115. P. Lodha and A.N. Netravali, Proc. of ICCE-7, 655 (2000).
116. P. Lodha and A.N. Netravali, *J. Mater. Sci.*, **37**, 3657 (2002).

117. P. Lodha and A.N. Netravali, *Recent Advances in polymer and composites*, Allied Publishers, New Delhi, India, 3 (2000).
118. S. Nam and A.N. Netravali, Proc. of ICCE-9 551 (2002).
119. A.N. Netravali and S. Chabba, *Materials Today*, 22-29 (2003).
120. A.K. Mohanty et al., *J. Mater. Sci.*, **35**, 2589 (2000)
121. A.K. Mohanty et al., *Compos. Sci. Technol.*, **60**, 1115 (2000).
122. A.K. Mohanty et al., *Composite*, *Part A*, **31**, 143 (2000).
123. A.S. Hermann et al., *Polym. Degrad. Stab.*, **59**, 251 (1998).
124. R. Kumar et al., *Industrial Crops and Products*, **16**, 155 (2002).
125. J.U. Otaigbe, Plastics Engineering, 37 (1998).
126. J.U. Otaigbe, D.O. Adams, *J. Environ. Polym*, **5**, 199 (1997).
127. J.U. Otaigbe and J.L. Jane, *J. Environ. Polym*, **5**, 75 (1997).
128. J. Zhang et al., *Polymer Preprints*, **39**, 162 (1998).
129. S. F. Thames and L. Zhou, Proc. of ICCE-5, 887 (1998).
130. S. F. Thames et al. Proc. of ICCE-6, 135 (1999)
131. L.T. Drzal et al., *Polymeric Materials: Sci. & Eng.*, 87, 117 (2002).
132. S. Chabba and A.N. Netravali, International workshop on 'Green' Composites, 1 (2002)
133. S. Nam, M.S. thesis, Cornell University, NY, (2002)
134. H. Takagi et al., International workshop on 'Green' Composites, 4 (2002).
135. S. Ochi et al., International workshop on 'Green' Composites, 22 (2002).
136. Y. Ichihara and H. Takagi, International workshop on 'Green' Composites, 26 (2002).
137. K. Goda et al., International workshop on 'Green' Composites, 8 (2002).
138. D.T. Grubb and L. Jelinski, *Macromolecules*, **30**, 2860 (1997).
139. P. Gould, Materials Today, **5 (12)**, 42 (2002).
140. T.D. Rathke and S.M. Hudson, *J. Macromol. Sci. Reviews*, **34**, 375 (1994).
141. S. Salmon and S.M. Hudson, *J. Macromol. Sci. Reviews*, **37**, 199 (1997)
142. S.D. Allen et al., *J. Am. Chem. Soc.*, **124**, 14284 (2002).
143. L.R. Reith et al., *J. Am. Chem. Soc.*, **124**, 15239 (2002).
144. Ph (Post harvest) Action News. Publication from FAO, No. 4, (2001).
145. J. Jane and S. Wang, U.S. patent 5,523,293 (1996).

146. S. Wang, H.J. Sue, J. Jane, *J. Macromol. Sci., Pure Appl. Chem. (Ed.)*, **33**, 557–569 (1996).
147. U. Kalapathy et al., *J. Am. Oil Chem. Soc.*, **72**, 507–510 (1995).
148. Y.M. Stuchell and J.M. Krochta, *J. Food Sci.*, **59**, 1332–1337 (1994).
149. O. Johnson, U.S. patent 1,460,757 (1923).
150. J.E. Kinsella, *J. Am. Oil Chem. Soc.*, **56**, 242-258 (1979).
151. R. Seal, Industrial soy protein technology. In: Grant, R.A. (Ed.), Applied Protein Chemistry. Appl. Sci. Pub. Ltd, 87–111 (1980).
152. T.L. Krinski and M.L. Scacciaferro, European Patent 083,851,3A2. (1998).
153. A.L. Lambuth, A.L., Soybean glues. In: Skeist, I. (Ed.), Handbook of Adhesives, 2nd ed. Van Nostrand, New York, pp. 172–180 (1977).
154. A.L. Lambuth, A.L., Blood and casein glues. In: Satas, D., Tracton, A.A. (Eds.), Coatings Technology Handbook. Marcel Dekker Inc, New York, pp. 519–530 (2001).
155. U. Kalapathy et al., *J. Am. Oil Chem. Soc.*, **73**, 1063–1066 (1996).
156. S. Chabba, G. F. Matthews and A. N. Netravali, *Green Chemistry*, **7**, 576-581 (2005).
157. S. Chabba and A. N. Netravali, *J. Mater. Sci.*, **40**, 6263 (2005).
158. S. Chabba and A. N. Netravali, *J. Mater. Sci.*, **40**, 6275 (2005).
159. I. Skeist, ed. Handbook of Adhesives. 1st and 2nd ed. Huntington, NY: Robert E. Kreiger Publishing Co., (1977).
160. C.V. Horie, Materials for Conservation: Organic Consolidants, Adhesives. Coatings. London: Butterworths & Co., (1987).
161. TAPPI, Starch and Starch Products in Paper Coating. Monograph No. 17, New York, NY: TAPPI, (1957).
162. S.H Imam, L. Mao, L. Chen, L.V. Greene, *Starch/Stärke*, **51(6)**, 225–229 (1999).
163. A.P Mathew, A. Dufresne, Biomacromolecules, **3**, 1101–1108 (2002).
164. A.J.F. Carvalho, A.A.S. Curvelo, J.M.A. Agnelli, *Int. J. Polym. Mater.*, **51**, 647–660 (2002).
165. F.G. Torres, O.H. Arroyo, C. Gomez , *J. Thermoplast. Compos. Mater.*, **20**, 207-223 (2007).
166. M.D.H. Beg, K.L. Pickering, S.J. Weal, *Mater. Sci. Eng. A*, **412**, 7-11 (2005).
167. E. Corradini, S.H. Imam, J.M.A. Agnelli, L.H.C. Mattoso, *J. Polym. Environ.*, **17**, 1–9 (2009).

168. A. Moubarik, B. Charrier, A. Allal, F. Charrier, A. Pizzi, *Eur. J. Wood Prod.*, 68, 167–177 (2010).